九州大学学術情報リポジトリ Kyushu University Institutional Repository

Dew-Point Evaporative Cooling for All Weather Application and PV Cooling: Thermodynamic and Entropy Generation Analysis

ヨウ, テイ

https://hdl.handle.net/2324/7363864

出版情報:Kyushu University, 2024, 博士(工学), 課程博士

バージョン: 権利関係:

Dew-Point Evaporative Cooling for All Weather Application and PV Cooling: Thermodynamic and Entropy Generation Analysis

Dissertation

YANG CHENG



November 2024

Interdisciplinary Graduate School of Engineering Science

Kyushu University, Japan

Dew-Point Evaporative Cooling for All Weather Application and PV Cooling: Thermodynamic and Entropy Generation Analysis

A dissertation submitted in partial fulfilment of the requirements for the award of the degree of

Poctor of Engineering

By

YANG CHENG



Supervisor: Professor Takahiko Miyazaki

Associate Professor Kyaw Thu

Interdisciplinary Graduate School of Engineering Science

Declaration

The declaration in this dissertation asserts that, unless explicitly referenced, the work

presented is original and has not been previously submitted, either in whole or in part, for any

other academic degree or qualification at this or any other institution. This dissertation reflects

my independent research and does not incorporate collaborative contributions, except where

clearly acknowledged in the text and Acknowledgements section. Submitted in partial

fulfillment of the requirements for the Doctor of Philosophy degree at the Interdisciplinary

Graduate School of Engineering Sciences, Kyushu University, Japan, this work stands as a

genuine account of my original research efforts.

YANG CHENG

2024.11.19

i

Acknowledgements

First and foremost, I would like to express my heartfelt gratitude to Professor Miyazaki Takahiko. I am deeply thankful for the opportunity he granted me to pursue my master's and doctoral degrees at Kyushu University, a prestigious institution. His profound expertise has enriched my academic knowledge and cultivated my ability to conduct independent research. Moreover, his patience and care provided immense mental support, inspiring me to persist in my academic endeavors.

I am equally grateful to Professor Kyaw Thu for his unwavering enthusiasm for work, which profoundly influenced my work ethic and approach. His exceptional academic guidance supported me in completing critical tasks such as mathematical modeling, data analysis, and paper writing. Beyond academics, his mentorship extended to daily life, offering invaluable support and advice.

I would also like to extend my thanks to our laboratory secretary, Yamato Yuri, for her meticulous assistance with my day-to-day administrative matters, including financial reimbursements and work-related tasks. My gratitude also goes to technical staff member Takata Nobuo for his guidance and support in equipment usage and experiment-related matters.

Furthermore, I wish to thank all my laboratory colleagues over the past five years. Their support extended beyond academics, providing companionship and encouragement in everyday life. Lastly, I am profoundly grateful to my parents. Despite the physical distance between us, their unwavering understanding and support have been my strongest foundation. Without them, completing my studies would not have been possible.

Table of Contents

Declaration	i
Acknowledgements	ii
Abstract	vi
List of Figures.	viii
List of Tables	xiii
Nomenclature	xiv
Chapter 1 Introduction	1
1.1 Background	1
1.2 Dew-point evaporative cooling	4
1.2.1 Analysis based on the first law of thermodynamics	4
1.2.2 Analysis based on the second law of thermodynamics	7
1.3 Applications	12
1.4 Objective	20
1.5 Thesis outline	21
Chapter 2 Thermodynamic and entropy generation analysis of the coun	nter-flow dew-point
evaporative cooling	23
2.1 Introduction	23
2.2 Description of the DPEC system	23
2.3 Methodology	25
2.3.1 Mathematical model	25
2.3.2 Entropy generation model	28
2.3.3 performance evaluation	29

2.3.4 Numerical approach	30
2.3.5 Experimental validation	31
2.4 Results and discussion	36
2.4.1 Behavior of humidity and temperature	36
2.4.2 Response of the entropy generation	40
2.4.3 Parametric analysis	45
2.5 Conclusions	60
Chapter 3 Dew-point evaporative cooling of PV panels	62
3.1 Introduction	62
3.2 Description of system	63
3.3 Methodology	65
3.3.1 Mathematical model	65
3.3.2 Performance evaluation	70
3.3.3 Simulation scheme	71
3.3.4 Ambient condition	73
3.3.5 Model validation	75
3.4 Results and discussion	76
3.4.1 Comparison of evaporative cooling and air-cooling system	76
3.4.2 Temperature distribution along the air channels	80
3.4.3 Effect of cooling system parameters	82
3.5 Conclusions	86
Chapter 4 Combined Dew-point evaporative cooling system for winter heating	88
4.1 Introduction	88
4.2 Description of system	89

4.3 Methodology	90
4.3.1 Mathematical model	90
4.3.2 Simulation scheme	95
4.3.3 Model validation	97
4.4 Results and discussion	98
4.4.1 Comparison of evaporative cooling and air-cooling system	98
4.4.2 Temperature and humidity behavior of air during the adsorption/desorption/	orption process
	102
4.5 Conclusions	106
Chapter 5 Conclusions and future prospects	108
5.1 Conclusions	108
5.2 Future prospects	109
References	111

Abstract

The growing global demand for energy-efficient cooling and heating solutions, driven by climate change and increasing energy consumption, necessitates innovative technologies to reduce environmental impact. This work presents a comprehensive investigation into dew-point evaporative cooling (DPEC) systems and their integration with advanced energy solutions, focusing on thermodynamic performance, system optimization, and potential applications.

The study commences with an entropy generation analysis of a counter-flow DPEC system, employing a dynamic mathematical model to evaluate mass and heat transfer processes. Results reveal that inlet air conditions, geometric parameters, and operational settings significantly influence entropy generation and system efficiency. For instance, higher inlet air temperatures enhance heat transfer but increase entropy generation, while optimized channel dimensions, such as smaller heights, improve wet-bulb efficiency.

Further, the research develops and evaluates an enhanced DPEC system for photovoltaic (PV) panel cooling. Simulations demonstrate that the addition of a second wet channel improves cooling performance, stabilizes PV surface temperatures, and elevates solar cell efficiency by up to 16.7%. However, the system's water consumption and dependency on ambient humidity necessitate further optimization and potential integration with predehumidification systems.

Lastly, the study explores the hybridization of DPEC, PV, and desiccant units for winter heating applications. Results indicate the system's capability to provide air at 28°C and 45% relative humidity, aligning with thermal comfort standards. Dynamic modeling validates its efficiency in maintaining PV panel performance while delivering energy-efficient heating.

Overall, this research highlights the DPEC system's versatility, suggesting future efforts should emphasize experimental validation, economic feasibility studies, and innovative integrations to enhance its practical impact and align with sustainable development goals.

List of Figures

Fig. 1.1. Energy demand for cooling based on efficient cooling scenario and baseline
scenario [13].
Fig. 1.2. Schematic of indirect evaporative cooling: (a) traditional IEC; (b) novel DPEC
Fig. 2.1. Schematic diagram of the DPEC system with a single stage
Fig. 2.2. Schematic diagram of each control volumes: (a) wet channel, dry channel, (b) wate
film and channel plate
Fig. 2.3. Simulation flowchart.
Fig. 2.4. Test experimental setup for DPEC system: for: (a)vertical flow direction; (b
horizontal flow direction; (c) environmental chamber
Fig. 2.5. Model validation with experimental setup under different inlet condition: (a) Inle
air temperature by setup 1; (b) Inlet air RH by setup 1; (c) Multiple experiments under the
same inlet condition by setup 2; (d) Inlet air RH by setup 2
Fig. 2.6. Error between measured temperature and simulated temperature
Fig. 2.7. Model validation with temperature data presented by Lin et al. [92]. (a) case 1; (b
case 2
Fig. 2.8. Transient behavior of temperature and humidity: (a) Dry channel air; (b) We
channel; (c) Channel plate; (d) Water film; (e) Wet air humidity
Fig. 2.9. Steady-state values distribution within channel length: (a) Temperature; (b
Humidity ratio
Fig. 2.10. Heat transfer along each element: (a) Dry channel layer; (b) Wet channel layer; (c
Plate layer; (d) Water film layer40
Fig. 2.11. Transient response of entropy generation in different location of the channel: (a)
= 0; (b) $x = 0.2L$; (c) $x = 0.4L$; (d) $x = 0.6L$; (e) $x = 0.8L$; (f) $x = L$

Fig. 2.12. Transient response of entropy generation: (a) Entropy generation in each layer by
heat transfer; (b) Entropy generation of wet air and water film by mass transfer; (c) Total
generation of DPEC system
Fig. 2.13. Entropy generation in each element in steady-state: (a) total generation for 4
layers; (b) by mass transfer; (c) by heat transfer within dry channel; (d) by heat transfer
within wet channel; (e) by heat transfer in Plate; (f) by heat transfer in water film
Fig. 2.14. The effects of different inlet temperature on entropy generation: (a) Dry channel
air; (b) Channel plate; (c)Wet channel air; (d) Water film
Fig. 2.15. Entropy generation involved in each layer at different inlet air temperatures: (a)
Dry channel air; (b) Channel plate; (c) Wet channel air; (d) Water film
Fig. 2.16. The effects of different inlet humidity on entropy generation: (a) Dry channel air;
(b) Channel plate; (c) Wet channel air; (d) Water film
Fig. 2.17. Entropy generation involved in each layer at different inlet air humidity: (a) Dry
channel air; (b) Channel plate; (c) Wet channel air; (d) Water film
Fig. 2.18. The wet-bulb effectiveness and the specific entropy generation at: (a) different
inlet air temperature; (b) different inlet air humidity
Fig. 2.19. The effects of different working ratio on entropy generation: (a) Dry channel air;
(b) Channel plate; (c) Wet channel air; (d) Water film
Fig. 2.20. Entropy generation involved in each layer at different working ratio: (a) Dry
channel air; (b) Channel plate; (c) Wet channel air; (d) Water film
Fig. 2.21. The effects of different air velocity on entropy generation: (a) Dry channel air; (b)
Channel plate; (c) Wet channel air; (d) Water film. 54
Fig. 2.22. Entropy generation involved in each layer at different inlet air velocity: (a) Dry
channel air: (b) Channel plate: (c) Wet channel air: (d) Water film

Fig. 2.23. The wet-bulb effectiveness and the specific entropy generation at: (a) different
working ratio; (b) different inlet air velocity
Fig. 2.24. The effects of different channel height on entropy generation: (a) Dry channel air;
(b) Channel plate; (c) Wet channel air; (d) Water film
Fig. 2.25. Entropy generation involved in each layer at different channel height: (a) Dry
channel air; (b) Channel plate; (c) Wet channel air; (d) Water film
Fig. 2.26. The effects of different channel length on entropy generation: (a) Dry channel air;
(b) Channel plate; (c) Wet channel air; (d) Water film
Fig. 2.27. Entropy generation involved in each layer at different channel length: (a) Dry
channel air; (b) Channel plate; (c) Wet channel air; (d) Water film
Fig. 2.28. The wet-bulb effectiveness and the specific entropy generation at: (a) different
channel height; (b) different channel length
Fig. 3.1. Schematic diagram for solar PV cooling system: (a) enhanced DPEC using two wet
channels; (b) traditional DPEC-based air sensible cooling; (c) temperature and humidity
profiles for two systems on the psychrometric chart
Fig. 3.2. Schematic diagram for each layer of PV module
Fig. 3.3. Comparison of local weather data on the 1st June and 1st August with the fitted
equations: (a) solar irradiance, (b) ambient air temperature; (c) wind speed
Fig. 3.4. Model validation with local weather data from Mahmood et al. [113]: (a) July 2 nd ;
(b) July 3 rd
Fig. 3.5. Comparison of temperature and solar cell efficiency of PV based on hourly
irradiance data with evaporative cooling and air cooling: (a) 1st June; (b) 1st August 78
Fig. 3.6. Solar cell efficiency of two cooling configurations based on: (a) 1st June; (b) 1st
August. 78

Fig. 3.7. Thermal efficiency improvement based on the weather data of: (a) 1st June; (b) 1st
August79
Fig. 3.8. Comparison of the PV temperature with different cooling methods and the weather
data of: (a) July 2 nd ; (b) July 3 rd
Fig. 3.9. Temperature and humidity ratio distribution of systems based on the weather data
of 13:00, 1st June: (a) DPEC; (b) temperature of each layer of PV module; (c) humidity
distribution for DPEC dry channel and wet channel 1; (d) humidity distribution for wet
channel 2 in PV module
Fig. 3.10. The effects of different channel lengths on (a) The temperature distribution of the
PV panel; (b) The solar cell efficiency and the thermal efficiency improvement
Fig. 3.11. The effects of different channel heights on (a) The temperature distribution of the
PV panel; (b) The solar cell efficiency and the thermal efficiency improvement
Fig. 3.12. The effects of different inlet air velocities on (a) The temperature distribution of
the PV panel; (b) The solar cell efficiency and the thermal efficiency improvement 85
Fig. 3.13. The effects of different working air ratios on (a) The temperature distribution of
the PV panel; (b) The solar cell efficiency and the thermal efficiency improvement 86
Fig. 4.1. Schematic diagram for the hybrid system for winter heating: the DPEC with PV
panel and desiccant90
Fig. 4.2. Schematic diagram each control volume for air and desiccant
Fig. 4.3. Simulation flowchart
Fig. 4.4. Model validation with experimental data from Priyadarshi et al. [156]
Fig. 4.5. Air temperature and humidity distribution of each unit: (a) temperature of DPEC;
(b) humidity of DPEC; (c) temperature of PV panel; (d) humidity of PV panel; (e)
temperature of desiccant unit: (f) humidity of desiccant unit

Fig. 4.6. PV panel system with natural air cooling: (a) schematic of system; (b) temperature
distribution
Fig. 4.7. Comparison of the air temperature and humidity change with different system. 102
Fig. 4.8. Temperature and humidity behavior of air during the adsorption/desorption process
(a) adsorption mode temperature profile; (b) adsorption mode humidity profile; (c)
desorption mode temperature profile; (d) desorption mode humidity profile; (e) uptake of
the adsorbent. 105
Fig. 4.9. Temperature and humidity distribution of air channel outlet: (a) temperature; (b)
humidity

List of Tables

Table 1.1 Recent study of dew-point evaporative cooling	9
Table 1.2 Application of dew-point evaporative cooling technologies	16
Table 2.1 Parameters of DPEC system.	31
Table 2.2 Specification of measuring devices.	34
Table 3.1 Geometrical parameters of PV module.	72
Table 3.2 Optical and thermal properties of layers.	72
Table 3.3 Nominal parameters of the reference system.	82
Table 4.1 Input parameters of desiccant module	96
Table 4.2 Input winter weather parameters used in simulation	96

Nomenclature

Abbreviations DPEC dew-point evaporative cooling PV photovoltaic **IEC** Indirect evaporative cooling RH relative humidity ratio Symbol A area (m²) specific heat capacity of the glass (J/kg K) cspecific heat capacity (J/kg K) c_p channel height (m) d half of air channel height (m) d_a half of desiccant layer thickness (m) d_b d_e effective thickness of channel plate and water film (m) D_{ab} mass diffusivity (m²/s) D_{w} mass diffusivity of water vapor in air (m²/s) D_b diffusion coefficient of water vapor in desiccant layer (m^2/s) gravitational acceleration (m/s²) g Gsolar irradiance (W/m²) h specific enthalpy (J/kg) (Chapter 2) h convective heat transfer coefficient (W/m²K) (Chapter 3, 4) h_m convective mass transfer coefficient (m/s) latent heat (kJ/kg) h_{fg} Jdiffusive flux (kg/m²s) thermal conductivity (W/m K) k permeability (m²) (Chapter 4) k convective mass transfer coefficient (m/s) k_m mass transfer coefficient of adsorption (1/s) k_m Llength (m)

Lewis number

Lw

mass flow rate (kg/s) ṁ

mass flow rate of water vapor (kg/s) m_w

Nu Nusselt number P pressure (Pa)

heat transfer rate (W) qQcooling capacity (W)

R gas constant of water vapor

Ra Rayleigh number

entropy generation (W/m³K) S_g

t time (s)

Ttemperature (K)

 T_a air temperature inside air channel (K)

 T_r reduced temperature (K m²/W)

velocity (m/s) и

velocity of air (m/s) u_a

adsorption uptake (kg/kg) W_b \overline{W}

equilibrium adsorption (kg/kg)

humidity ratio (kg/kgDA) x

Greek symbols

convective heat transfer coefficient (W/m²K) (Chapter 2) α

absorption coefficient (Chapter 3) α

convective mass transfer coefficient (m/s) α_m

thermal diffusivity of desiccant layer (m²/s) α_b

δ thickness (m)

temperature coefficient (1/K) В

emissivity ε

porosity (-) (Chapter 4) ε

transmittance τ density (kg/m³) ρ

Density of air (kg/m³) ρ_a

Density of desiccant layer (kg/m³) ρ_{s}

Density of water vapor inside desiccant layer (kg/m³) ρ_w

solar cell efficiency η_T thermal efficiency η_{th}

ν viscosity (Pa s)

γ angle of the PV panel to the horizontal (rad)

Subscripts

a ambient

ad total of the adhesivead adsorption (Chapter 4)

air air

air_ec air from evaporative cooling

air_acair from air-coolingbdesiccant layer

cooling cooling

cv control volume

dadry aireeffectivegglass

h heat transferi interfacial value

m mass transfer

sky sky

PV photovoltaic gap air gap

top side of glass

w force convection wind

free free convection EVA encapsulant

TEDtedlargladhesiverefreferenceplchannel platesupplysupply airwawet airwfwater film

e sum of water film and channel plate (Chapter 3)

sat saturation

specspecific entropy generationyy-directionzz-direction

Chapter 1 Introduction

1.1 Background

Thermal comfort refers to a state in which individuals feel comfortable without experiencing noticeable sensations of being too hot or too cold, as influenced by factors such as ambient temperature, humidity, and airflow [1]. In a workplace environment, the suitability of temperature and humidity directly impacts employees' concentration, mood, and physical comfort. Experimental findings by Geng et al. [2] indicate that most occupants find a thermal environment of 24°C satisfactory. Optimal productivity is achieved when individuals perceive the environment as neutral or slightly cool. Enhanced thermal satisfaction positively influences productivity. Other studies [3–6] have also demonstrated that excessively low or high temperatures can lead to physical discomfort among employees, diverting their attention and subsequently reducing work efficiency. An essential aspect of maintaining indoor thermal comfort is space cooling. Studies [7–10] have demonstrated that reducing indoor temperatures significantly enhances the comfort and health of occupants. Air conditioning, plays an increasingly important role in maintaining indoor comfort across various buildings. Its significance is particularly evident in hot and arid regions, where it has become an indispensable aspect of daily life to address the growing demand for thermal comfort and efficient temperature regulation [11,12].

However, with the intensification of global warming, summer temperatures continue to rise yearly, leading to a significant increase in indoor cooling demand. According to a report [13] by the International Energy Agency (IEA), the global stock of air conditioning units reached 2 billion in 2018 and is projected to double by 2050. For developing countries and emerging

economies, the accelerating pace of urbanization has resulted in an increasing reliance on cooling systems in residential and office spaces. This trend poses two substantial societal challenges: heightened energy consumption and increased carbon dioxide emissions. According to the IEA report [14], energy consumption and carbon emissions associated with space cooling have approximately tripled compared to 1990 levels. In 2022, global energy consumption for cooling reached 7.6 EJ, while CO2 emissions totaled 1.02 Gt. Furthermore, energy consumption for space cooling continues to grow at an annual rate of around 4%.

Given the current energy scenario, the development of more efficient air conditioning systems demonstrates significant potential in reducing energy consumption and carbon emissions associated with space cooling [15–21]. As shown in Fig. 1.1 [13], (a) indicates that under the efficient cooling scenario, energy demand for cooling could be reduced by approximately 45%. (b) further highlights that, based on the efficient cooling scenario, peak electricity demand by 2050 can be significantly lower than the baseline projections for regions such as the United States, China, South Korea, and the Middle East, with levels even falling below those recorded in 2016. Conversely, for countries like Indonesia, India, Mexico, Brazil, and South Africa, while the 2050 demand is projected to exceed 2016 levels, it is still markedly reduced compared to the baseline scenario.

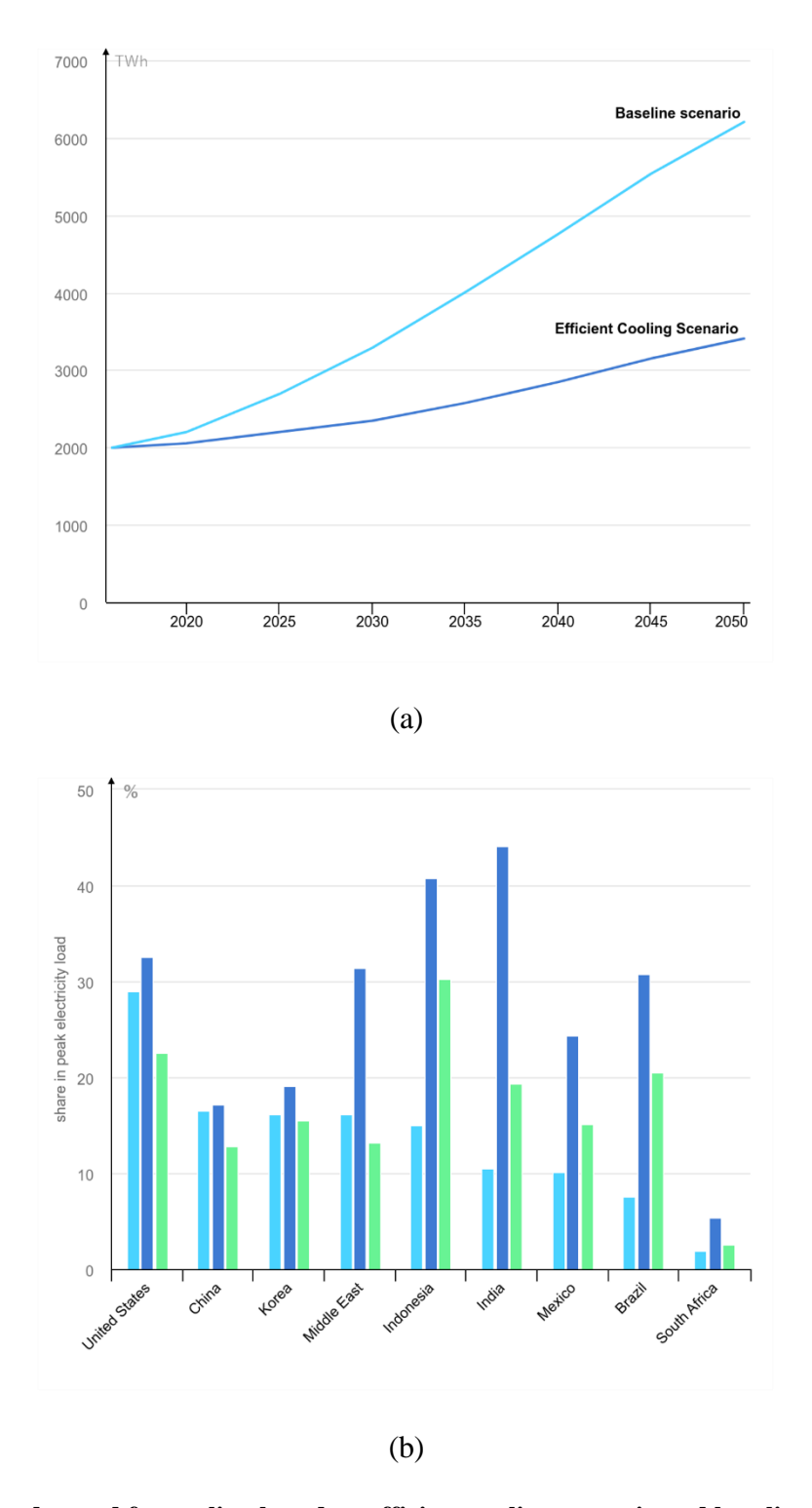


Fig. 1.1. Energy demand for cooling based on efficient cooling scenario and baseline scenario [13].

On one hand, efforts have been focused on improving traditional air conditioning systems.

Zhang et al. [22] integrated a phase change material (PCM) to air heat exchanger into the system,

achieving energy savings of at least 16%, with a maximum reduction of 44.7%. Sandong Omgba et al. [23] proposed a novel solar-assisted air conditioning system, introducing a parabolic trough concentrator sub-cycle integrated with a traditional vapor compression cycle, which resulted in a 25.3% energy savings. Elhelw et al. [24] incorporated evacuated tubes into a conventional cooling system, and experimental results showed a 20.3% increase in COP and an 8.22% reduction in compressor energy consumption. Martínez et al. [25] added evaporative pre-cooling before the condenser, demonstrating through experiments that the system achieved a 43% reduction in energy consumption. On the other hand, a low-energy, refrigerant-free, and simple cooling technology that utilize both sensible and latent heat [26,27], namely, evaporative cooling, capitalizing on the water evaporation as a heat-absorption mechanism, has been researched for several decades [28–31]. In response to the growing trends of energy conservation and emission reduction, researchers have increasingly focused on optimizing traditional direct and indirect cooling systems: Mao et al. [32] proposed the use of cold-mist direct evaporative cooling to maintain an optimal working environment in data centers. This solution successfully kept the data center temperature within 23.57-25.58°C while reducing the cooling energy consumption by 14-41%. Khan et al. [33] introduced a hybrid system combining direct and indirect evaporative cooling, achieving a system performance with a COP of 35.2, a cooling capacity of 16.8 kW, and a wet-bulb efficiency of 85%, as determined through realtime testing under operational conditions. Gao et al. [34] utilized low-temperature exhaust air from indoor air-conditioned spaces as the working air for an indirect evaporative cooler, enhancing the cooling effect of the IEC on primary air by 23.7%.

1.2 Dew-point evaporative cooling

1.2.1 Analysis based on the first law of thermodynamics

Although advancements have been made in improving the efficiency and reducing the energy consumption of traditional evaporative cooling systems, their performance is often limited by the wet-bulb efficiency. As a result, significant breakthroughs in efficiency remain challenging to achieve within the constraints of these systems. To address the limitations of traditional evaporative cooling systems, an innovative technology known as Dew-Point Evaporative Cooling (DPEC) has been introduced [35–38]. Grounded in the principles of indirect evaporative cooling, DPEC has shown superior efficiency when compared to conventional systems of a similar nature. As depicted in Fig. 1.2, the DPEC system utilizes a segment of the supply air within the dry channel as the working air. The greater temperature difference between the working air and the wet channel enhances the mass and heat transfer processes in the adjacent wet channel. In theory, the exhaust air at the outlet of the wet channel reaches saturation, as the supply air is able to achieve its dew-point temperature at the exit of the dry channel.

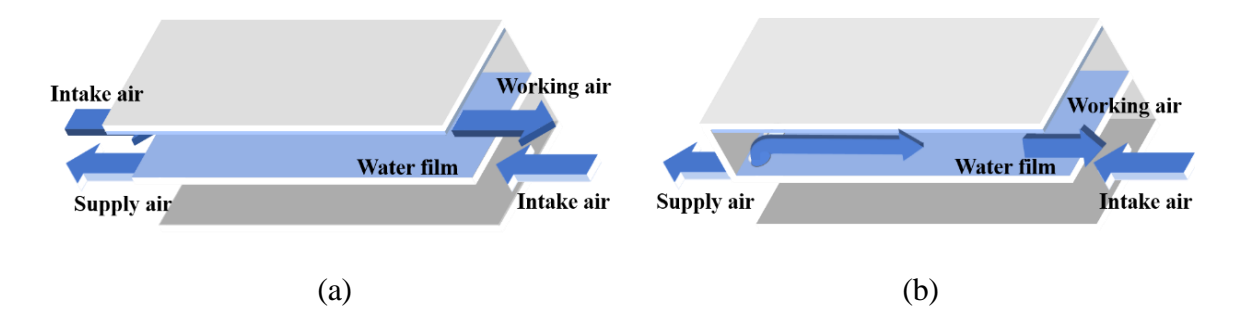


Fig. 1.2. Schematic of indirect evaporative cooling: (a) traditional IEC; (b) novel DPEC.

Many researchers have conducted comprehensive analyses of this novel technology, utilizing both experimental and simulation-based approaches from various perspectives. These studies have focused on optimizing the DPEC system's performance, examining factors such as heat and mass transfer efficiency, and exploring its potential applications in different

environments and operational conditions. From the inlet air properties point of view, Anisimov et al. [39–41] demonstrated that DPEC systems achieve particularly high efficiency in hot and arid climates. The system's thermodynamic performance is significantly influenced by the temperature and humidity of the incoming air. Regarding operational conditions, Pandelidis et al. [42] emphasized the importance of the working ratio on system efficiency, recommending a triangular configuration for optimal regenerative exchangers. In terms of channel geometry, Hasan [43,44] explored four DPEC configurations, concluding that the combined parallelregenerative cooler exhibited the highest wet-bulb efficiency. Lee et al. [45] further improved cooling performance by incorporating fins in the wet air channel, achieving temperatures below the wet-bulb temperature, with optimal performance at a working ratio of 0.3. Other studies have expanded understanding of DPEC systems from various angles. Lin et al. [46] conducted a parametric study, revealing a wet-bulb efficiency range of 0.42 to 1.46 and offering insights into heat transfer and evaporation intensity. Gupta et al. [47] analyzed DPEC performance under New Delhi's climate conditions and provided an economic cost analysis. Experimental work by Riangvilaikul and S. Kumar [48,49] achieved a dew-point efficiency of 0.92 and a wet-bulb efficiency of 1.14. Pakari et al. [50] developed and experimentally validated one-dimensional and three-dimensional models within a counter-flow structure, achieving a wet-bulb efficiency of 1.25.

Although DPEC technology has been studied for decades, yielding numerous remarkable results, the growing demand for energy and the increasing need for efficient technologies mean that dew-point evaporative cooling continues to attract the attention of researchers. This ongoing interest suggests that the technology still holds significant untapped potential. Table 1.1 summarizes the recent efforts by researchers in the development of DPEC systems over the past two years. Most studies focus on optimizing the geometric configuration to achieve higher

cooling efficiency, or on developing models with greater accuracy that enable simulation results to more closely align with real-world engineering applications and product optimization.

1.2.2 Analysis based on the second law of thermodynamics

Thermodynamic analyses of the DPEC system have been conducted using experimental and simulation data within the framework of the first law of thermodynamics. In contrast, entropy generation analysis provides an effective approach to achieving a more comprehensive evaluation of the system's thermodynamic performance. A few studies have begun applying second-law thermodynamic principles to provide deeper insights into various thermodynamic systems. Thu et al. [51] applied transient entropy generation analysis to evaluate heat exchange in adsorption-desorption processes, highlighting inefficiencies in mass and heat transfer. Mahdi et al. [52] used an entropy generation model to optimize conditions for a heated horizontal cylinder. Sachdeva et al. [53] investigated the ejector refrigeration cycle via exergy analysis and conducted a parametric study. Kumar et al. [54] employed an entropy generation model to enhance insights into absorber surfaces. For the DPEC system, entropy generation analysis is crucial for both gaining a deeper understanding of the thermodynamic performance, as well as for their practical engineering applications. In the context of evaporative cooling, it helps identify inefficiencies such as heat transfer losses and non-ideal mass transfer between air and water. By quantifying the irreversibility of the process, entropy generation highlights areas where energy dissipation occurs as heat, ultimately impacting the system's overall efficiency. Minimizing entropy generation allows the system to operate closer to its theoretical maximum efficiency, leading to more effective cooling with reduced energy input. Studies applying second-law thermodynamic analysis to the DPEC system have begun to emerge: Wang et al. [55] developed an entropy analysis model to optimize the DPEC system structure by adjusting parameters through system-wide entropy generation analysis. Aziz et al. [56], designed a DPEC system for seawater desalination, analyzing entropy generation within each system channel. Some other studies [57–60] focus on exergy analysis, employing numerical analyses of exergy flow and efficiency to investigate the application of dew point evaporative cooling technology.

Table 1.1 Recent study of dew-point evaporative cooling

Year	Authors	Method	Inlet parameters	Validation		Features
			T:30-40°C		1.	The indirect evaporative cooling was combined with the air-cooled
2024	Duan et al. [61]	Evn/Sim	x:30-80%RH	Experimental data		thermoelectric cooling technology.
2024		Exp/Sim	r:0.2-0.8		2.	The system performance was carried experimentally, and the
			v:76.8-144g/s			optimization was conducted by numerical model.
			T:30-40°C		1.	A compact mixed-flow DIEC system was proposed.
2024	Lings at al. [62]	Eve	x:17-50%RH		2.	3 different water distribution system was discussed, and wick
2024	Urso et al. [62]	Exp	r:0.4-0.8	-		materials were tested directly in the prototype experimental setup.
			v:389kg/h			
2024	Pandelidis et al.	Eve /Sim		Evenorimental data	1.	The performance of the Dew-Point Cooling Tower was investigated.
2024	[63]	Exp/Sim	-	Experimental data	2.	The application potential of DPCT in different climatic was discussed.
					1.	Configuration that eliminates the U-turn of the working air was
			T:33°C			proposed.
2024	Wang et al.	Evn/Sim	x:56.14%RH	Experimental data	2.	Working ratios of 0.5-0.6 shows the optimal cooling coefficients of
2024	[64,65]	Exp/Sim	r:0.5			performance.
			$v:556 \text{ m}^3/\text{h}$		3.	Metallic material channel prefers higher flow rates, while plastic
						prefers lower flow rates.
2024	Güzelel et al.	Sim	T:25-45°C	Published data	1.	4 novel flow configurations have been compared with the traditional
2024	[66]	SIIII	x:6-26g/kg [DA]			counter-flow indirect evaporative cooler.

			r:0.2-0.8 v:1-5m/s		2.	Multiple aperture air passages have the lower water consumption per cooling capacity and COP.
2024	Wu et al. [67]	Exp/Sim	T:30-38°C x:12-24g/kg [DA] r:0.2-0.8 v:2-4m/s	Experimental data	1. 2. 3.	The enhanced DPEC with rib-roughened dry channels was investigated. A novel low-Reynolds number CFD model was developed. Convective heat transfer can be enhanced by the vortices near the ribs.
2024	Xu et al. [68]	Exp/Sim	v:340-2380m ³ /h	Experimental data	 2. 	The effect of internal heat and humidity change of channel was considered. Actual experimental data was introduced to improve the accuracy of the numerical model.
2023	Chakraborty et al. [69]	Exp/Sim	T:26-40°C x:50%RH	Experimental data	 2. 	Study for building installation ready full-size equipment was discussed. Study on the impact of primary air condensation on the performance of an M-cycle IEC was proposed.
2023	Wang et al. [70]	Exp	T:32-33°C r:0.49 v:175-400m ³ /h	-	 2. 	A new configuration which aims to solve the uneven working air and high-pressure drop was proposed. The pressure drop can be reduced 3 times compare to the traditional counter-flow configuration.
2023	Pacak et al. [71]	Sim	-	Published data	 1. 2. 	A novel heat exchanger geometry (with a shape optimized) was proposed. A CFD model focus on the calculation of air distribution and pressure

						drop was developed.
					3.	The influence of air distribution on the cooling capacity of the system was analyzed.
2023	Zhu et al. [72]	Sim	T:25-45°C x:6.9-26.4g/kg [DA] r:0.33 v:2.4m/s	Published data	1.	A three-dimensional CFD model of regenerative dew-point evaporative cooling was developed. The water distribution effects on dew- point evaporative cooling was discussed.
2023	Gao et al. [73]	Sim	T:30-38°C x:12-20g/kg [DA] r:0.33 v:2m/s	Validated by a plate-type cooler data	 2. 3. 	A novel counter-flow tubular architecture was proposed. A rotating axisymmetric mathematical model based on continuity, momentum and energy equations was established. The product air temperature from tubular system can be 1.6-3.0°C lower than the traditional plate type under tested condition.
2022	Comino et al. [74]	Exp/Sim	T:32-43°C x:6-13g/kg [DA] r:0.2-0.8 v:3000-5000m ³ /h	Experimental data	 2. 3. 4. 	Discusses the potential for cooling and ventilation of different type of building in European. Experimental study was carried under different inlet air conditions. Simulation model was developed based on ε -NTU method. Different working ratios have been proposed for office, restaurant and auditorium application.

1.3 Applications

While some researchers remain focused on improving the performance of DPEC systems, others have begun exploring their applications and investigating the potential for commercialization. As illustrated in Table 1.2, some studies target small-scale devices, such as cooling vests for workers, thermal management modules for electronic CPUs, and battery cooling systems. Meanwhile, others have concentrated on large-scale applications, such as cooling systems for data centers to ensure operational safety. Puglia et al. [75] examined the water consumption issue in DPEC systems and explored using water generated by fuel cell chemical reactions to replenish the wet channels. To address the efficiency limitations of DPEC systems under high-humidity conditions, significant efforts have been directed toward hybrid systems that integrate desiccants with DPEC technology. These approaches include pre-cooling the inlet air, optimizing geometric configurations, or introducing additional components to enhance system performance. Among these applications, there are two specific directions that have shown promising feasibility for practical implementation. However, these directions remain relatively unexplored and warrant further investigation to fully understand their potential and optimize their performance.

(1) PV cooling

Evaporative cooling, as an efficient and low-energy-consumption technology, holds great potential for meeting the cooling demands of solar panels [76–78]. Several studies have demonstrated its benefits. Lucas et al. [79] a used an evaporative solar chimney on the rear of PV panels, achieving a solar cell efficiency increase from 4.9% to 7.6% on a typical summer day in the Mediterranean. Haidar et al. [80,81] implemented an experimental setup with wetted materials on the backside of PV panels, reducing surface temperature by up to 20 °C and

improving efficiency by approximately 14%. Mahmood et al. [82] designed an evaporative cooling system beneath the PV panels with cellulose cooling pads of various thicknesses and water flow rates, achieving efficiency gains of 7.4%, 10.5%, and 11.2% with increasing pad thickness. Žižak et al. [83] reported over 20 °C temperature reduction and a 9.6% power output increase by supplying water to the panel's backside. Alktranee et al. [84] compared evaporative cooling to aluminum fins, finding a 22.3% temperature reduction with evaporative cooling versus only 6.7% with aluminum fins. Dew-point evaporative cooling, as an advanced version of traditional evaporative cooling, offers potential advantages for solar panel cooling. However, its performance in this specific application remains largely unknown. Consequently, exploring and evaluating the feasibility and effectiveness of DPEC as a cooling solution for solar panels has become one of the primary research directions and objectives of this study.

(2) Winter heating

On the other hand, most of the applications mentioned in the literature review focus on the cooling capabilities of DPEC. A key area of interest and research in this study is how to extend the application of this efficient technology to winter conditions. Specifically, the objective is to explore ways to utilize the DPEC system not only for cooling purposes, such as summer air conditioning and electronic component cooling, but also to adapt it for effective operation in winter. This would enable the development of a versatile, year-round operational system. For winter heating, there are some heating systems that utilize waste heat recovery, incorporate phase-change materials, or adopt hybrid designs with renewable sources, like solar-assisted heating, are increasingly explored as sustainable alternatives. Kumar Sharma et al. [85] investigated the winter performance of a transcritical CO₂-based air-conditioning system, highlighting that while the system's COP surpasses summer performance, frosting issues arise due to reduced evaporator temperatures. Qu et al. [86,87] implemented four different

intermittent heating modes in a radiant air-conditioning system, demonstrating energy savings of 22%-48% compared to continuous heating modes. Dong et al. [88] proposed an innovative hybrid radiant-convection heating system, which combines the advantages of both radiant and convective heating, enhancing heating capacity by 28.5%-58.9%. Yang et al. [89] developed a hybrid air-conditioning system featuring two-stage energy recovery and conducted a theoretical analysis of its winter performance, revealing energy savings of 44%. Li et al. [90] presented experimental results for a solar PV air-conditioning system, indicating that its winter heating performance in Shanghai's climate is inferior to conventional solar thermal collectors. Said et al. [91] explored the coupling of phase-change materials (PCM) with air-conditioning systems, showing a 22% increase in winter COP and a 2.8% improvement in energy savings for winter heating.

Besides, many researchers have focused on integrating air-conditioning systems with desiccant technologies to improve performance. Zhang et al. [92] proposed a novel system combining two dehumidification wheels and a heat pump, designed to humidify supply air during winter and meet year-round humidity requirements for residential applications. Results indicated that the system performs well across various climate conditions. Ge et al. [93] studied the winter performance of an air-conditioning system incorporating a desiccant-coated heat exchanger, aiming to address limitations of conventional desiccant wheel systems. This research examined the feasibility of the system under different climatic scenarios. Building upon this, Zhang et al. [94] integrated solar energy with the system and analyzed the effects of various environmental parameters on its performance. Additionally, Nain et al. [95] combined solar energy with a desiccant-coated concentric tube heat exchanger to enable continuous humidification of dry air. Performance results demonstrated that the proposed system provides consistent heating and humidification in the dry, cold regions of northern India. The DPEC

system combined with desiccants has demonstrated its effectiveness in enhancing cooling performance. If such a high-efficiency system could be adapted for winter heating, it would be intriguing to investigate whether its heating performance surpasses that of the conventional heating systems mentioned earlier. This prospect holds significant potential and is worthy of further exploration.

Table 1.2 Application of dew-point evaporative cooling technologies

Year	Authors	Method	Inlet parameters	Validation		Features
2019	Raad et al. [96]	Exp/Sim	T:36°C x:42%RH v:0.8, 1.4, 2.3 m/s	Experimental data	 2. 3. 	A dew point evaporative cooling (DPEC) technique was applied to design a cooling vest aimed at the worker's back. The system's impact on human thermal comfort was analyzed using a cooling model coupled with a bio-thermal model. Results demonstrated that the M-cycle cooling vest reduced the back temperature by 1.27°C and enhanced thermal comfort for 38% of the
2023	Lin et al. [97]	Exp/Sim	T:30-4°C0 x:10-19g/kg [DA] r:0.33-0.79 v:2.0-4.5m/s	Experimental data	 2. 	wearers. A novel pseudo-4D battery model was developed to investigate the thermal behavior of batteries, integrating dew point evaporative cooling (DPEC) into the battery thermal management system. Utilizing the DPEC method effectively reduced battery temperatures by 3–13.6°C with the 8.9-28.9COP.
2021	Dizaji et al. [98]	Exp	T:40°C x:19g/kg[DA] r:0.5 v:0.001-0.08kg/s	-	 2. 	A micro-scale dew point evaporative cooler with a heat transfer area of 64 cm ² was proposed for CPU thermal management applications. Under optimal operational and design conditions, this micro cooler effectively lowers CPU temperatures and enhances cooling efficiency.
2024	Puglia et al. [75]	Exp	-	-	1.	The feasibility of utilizing recovered water from hydrogen PEM fuel cell exhaust to replenish the moisture in the wet channels of a DPEC system was investigated, and the cooling capacity of the system was evaluated.

					2.	Results indicated that 10% of the water required for the evaporative cooling system could be supplied by the water produced through the hydrogen reaction.
2023	Ma et al. [99]	Exp	-	-	1.	An innovative DPEC system was designed, constructed, and installed, incorporating features such as high-absorbency and diffusion-capable wick materials, an intermittent water supply, a flow-adjustable water pump, and an optimized fan configuration. The system was tested in a real-time data center environment. The system demonstrated an average COP of 29.7, achieving a 90% energy savings for the data center.
2024	Yan et al. [100]	Sim	T:36°C x:40%RH r: 0.8 v:1.5m/s	Published data	 1. 2. 3. 	A DPEC system was proposed for data center cooling applications. The system employed Response Surface Methodology (RSM) to correlate eight design parameters with three evaluation metrics. Multi-objective optimization was conducted using a Genetic Algorithm (GA) to achieve superior cooling performance and efficiency, with results indicating a COP exceeding 61.3.
2022	Güzelel et al. [101]	Sim	T:20-40°C x:8-15g/kg[DA]	Published data	 2. 	A mathematical framework was derived to simulate the performance of a desiccant-wheel-based air conditioning system incorporating two heat recovery devices: DPEC and a direct evaporative cooler. The influence of indoor air and exhaust air mixing ratios on system performance was evaluated, revealing that the maximum COP of 0.78

						occurred in October.
	Pacak et al. [102]	Exp			1.	Pre-cooling the air entering the desiccant wheel using DPEC was proposed
						to enhance the efficiency of the adsorption system.
2023				_	2.	Results indicated that pre-cooled air improved the dehumidification rate of
2023						the desiccant wheel from 1.4 to 1.9. Additionally, achieving the same
						dehumidification rate allowed for a 15°C reduction in regeneration temperature.
					1.	An experimental evaluation of the combined DPEC and desiccant wheel
	Romero- Lara et al. [103]	Exp	T:24-40°C x:8-14g/kg[DA] r:0.3-0.7 v:1000-2000m ³ /h			system was conducted, involving 64 tests to validate the system's
						performance, resulting in the development of several comprehensive
2024				-		empirical models.
					2.	Four performance indicators were established: (1) dehumidification
						capacity, (2) dehumidification capacity per unit power, (3) dew point
						efficiency, and (4) cooling capacity per unit power.
					1.	The cooling capacity and water utilization efficiency of the desiccant wheel
	Lai et al. [104]	Sim	T:30-45°C x:50-80%RH r:0.1-0.6			and DPEC system were optimized using the Response Surface
				Published data		Methodology (RSM). The optimization targeted four critical parameters:
2024						temperature, humidity, water consumption rate, and the coefficient of
						performance (COP).
					2.	Under Australian climatic conditions, the optimized system was capable of
						supplying air with a temperature below 19°C and humidity below 11.51

						g/kg dry air.
2024	Chun et al. [105]	Sim	T:31.5°C x:80%RH v: 300m ³ /h	Published data	1.	A novel dual-return-air desiccant-based DPEC system was proposed, and a corresponding mathematical model was developed.
2024	Chen et al. [106]	Exp/Sim	T:27-35°C x:16-21g/kg [DA] v:0.5-5.5m/s	Experimental data	 2. 	An integrated dehumidification and dew point evaporative cooler system was developed, and the transient and steady-state behaviors of the integrated system were analyzed. The results indicate that the system achieved a dew point efficiency of 0.9, a COP of 15.9 for the DPEC, and an electrical COP of 6.43 for the integrated system.

1.4 Objective

The primary objective of this doctoral research is to address the research gaps in the field of dew-point evaporative cooling (DPEC) systems. It aims to enrich performance studies on DPEC from various perspectives, provide insights and strategies for system optimization, and explore the potential applications of DPEC systems across different fields. Grounded in the laws of thermodynamics, this study analyzes and characterizes the heat and mass transfer behaviors within the system.

The entropy generation model of the DPEC system is investigated through simulations, aiming to achieve the following specific objectives: (1) understanding the fundamental principles of the DPEC system, including the heat and mass transfer processes within its channels, from the perspective of the second law of thermodynamics, while exploring the system's transient responses; (2) analyzing the impact of heat flows in different system layers on entropy generation; (3) conducting a parametric study to evaluate the influence of various input parameters on system entropy generation. This model facilitates a comprehensive analysis of how different factors influence the thermodynamic performance, enabling the identification of optimal operating conditions for enhanced efficiency under the second law framework.

The detailed objectives of PV panel cooling are: (1) to understand the mechanisms of the heat and mass transfer process in the PV panel with the enhanced cooling system and explore their dynamic behaviors in different climate conditions; (2) to explore the feasibility of DPEC system for cooling PV panels and to predict the system performance under different design and operating conditions; (3) to analyze the impact of input parameters on system performance.

The performance of a hybrid DPEC system integrated with photovoltaic (PV) panels and a desiccant unit for winter heating is analyzed through simulations, with the following specific

objectives: (1) to investigate the thermal performance of the hybrid system in winter conditions, focusing on the synergy between the DPEC-PV and desiccant units in providing effective space heating; (2) to understand the heat transfer and energy conversion processes within the system, emphasizing the interaction between the PV panels, DPEC unit, and desiccant unit under varying environmental conditions; (3) to provide design recommendations to optimize the hybrid system for specific winter heating scenarios, ensuring practical feasibility and sustainable operation; (4) to assess the hybrid system's overall energy efficiency and identify optimal operating parameters that enhance heating performance.

1.5 Thesis outline

This thesis is structured into five chapters, systematically addressing key aspects of the research on dew-point evaporative cooling (DPEC) systems. Each chapter is designed to progressively build an understanding of the system's performance, its integration with other technologies, and its potential applications. The organization is as follows:

Chapter 1 Introduction

Provides an overview of the current energy landscape for space cooling, emphasizing the growing challenges of energy consumption and carbon emissions. It includes a detailed review of literature covering advancements in traditional air conditioning systems, improvements in direct and indirect evaporative cooling technologies, and the concept, developments, and applications of DPEC systems.

Chapter 2 Thermodynamic and entropy generation analysis of the counterflow dew-point evaporative cooling This chapter delves into the second-law thermodynamic analysis of the DPEC system, focusing on entropy generation and the heat and mass transfer mechanisms within the system. The transient and steady-state responses of the system under varying conditions are explored.

Chapter 3 Dew-point evaporative cooling of PV panels

Explores the integration of DPEC technology into solar panel cooling systems. This chapter investigates the thermal management benefits for photovoltaic (PV) systems, quantifies energy savings, and assesses water consumption and operational feasibility under varying environmental conditions.

Chapter 4 Combined Dew-point evaporative cooling system for winter heating

Focuses on modeling and analyzing a hybrid system incorporating DPEC, photovoltaic, and desiccant units. This chapter describes the temperature and humidity distribution within the system, offering insights into its thermal performance under winter heating conditions.

Chapter 5 Conclusions and future prospects

Summarizes the key findings, highlights the contributions of this work to the field of energyefficient cooling and heating systems, and provides recommendations for future research directions.

This structured approach ensures a comprehensive investigation of the DPEC system and its hybrid configurations, addressing both theoretical and practical aspects to contribute to sustainable energy solutions.

2.1 Introduction

As mentioned in the literature review in Chapter 1, although some second-law analyses of DPEC systems have been conducted, most emphasize system-environment interactions, with limited focus on internal entropy generation, and research on transient entropy generation in DPEC systems, in particular, remains scarce. Therefore, in this chapter, a transient entropy generation model was developed in this chapter aiming to enhance the theoretical understanding of the second law of thermodynamics in the context of DPEC systems and provide a clearer insight into their thermodynamic performance. This model, based on the second law of thermodynamics, captures the transient response of both external and internal irreversibility. It computes the total entropy generation of the system and quantifies the contributions from irreversible heat flows and mass transfer within each layer.

2.2 Description of the DPEC system

Fig. 2.1 illustrates a counter-flow configuration for a single-stage DPEC system, consisting of two sets of channels: a wet air channel and a dry air channel. The system accommodates three distinct airstreams: (1) intake air, (2) supply air, and (3) working air. Intake air, characterized by low humidity and high temperature, is drawn from the ambient environment

Thermodynamic and entropy generation analysis of the counter-flow dew-point evaporative cooling and directed into the dry air channel. Convective heat transfer between the channel plate and the dry air reduces the intake air temperature. At the end of the dry air channel, part of the cooled air is diverted as supply air to the workspace, while the remaining air continues into the wet channel as working air. In the wet channel, evaporation occurs due to the moisture content difference between the saturated water vapor near the water film and the working air. The heat required for this evaporation is supplied by the adjacent dry channel. As a result, the supply air exiting the dry channel is effectively cooled, approaching the dew-point temperature. From the psychrometric chart, it is evident that when higher temperature intake air enters the DPEC system, the heat transfer process leads to a reduction in air temperature in the dry channel, while humidity remains constant, resulting in a horizontal curve. As the air moves into the wet channel and becomes working air, the combined mass and heat transfer processes cause both air temperature and humidity to rise, quickly reaching a saturated state. The working air then continuously absorbs heat from the dry channel, leading to an increase in temperature along the line corresponding to 100% relative humidity.

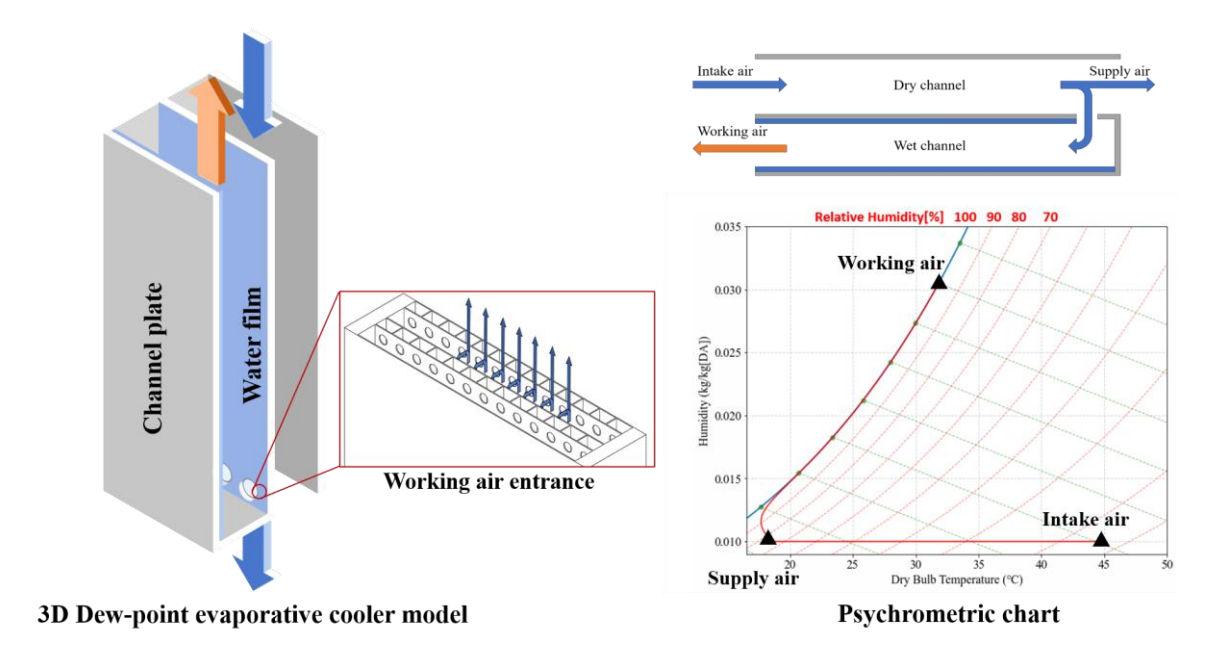


Fig. 2.1. Schematic diagram of the DPEC system with a single stage.

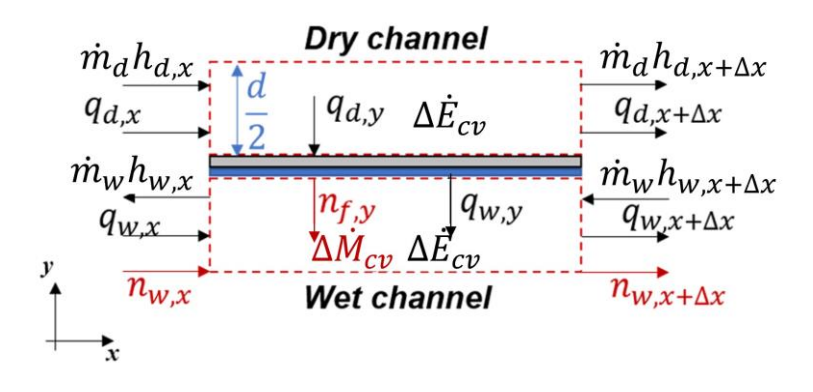
2.3 Methodology

2.3.1 Mathematical model

The DPEC system consists of multiple layers, further divided into numerous identical elements using a grid meshing technique. Each element includes a dry channel layer, a water film layer, a wet channel layer, and a channel plate layer, as shown in Fig. 2.2. To gain insight into the thermodynamic behavior of the DPEC system, a transient model has been developed, based on the following assumptions:

- (1) Adiabatic circumstances between the channel unit and its environment.
- (2) The water film within the wet channel is stagnant and saturated.
- (3) The air density remains constant inside the dry channel.
- (4) The characteristics remain consistent throughout the control volume.

The unsteady state mathematical model was formulated and modified based on the model presented by Miyazaki et al. [107], and Lin et al. [46,108]. Below are the specifics of the governing equations:



(a)

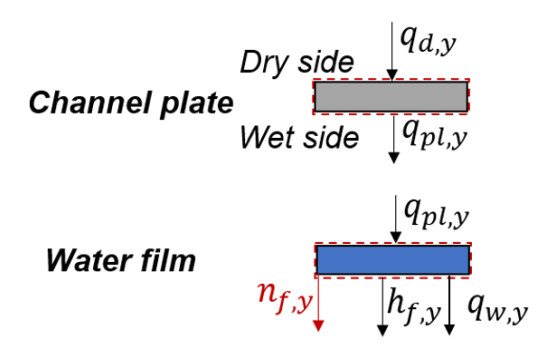


Fig. 2.2. Schematic diagram of each control volumes: (a) wet channel, dry channel, (b) water film and channel plate.

(b)

(1) Dry channel

In the dry channel, the equation describing the energy balance for a layer element is as follows:

$$\rho_{da}c_{p,da}\frac{dT_{da}}{dt} = k_{da}\frac{d^{2}T_{da}}{dx^{2}} - \rho_{da}c_{p,da}u_{da}\frac{dT_{da}}{dx} - \frac{2\alpha_{da}}{d}\left(T_{da} - T_{pl}\right) \tag{1}$$

The right-hand side expressions of Eq. (1) are the air heat conduction of the longitudinal direction, which is resulting from the temperature differential of the input and output air of the control volume. The second term is the advection term caused by the transport of sensible heat by the moving dry air. The third term is the convective heat transfer between channel plate and dry air due to the temperature different between them.

At steady state, the energy balance of dry air is written as:

$$\rho_{da}c_{p,da}u_{da}\frac{dT_{da}}{dx} = k_{da}\frac{d^{2}T_{da}}{dx^{2}} - \frac{2\alpha_{da}}{d}(T_{da} - T_{pl})$$
(2)

(2) Wet channel

Considerations are based on mass and energy balance in the wet channel, governing equations are given as:

$$\rho_{wa}c_{p,wa}\frac{dT_{wa}}{dt} = k_{wa}\frac{d^{2}T_{wa}}{dx^{2}} - \rho_{wa}c_{p,wa}u_{wa}\frac{dT_{wa}}{dx} + \frac{2\alpha_{wa}}{d}(T_{wf} - T_{wa})$$
(3)

$$\frac{dx_{wa}}{dt} = k_{m,wa} \frac{d^2 x_{wa}}{dx^2} - u_{wa} \frac{dx_{wa}}{dx} + \frac{2\alpha_{m,wa}}{d} (x_{sat} - x_{wa})$$
(4)

The Eq. (3) encompasses the air heat conduction of the longitudinal direction, the advection term and convective heat transfer term. While the Eq. (4) denotes the dispersion alone channel length direction, translated mass from inlet to outlet of the control volume and, mass transfer between the saturated air around the water film and the working air owing to the difference in vapor density.

In a state of equilibrium, the above equations are transformed into:

$$\rho_{wa}c_{p,wa}u_{wa}\frac{dT_{wa}}{dx} = k_{wa}\frac{d^{2}T_{wa}}{dx^{2}} + \frac{2\alpha_{wa}}{d}(T_{wf} - T_{wa})$$
 (5)

$$u_{wa} \frac{dx_{wa}}{dx} = k_{m,wa} \frac{d^2 x_{wa}}{dx^2} + \frac{2\alpha_{m,wa}}{d} (x_{sat} - x_{wa})$$
 (6)

(3) Channel plate

The temperature of water film and the channel plate is determined by taking into account the temperature difference between the channel plate and air. In this scenario, the temperature of the wet side channel plate is identical to that of the water film. The energy balance equation is expressed as follows:

$$\rho_{pl}c_{p,pl}\frac{dT_{pl}}{dt} = \alpha_d (T_{da} - T_{pl}) - \frac{k_e}{d_e} (T_{pl} - T_{wf})$$
(7)

Here, d_e is the effective thickness of water film and channel plate, which is determined by $d_e = d_{pl} + d_{wf}$. k_e is defined as the effective conductivity of water film and channel plate are calculated by $\frac{d_e}{k_e} = \frac{d_{pl}}{k_{pl}} + \frac{d_{wf}}{k_{wf}}$

(4) Water film

The equation that governs the behavior of the water film is as follows:

$$\rho_{wf}c_{p,wf}\frac{dT_{wf}}{dt} = \frac{k_e}{d_e}(T_{pl} - T_{wf}) - \alpha_{wf}(T_{wf} - T_{wa}) - \alpha_{m,wf}h_{fg}\rho_a(x_{sat} - x_{wa})$$
 (8)

 h_{fg} in Eq. (8) represents the latent heat of evaporation process, computed using the CoolProp library [109].

In the above model, the Nusselt number value is fixed at 7.45. [110] by ignoring the inlet effect and the diffusion coefficient is given as:

$$\alpha_m = 104.91143 \times 10^{-6} \times T^{1.744} / P (If T < 80^{\circ}C)$$
 (9)

$$\alpha_m = 805.2375 \times 10^{-6} / P \times T^{\frac{5}{2}} / (T + 190) \ (If T > 80^{\circ}\text{C})$$
 (10)

The function used to calculate the Lewis number, utilized for computing the latent heat, is formulated as:

$$Lw = 4185.5 \times (751.78 - 0.5655 \times T_{wf}) \tag{11}$$

2.3.2 Entropy generation model

Irreversible losses in the thermodynamic and mass transfer processes are quantified by entropy generation, which serves as a key indicator for evaluating the thermodynamic performance of the DPEC system. A comprehensive analysis of these losses involves examining the mass and heat transfer within specific control volumes: the wet channel, dry channel, water film, and channel plate. Accordingly, the entropy generation model in this section is divided according to the control volumes defined in Section 2.3.1.

As depicted in Fig. 2.2, for the dry channel within the control volume, the energy balance equation can be given as:

$$\Delta \dot{U}_{cv} = q_x - q_{x + \Delta x} + m_d (h_{d,x} - h_{d,x + \Delta x}) - q_{d,y}$$
 (12)

In Eq. (12), the general energy balance is determined by internal energy, encompassing conduction and flow within the air, and external energy, involving convective heat transfer between the channel plate and air.

The entropy generation by the irreversible heat flow inside the control volume can be represented as [111]:

$$s_{g,h} = -\frac{1}{T^2} \boldsymbol{q} \cdot \nabla T \tag{13}$$

where the entropy generation caused by the mass transfer can be simplified as [111]:

$$s_{g,m} = -\frac{1}{T} \nabla \mu_i \mathbf{J} \tag{14}$$

the diffusive flux **J** can be calculated by:

$$J = \rho_{wa} \alpha_{m,wa} (x_{sat} - x_{wa}) \tag{15}$$

Base on the above Eq. (12), (13), (14), and (15), each term in Eq. (12) can be treated as irreversible heat flow and substituted into Eq. (13) to calculate the entropy generation. Thus, in this model, for dry air, the entropy generation within each control volume due to the heat transfer processes can be computed. For wet air and water film, the entropy generation resulting from mass transfer can be determined through Eq. (14) and (15).

2.3.3 performance evaluation

The wet-bulb effectiveness is a generally employed evaluation for assessing the efficacy of the DPEC system, which is expressed as:

$$\varepsilon_{wb} = \frac{T_{da,in} - T_{da,out}}{T_{da,in} - T_{wh,in}} \tag{16}$$

The overall cooling capacity is described by:

$$Q_{-cooling} = m_{da} \dot{c}_{p,da} \left(T_{da,in} - T_{da,out} \right) \tag{17}$$

And the specific entropy generation can be given as:

$$s_{g,spec} = \frac{s_g}{Q_{-cooling}} \tag{18}$$

2.3.4 Numerical approach

The dynamic calculation of the DPEC system involves solving the Eq. (1), (3), (4), (7) and (8) in Section 2.3.1. The geometries of DPEC system are given in Table 2.1. The simulation is subject to the subsequent boundary conditions:

(1) The dry channel initial conditions:

$$T_{da_in} = T_{ambient}, x_{da} = x_{ambient}$$
 (19)

(2) The wet channel initial condition:

$$T_{wa_in} = T_{da_out}, x_{wa_in} = x_{da}$$
 (20)

(3) The conditions at the boundaries of other layers in the DPEC system are described as:

$$\frac{dT_{pl}}{dx}\Big|_{x=0} = \frac{dT_{pl}}{dx}\Big|_{x=L} = \frac{dT_{wf}}{dx}\Big|_{x=0} = \frac{dT_{wf}}{dx}\Big|_{x=L} = 0$$
 (21)

The finite difference method was applied to solve the differential equations in the DPEC model, with a non-linear optimization approach implemented in the Python environment. The length direction was discretized into 50 elements, and the time grid was set to 30 intervals. The simulation algorithm is shown in Fig. 2.3.

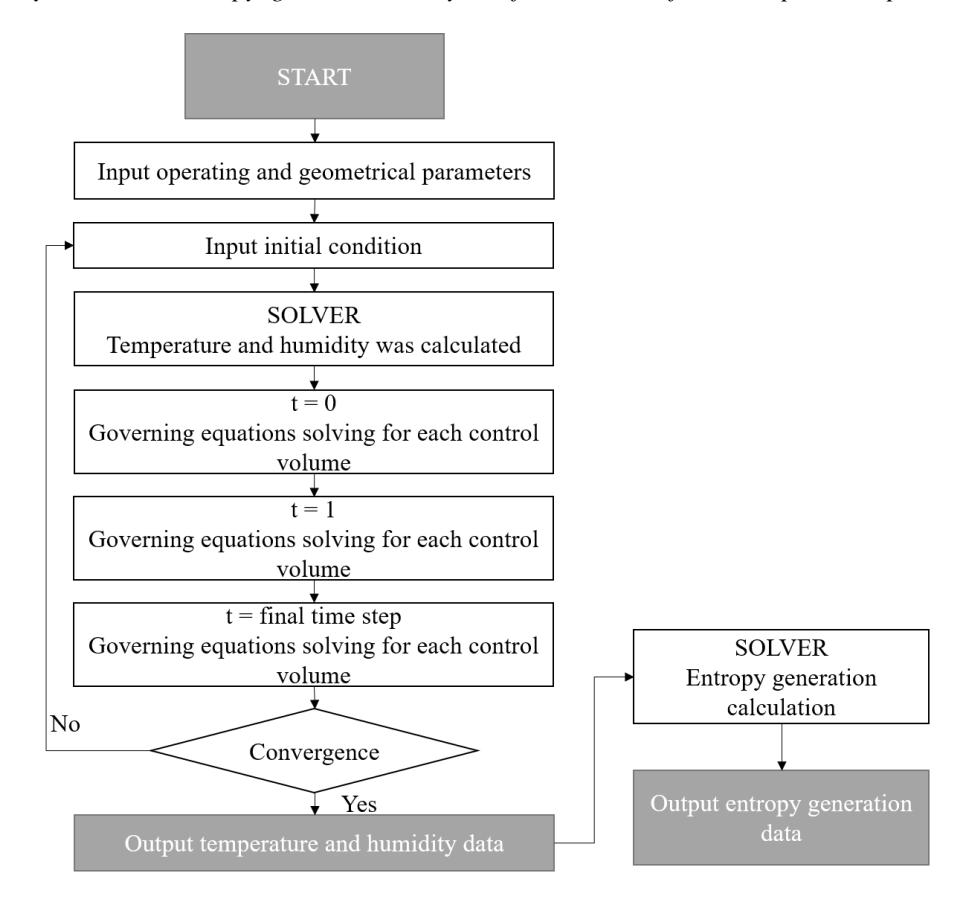


Fig. 2.3. Simulation flowchart.

Table 2.1 Parameters of DPEC system.

Parameters	Value
Air inlet temperature (°C)	35
humidity ratio (kg/kg [DA])	0.0123
Wall thickness(m)	4.5e-4
Channel length(m)	1.0
Channel width(m)	8.3e-2
Channel height(m)	4.5e-3
Working air ratio (-)	0.5

2.3.5 Experimental validation

Two versions of DPEC systems were fabricated to validate the developed numerical model. Experiments were conducted in the environmental chamber, as depicted in Fig. 2.4. Setup 1 is vertically oriented, consisting of two pairs of 1m long channels. Intake air is introduced from the top by fans, with a portion exiting as supply air from the bottom. The remaining air, designated as working air, flows through the wet channels and exits from the top. This setup faces challenges such as pressure losses from the long channel length and experimental data biases due to the limited number of channels. Air conditions were adjusted within a range of 35% to 45% relative humidity and 25°C to 35°C. On the other hand, setup 2 is horizontally arranged with eight pairs of 0.6m long channels. Intake air enters from the right side, facilitated by three sets of fans. After passing through the dry channels, a portion of the cooled air exits from the left side, while the rest continues as working air through the wet channels, exiting on the right side. Compared to Setup 1, Setup 2 has more channels and shorter lengths, reducing pressure losses and improving the accuracy of temperature and humidity measurements. It underwent four initial tests under the same conditions, followed by experiments with varying

inlet relative humidity, with data collected for each test.

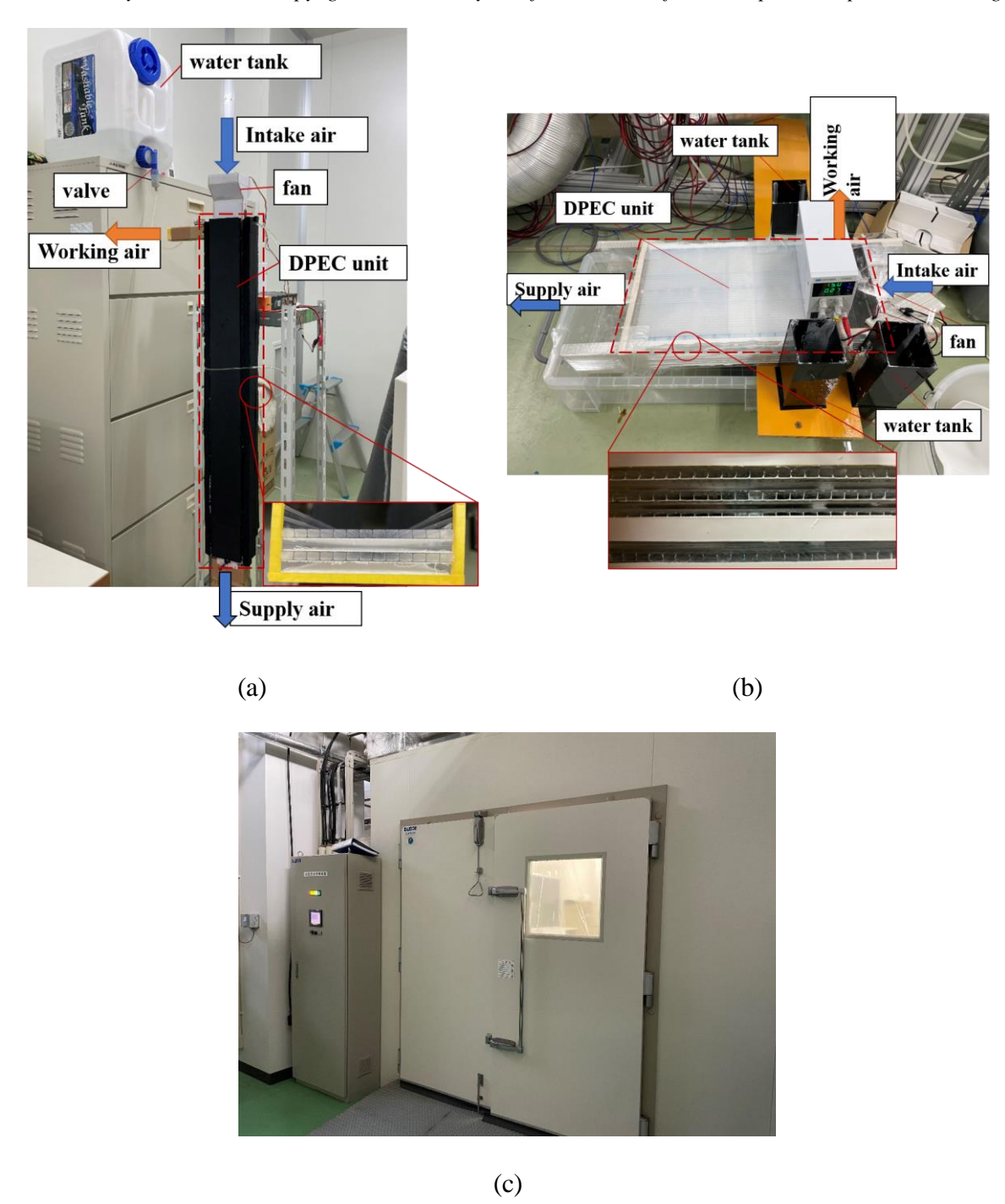


Fig. 2.4. Test experimental setup for DPEC system: for: (a)vertical flow direction; (b) horizontal flow direction; (c) environmental chamber.

Four key parameters (moisture content and temperature of the inlet, exhaust, and supply air) were measured using a Thermo-Hygrometer testo 605i (sensor accuracy provided in Table 2.2). Experimental data were used to validate the current model, as shown in Fig. 2.5. The model

Thermodynamic and entropy generation analysis of the counter-flow dew-point evaporative cooling demonstrated good predictive capability for the DPEC system temperature, with discrepancies ranging from 3.5% to 15.8% for Setup 1 and 3% to 12% for Setup 2, as depicted in Fig. 2.6. Additionally, the model was validated using experimental data from [112] for a counter-flow DPEC system under specific supply air conditions: (a) 32.6°C and 14 g/kg, and (b) 38.2°C and 10.2 g/kg. The temperature distribution along the channel was compared with model results, as shown in Fig. 2.7. The maximum discrepancies between the model and experimental data were 1.4°C (4%) for case (a) and 1.42°C (7.3%) for case (b). Overall, the average discrepancy between the simulation results and experimental data confirms the model's accuracy and predictability.

Table 2.2 Specification of measuring devices.

		-		
Instruments	Model	Parameters	Measurement range	Accuracy
Thermo-	Testo	Temperature	-20 to +60° C	±0.8° C (-20 to 0° C)
Hygrometer	605i	(° C)	-20 to +00 C	$\pm 0.5^{\circ}$ C (0 to 60° C)
	Testo 605i	Relative humidity (%)		±3%RH (10%-35%RH)
				±2%RH (35%-65%RH)
Thermo-			0.4000/DII	±3%RH (65%-
Hygrometer			0-100%RH	90%RH)
				±5%RH (<10% or
				>90%RH)
Thermo-	Testo	Ela la ait	0.20/-	±0.1m/s (0-2m/s)
Anemometer	405i	Flow velocity	0-30m/s	±0.3m/s (2-15m/s)

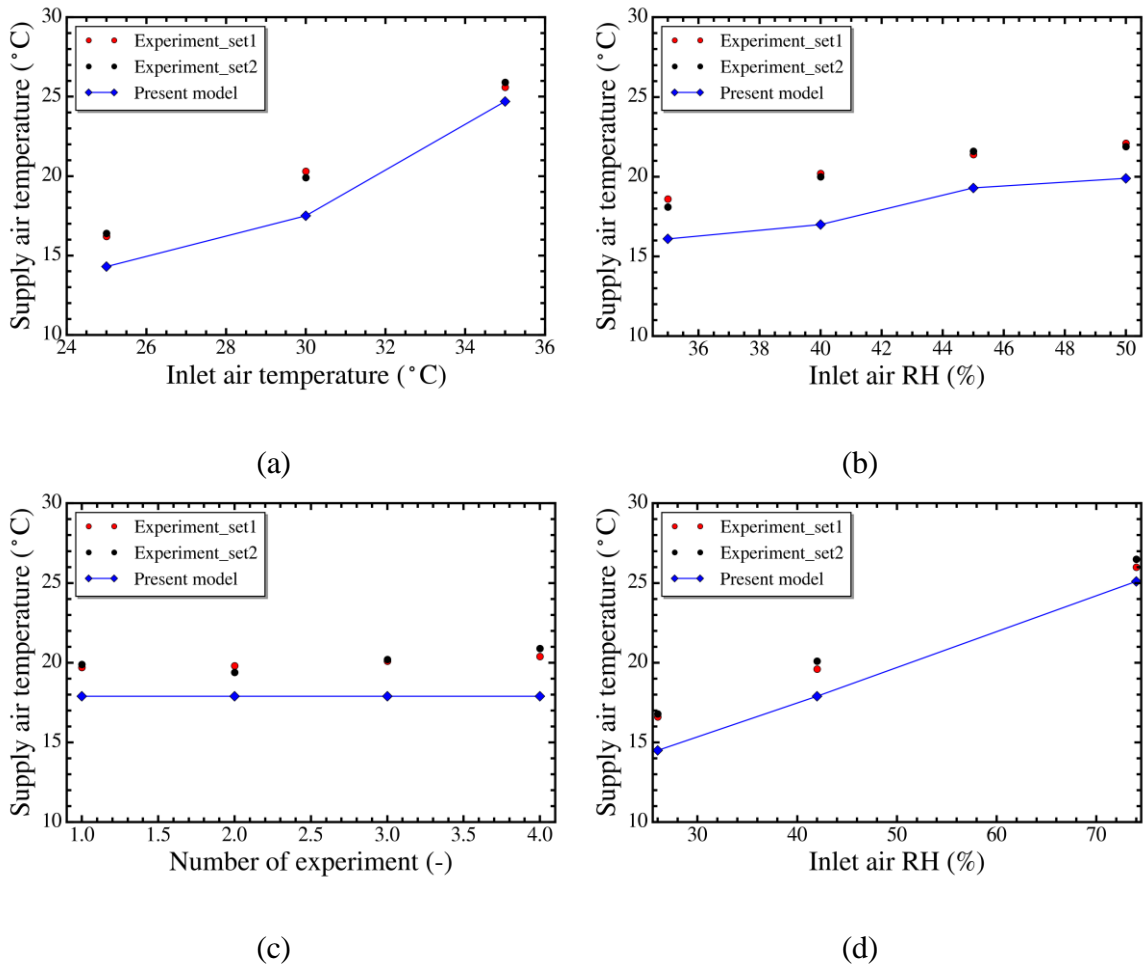


Fig. 2.5. Model validation with experimental setup under different inlet condition: (a) Inlet air temperature by setup 1; (b) Inlet air RH by setup 1; (c) Multiple experiments under the same inlet condition by setup 2; (d) Inlet air RH by setup 2.

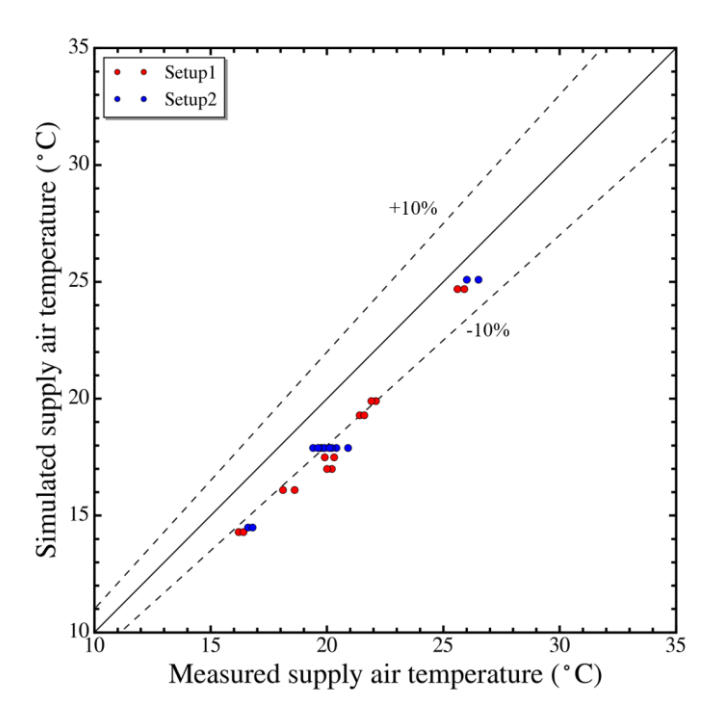


Fig. 2.6. Error between measured temperature and simulated temperature.

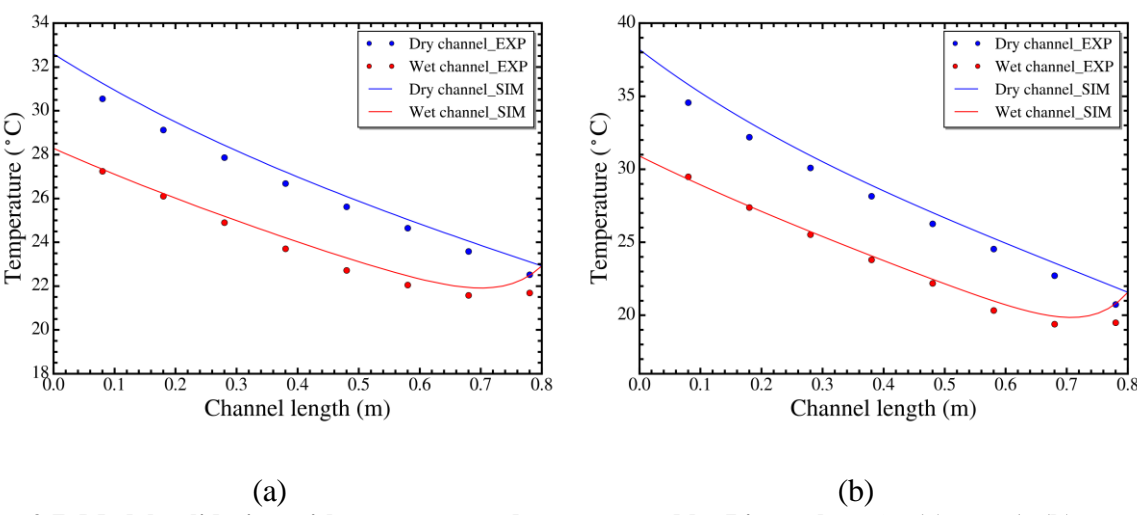


Fig. 2.7. Model validation with temperature data presented by Lin et al. [112]. (a) case 1; (b) case 2.

2.4 Results and discussion

2.4.1 Behavior of humidity and temperature

A dynamic analysis of the DPEC system with counter-flow configuration was performed using prescribed inlet air conditions. The temperature of the inlet air was maintained at 35°C with a humidity level of 12g/kg. The section focused on exploring the distribution of humidity and temperature at different positions within the channel.

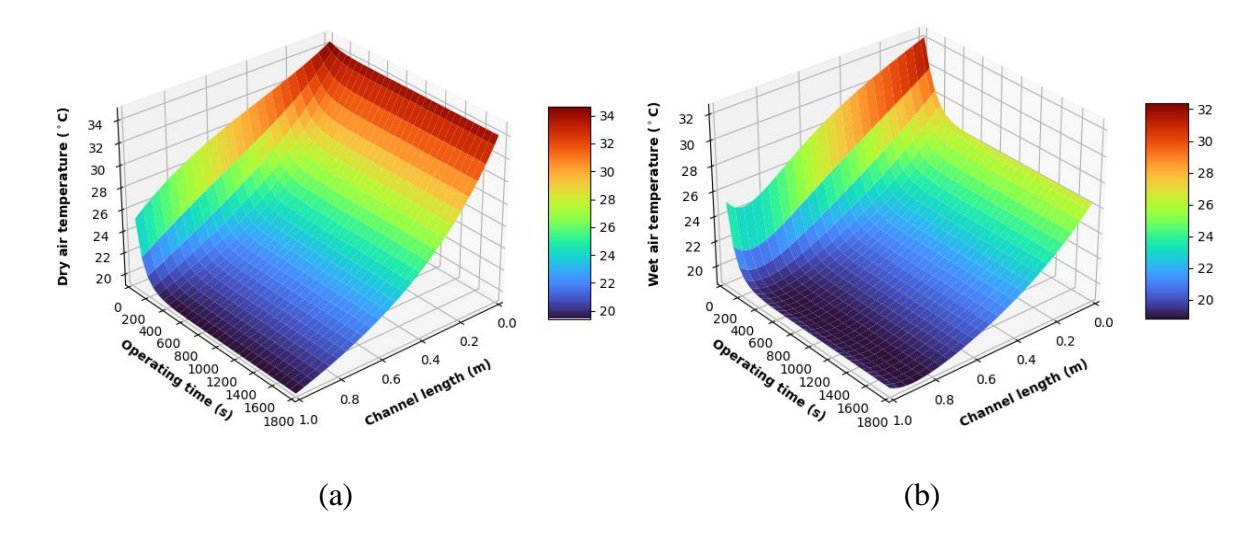
Fig. 2.8 (a) shows the temperature distribution within the dry channel, where the air temperature gradually decreases due to continuous convective heat transfer. As a portion of the supply air enters the wet channel and becomes working air, the temperature distribution of the dry air and working air at the wet channel's entrance is identical. However, the temperature of the working air decreases, as shown in Fig. 2.8 (b). This reduction occurs because, at this point, the temperature of the water film is lower than that of the air, leading to sensible heat transfer from the water film to the working air. The minimum temperature is reached when the air temperature equals the water film temperature. After this point, the working air temperature begins to rise gradually. This increase is due to the continued evaporation of the water film, which absorbs heat from the adjacent dry channel. As a result, the water film temperature exceeds that of the air, facilitating further heat transfer. Over time, as the outlet supply air temperature decreases, the inlet working air temperature also decreases, leading to a decline in the working air temperature distribution within the wet channel. The temperature distributions of the water film and channel plate, shown in Fig. 2.8 (c) and (d), follow a similar trend to the dry air. As the system transitions from an unsteady to a steady state, the temperatures of the water film and channel plate at the channel entrance decrease.

Fig. 2.8 (e) illustrates the distribution of humidity ratio in the moist air across the wet channel. Upon entering the wet channel, the working air humidity steadily increases, quickly reaching saturation. Even when saturated, the humidity ratio continues to rise as the water film absorbs heat from the adjacent channels, maintaining evaporation. During the transient

Thermodynamic and entropy generation analysis of the counter-flow dew-point evaporative cooling response, the working air temperature is higher in the first 200 seconds, which leads to a higher absolute saturated humidity during this period. Consequently, the humidity of the working air at the outlet is higher during the initial 200 seconds. As the operating time progresses, the working air temperature decreases, leading to a corresponding decrease in the humidity of the working air.

Fig. 2.8 (a) to (e) illustrate the distribution of humidity ratio and temperature within the wet and dry channels, water film, and channel plate. A significant change is observed during the first 200 seconds, followed by a gradual approach to equilibrium between 200 and 500 seconds. After 500 seconds, the supply air temperature shows minimal variation, indicating that the system has reached a steady state, as confirmed by the air temperature and humidity data presented in Fig. 2.9.

Fig. 2.10 depicts the heat flow distribution along the length of the channel for each layer. This not only provides a visual representation of heat transfer through the various layers but also serves as a reference for assessing the entropy generation associated with irreversible heat flow.



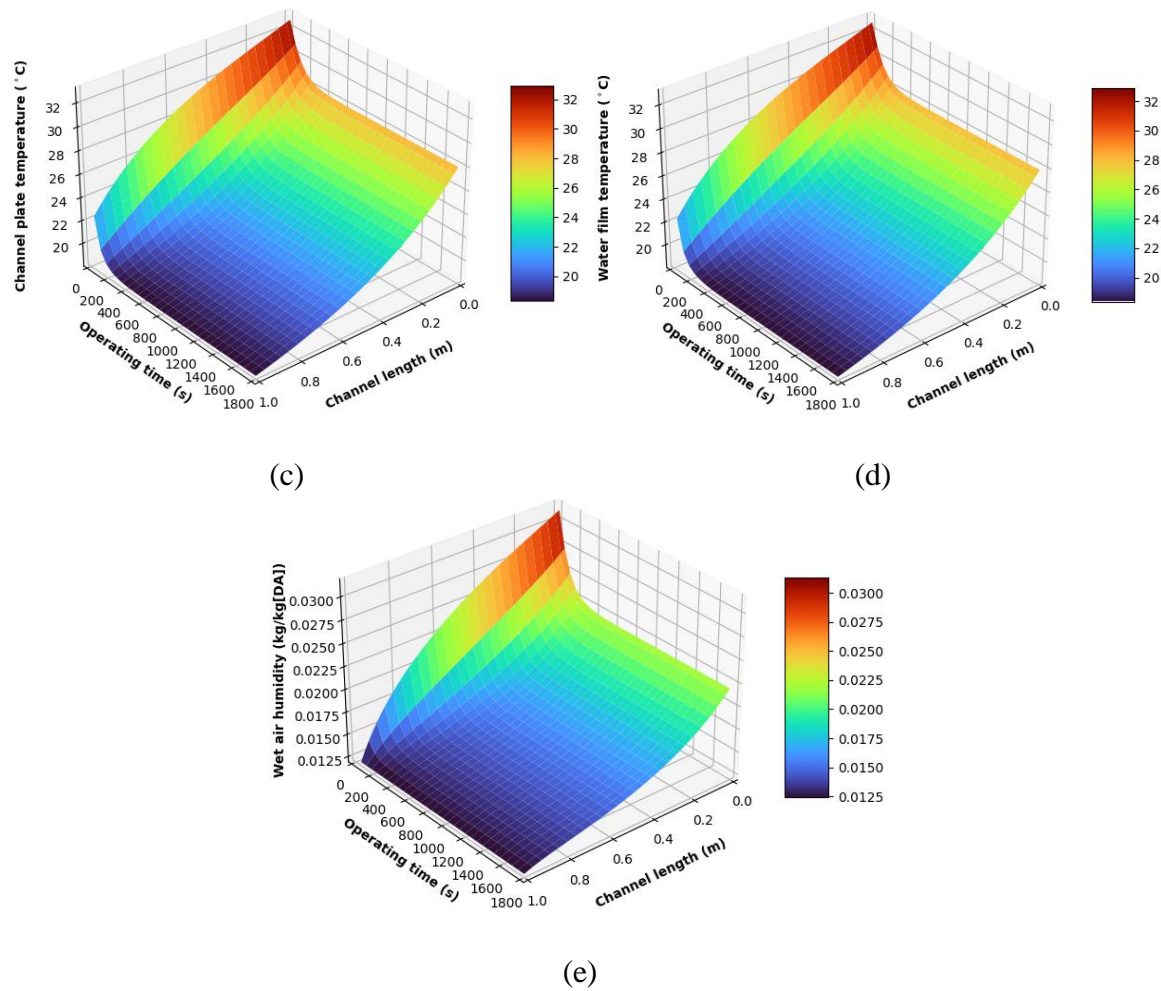


Fig. 2.8. Transient behavior of temperature and humidity: (a) Dry channel air; (b) Wet channel; (c) Channel plate; (d) Water film; (e) Wet air humidity.

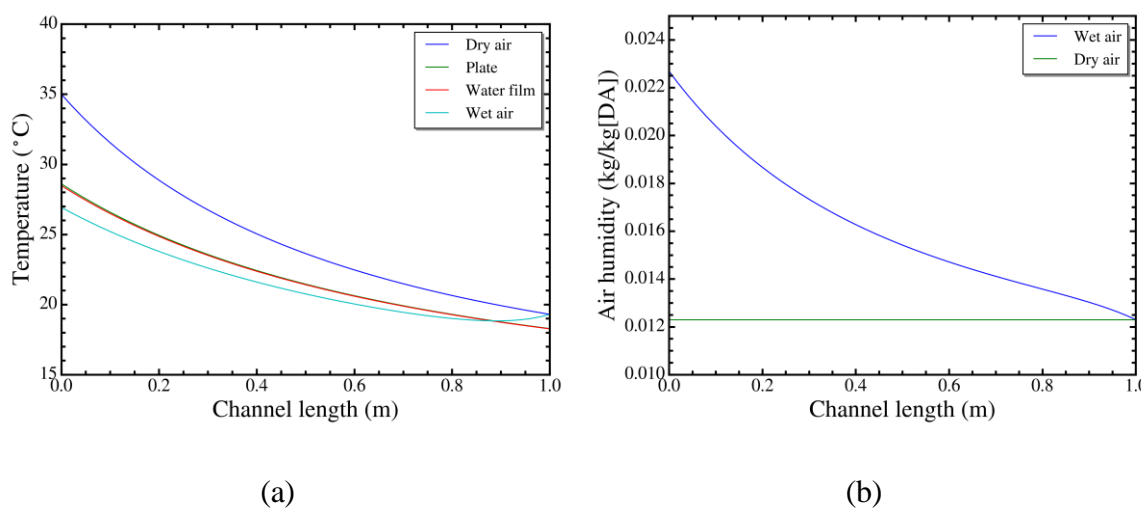


Fig. 2.9. Steady-state values distribution within channel length: (a) Temperature; (b) Humidity ratio.

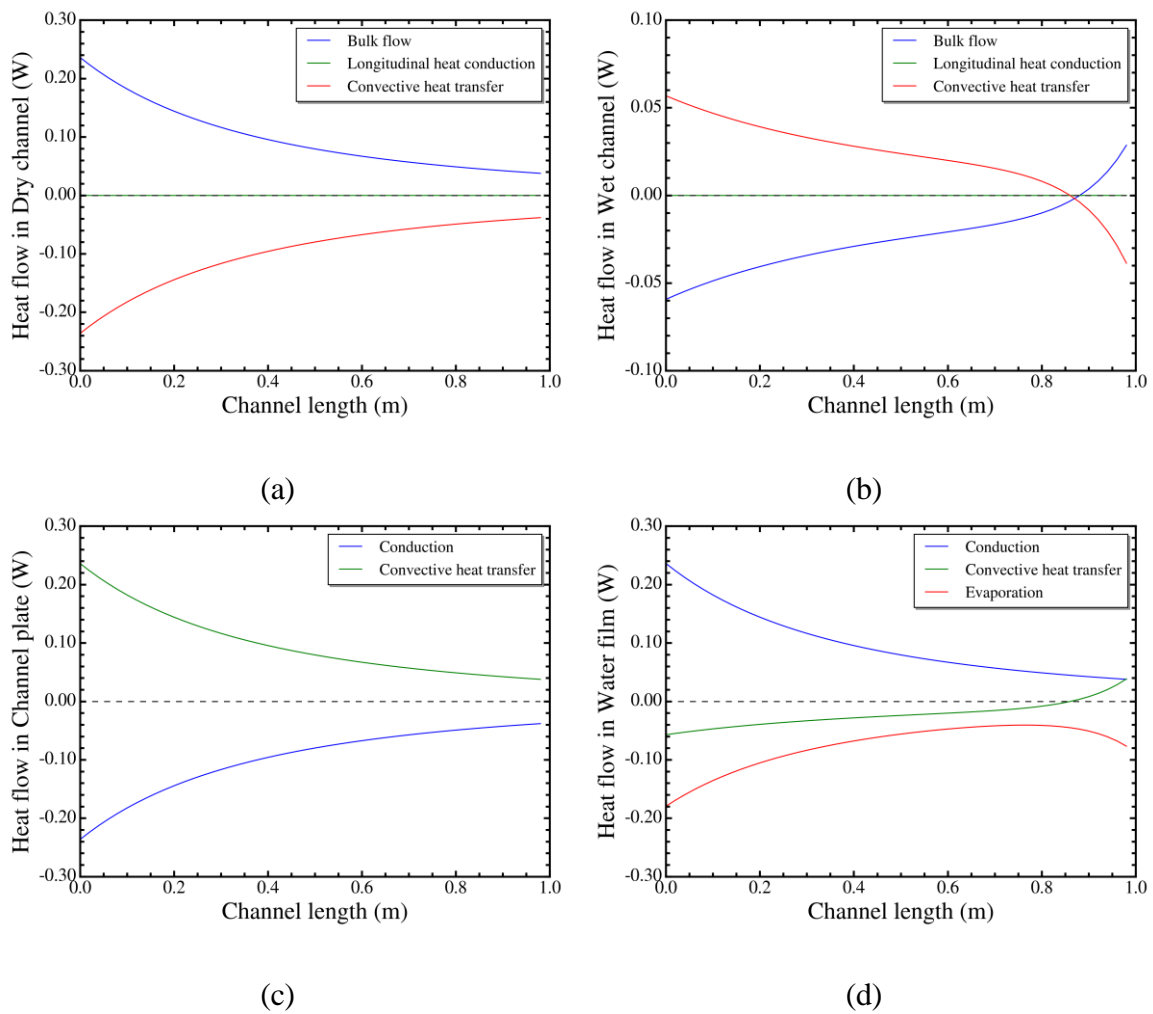


Fig. 2.10. Heat transfer along each element: (a) Dry channel layer; (b) Wet channel layer; (c) Plate layer; (d) Water film layer.

2.4.2 Response of the entropy generation

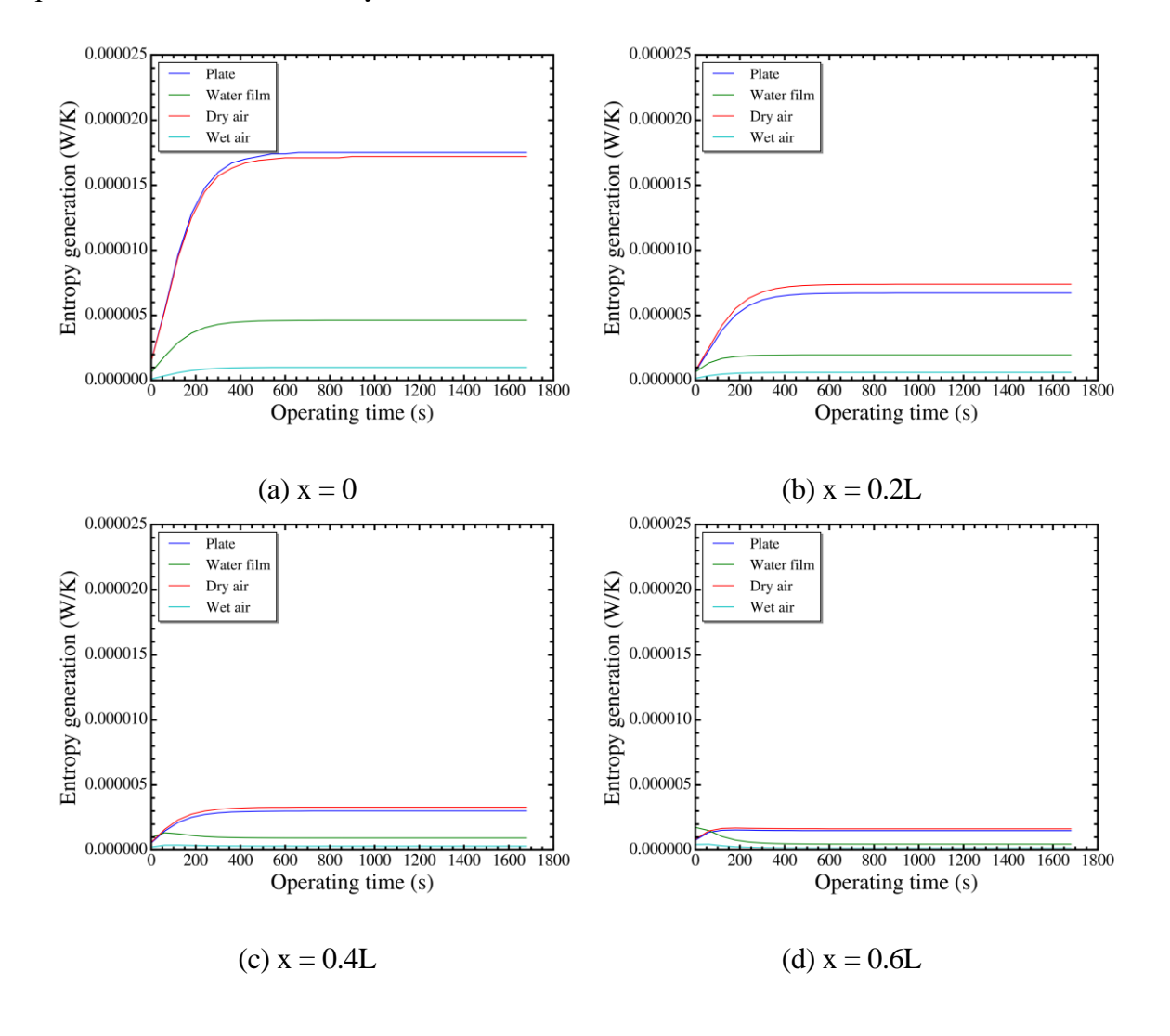
1) Transient point of view

This section evaluates the dynamic entropy generation under the previously specified operating conditions by examining entropy generation at various positions along the channels. Fig. 2.11 illustrates the transient entropy generation at positions 0.2L, 0.4L, 0.6L, 0.8L, and 1L along the channel length.

Fig. 2.11 (a) and (b) illustrate entropy generation at the channel's entrance region. Due to the notable temperature difference between the channel plate and dry air upon entry, convective Thermodynamic and entropy generation analysis of the counter-flow dew-point evaporative cooling heat transfer—especially between the channel plate and dry air—dominates this area, resulting in high entropy generation from heat transfer. As air progresses to 0.2L, the entropy generation from heat transfer decreases with the reduced temperature gradient between the dry air and channel plate. In Fig. 2.11 (c) to (e), entropy generation for the dry air and channel plate continues to decline as dry air temperature drops along the channel. Before reaching steady state (0s to 500s), approaching the dry channel exit (wet channel entrance) increases evaporation. This intensified water vapor transfer between working air and the water film raises entropy generation in the water film within the wet channel. Fig. 2.11 (f) shows that at the wet channel entrance, the humidity difference between the water film and working air peaks, driving intense evaporation and a marked rise in water film entropy generation. As the system stabilizes, entropy generation in the wet air and water film declines. Additionally, during the transient state, the high temperature gradient between the channel plate and dry air results in substantial entropy generation, which then decreases as the system reaches steady state and the temperature difference diminishes.

Fig. 2.12(a) presents the entropy generation distribution along the channel length across all layers. Notably, entropy generation is higher in dry air than in wet air. This difference arises primarily because, at the dry channel outlet, part of the air exits as product air (cooling source), while the remainder moves into the wet channel. Once the system reaches a steady state, the temperature difference between the channel plate and dry air peaks, leading to an increase in entropy generation within the dry air and channel plate over time. The entropy generation curves for wet air and the water film exhibit a consistent downward trend. During the transient state, the substantial humidity difference between the wet air and water film leads to higher entropy generation. However, as the system progresses towards steady state, this humidity difference diminishes, resulting in a gradual reduction in entropy generation for both the wet

Thermodynamic and entropy generation analysis of the counter-flow dew-point evaporative cooling air and water film. In Fig. 2.12(b), the entropy generation from mass transfer processes between the water film and wet air is shown. The water film comprises solely water vapor, while wet air includes both water vapor and dry air, resulting in numerical distinctions. The reduction in mass exchange during the transition to a steady state contributes to the decreasing trend in entropy generation. Fig. 2.12(c) illustrates the transient response of the system's total entropy generation. The results show that, while different heat and mass transfer processes impact entropy generation across channel areas, the total entropy generation approximates that of dry air and the channel plate. This suggests that the entropy generation in dry air and the channel plate dominates the overall system's behavior.



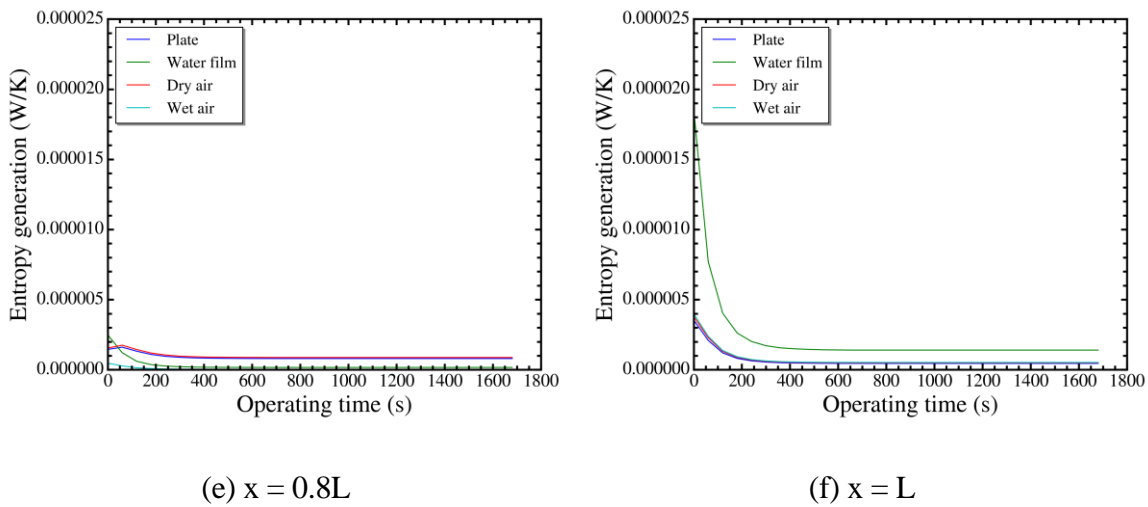


Fig. 2.11. Transient response of entropy generation in different location of the channel: (a) x = 0; (b) x = 0.2L; (c) x = 0.4L; (d) x = 0.6L; (e) x = 0.8L; (f) x = L.

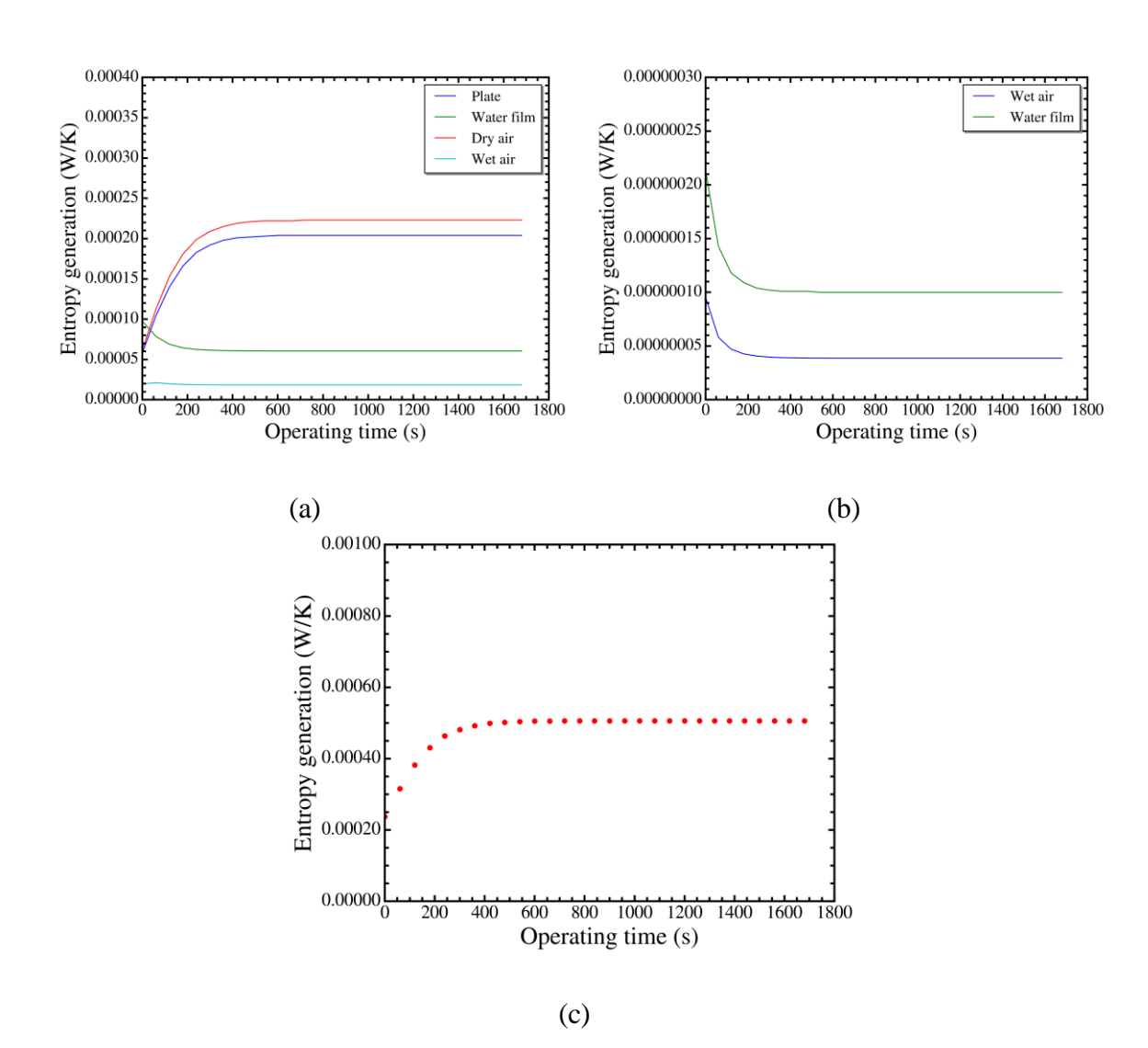
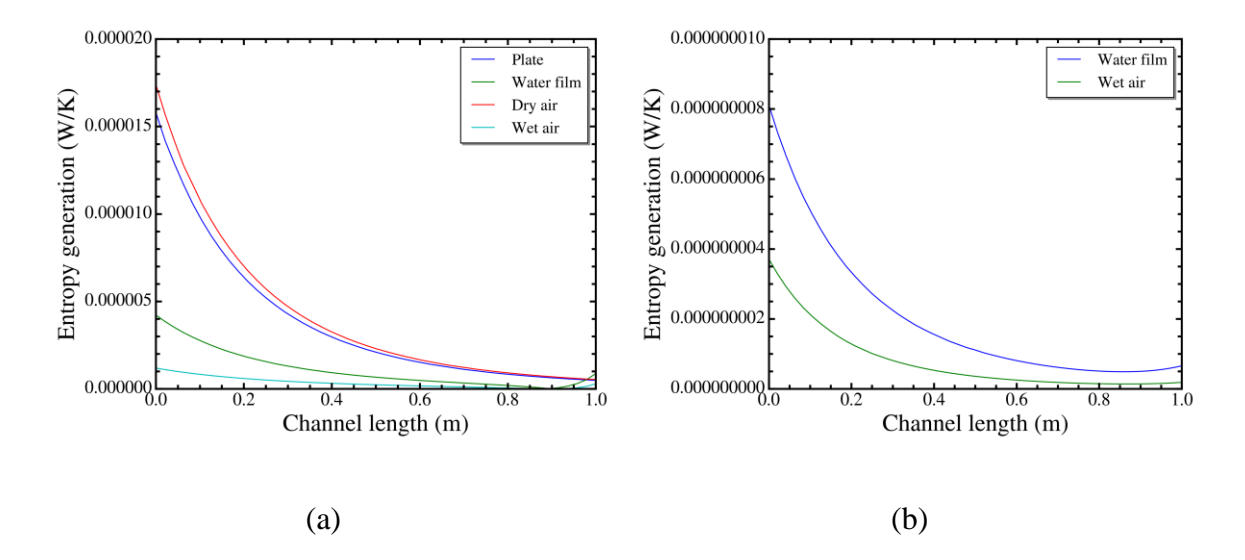


Fig. 2.12. Transient response of entropy generation: (a) Entropy generation in each layer by heat transfer; (b) Entropy generation of wet air and water film by mass transfer; (c) Total generation of DPEC system.

2) Steady-state point of view

Fig. 2.13 (a) displays the entropy generation distribution along the channel length across various layers. With diminishing temperature gradients, the heat transfer between layers decreases, resulting in an overall decline in entropy generation. Fig. 2.10 (b) and (d) reveal that, due to vigorous mass and heat transfer near the wet channel's entrance, the entropy generation of both wet air and the water film initially decreases and then increases along the wet channel, reaching a minimum when the water film and working air temperatures equalize. Fig. 2.13(b) highlights entropy generation within the wet channel from mass transfer between the water film and wet air. Fig. 2.13 (c)-(f) illustrate entropy generation from specific heat flows within individual layers. The figures demonstrate that, despite identical heat flows, variations in temperature differences among layers lead to differing entropy generation levels, offering valuable insights into optimizing the efficiency of the DPEC system.



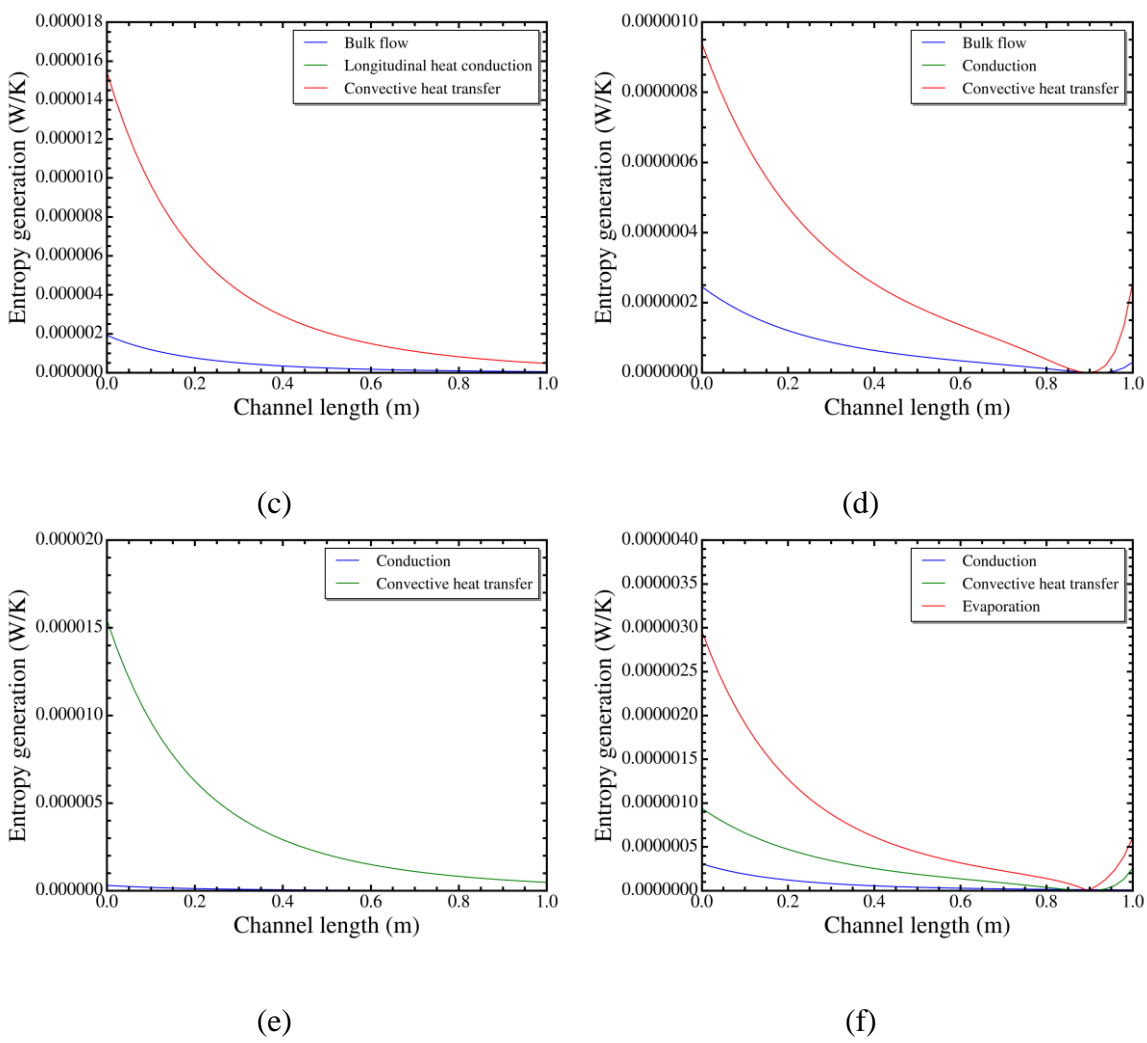


Fig. 2.13. Entropy generation in each element in steady-state: (a) total generation for 4 layers; (b) by mass transfer; (c) by heat transfer within dry channel; (d) by heat transfer within wet channel; (e) by heat transfer in Plate; (f) by heat transfer in water film.

2.4.3 Parametric analysis

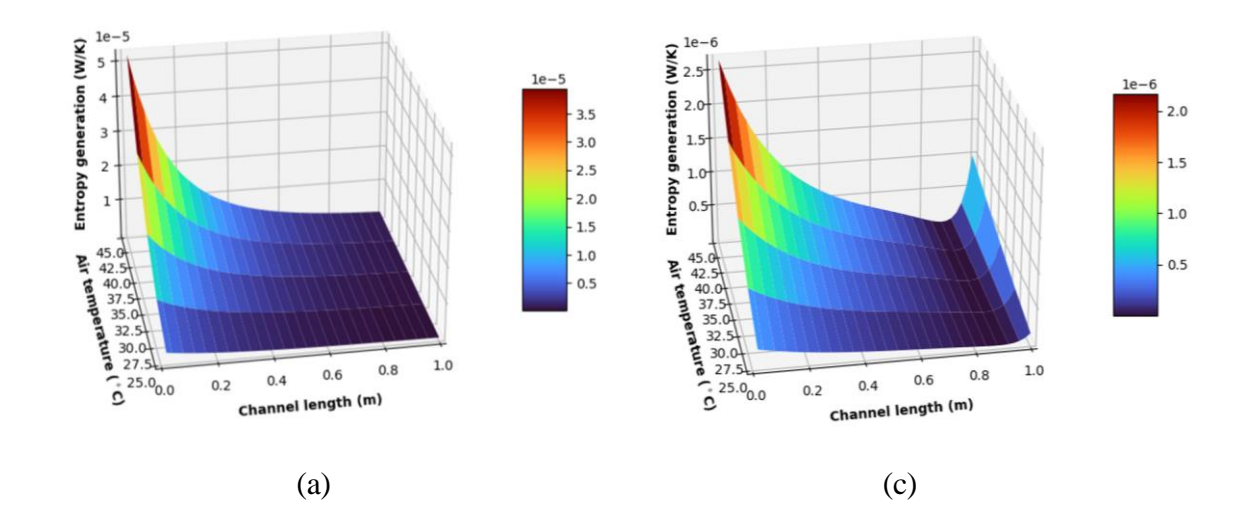
This section delves into the impact of altering input parameters, encompassing inlet air condition, operating condition and geometry on the entropy generation of the DPEC system.

1) Effect of inlet air condition

For inlet air conditions, the primary factors are air temperature and humidity. The temperature of incoming air, ranging from 25 to 45°C, significantly affects the system's entropy

Thermodynamic and entropy generation analysis of the counter-flow dew-point evaporative cooling generation, as shown in Fig. 2.14 (a) to (d). Variations in inlet temperature impact the entropy generation across each layer of the DPEC system. Higher inlet temperatures result in increased temperature differentials among layers, thereby intensifying heat transfer processes within the channel and leading to greater entropy generation. Notably, an increase in inlet air temperature proportionally raises the entropy generation at the entrance of the water film and wet channel.

Fig. 2.15 (a) to (d) illustrates the effect of various heat flows across layers on entropy generation. As inlet air temperature rises, enhanced heat transfer processes elevate entropy generation across all layers. In the dry air, entropy generation is primarily influenced by convective and advection heat transfer, with longitudinal conduction having a minor effect in both dry and wet air. In wet air, convective heat transfer predominates due to the temperature differences between the channel plate and air. In the channel plate, only convective heat transfer and vertical heat conduction contribute to entropy generation. For the water film, the latent heat of vaporization is a key factor, increasing with temperature and thus adding to the entropy generation.



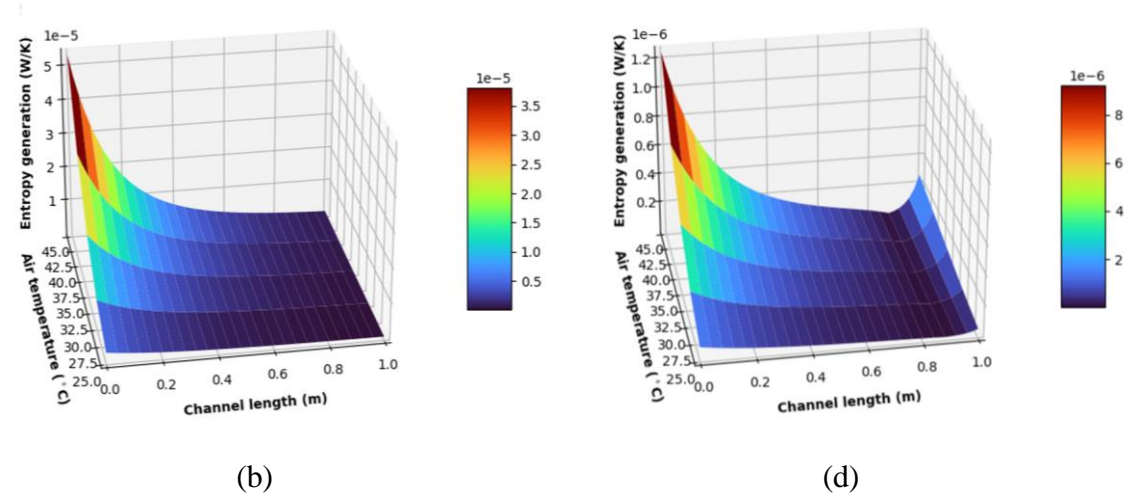


Fig. 2.14. The effects of different inlet temperature on entropy generation: (a) Dry channel air; (b) Channel plate; (c) Wet channel air; (d) Water film.

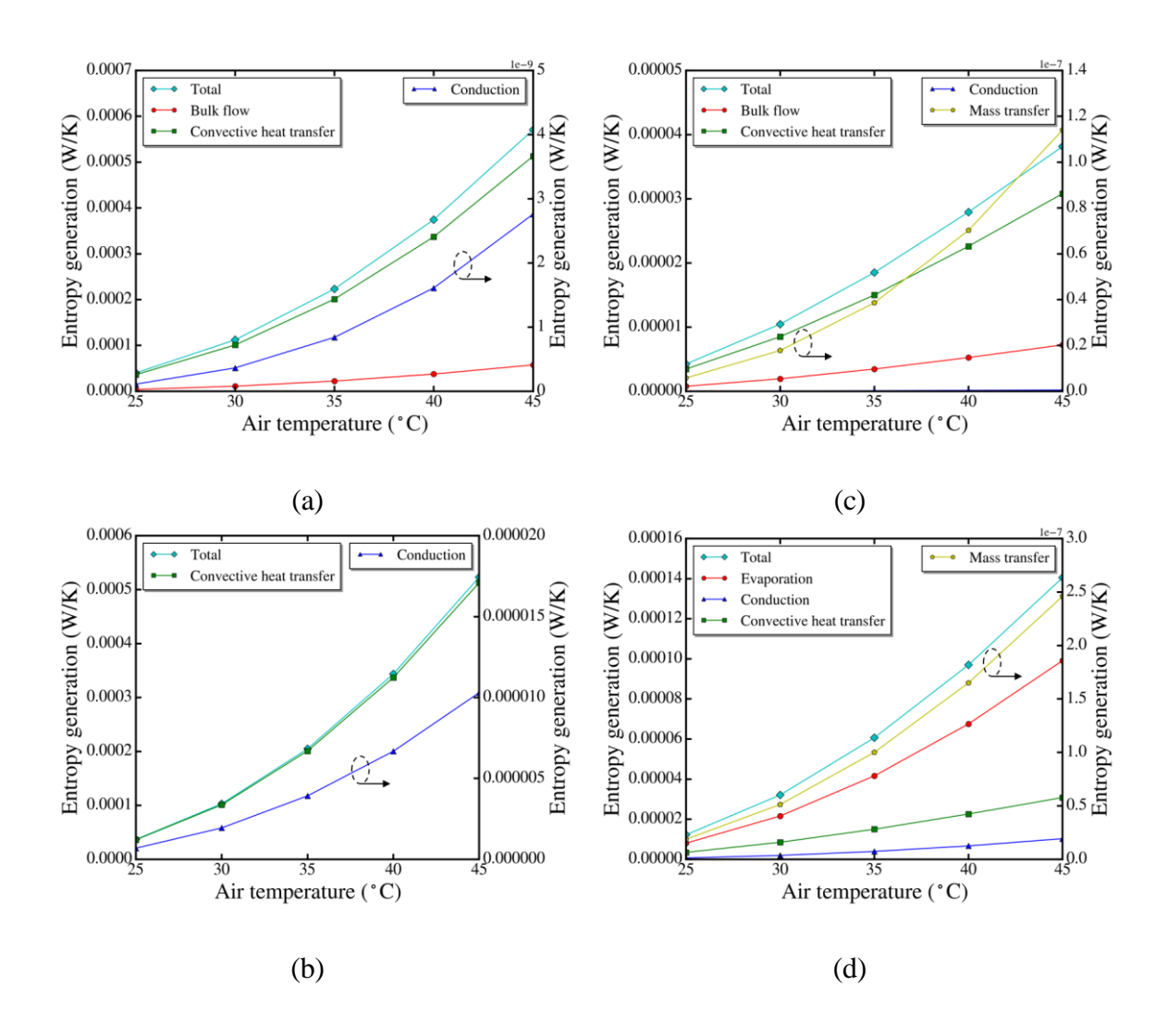


Fig. 2.15. Entropy generation involved in each layer at different inlet air temperatures: (a) Dry channel air; (b) Channel plate; (c) Wet channel air; (d) Water film.

On the other hand, the humidity, ranging from 8 to 24 g/kg, directly impacts system performance, as illustrated in Fig. 2.16 (a) to (d). As inlet air humidity increases, the potential for evaporative cooling decreases, weakening the evaporation-driven heat transfer between channels. In the dry channel and channel plate, reduced temperature differentials between the air and plate limit heat transfer, resulting in a downward trend in entropy generation. Conversely, for wet air and the water film, the humidity difference between the air and saturated water vapor influences entropy generation in the wet channel. With rising inlet air humidity, the air nears saturation, which restricts mass transfer and lowers entropy generation accordingly.

Fig. 2.17 (a) to (d) further demonstrates that higher humidity reduces the evaporative cooling potential, thereby weakening heat exchange. For dry air and the channel plates, convective and advective heat transfer, as well as longitudinal conduction, show a declining trend due to reduced temperature gradients. In the case of wet air and the water film, higher inlet air humidity reduces the humidity gradient, approaching saturation and thus decreasing entropy generation associated with mass transfer.

Fig. 2.18 (a) shows that an increase in inlet air temperature leads to higher specific entropy generation, thereby reducing the system's wet-bulb efficiency. In contrast, as depicted in Fig. 2.18 (b), an increase in inlet air humidity has a suppressive effect on the system's heat and mass transfer processes. This rise in humidity lowers system efficiency, while simultaneously decreasing irreversible heat loss due to the weakened heat transfer processes.

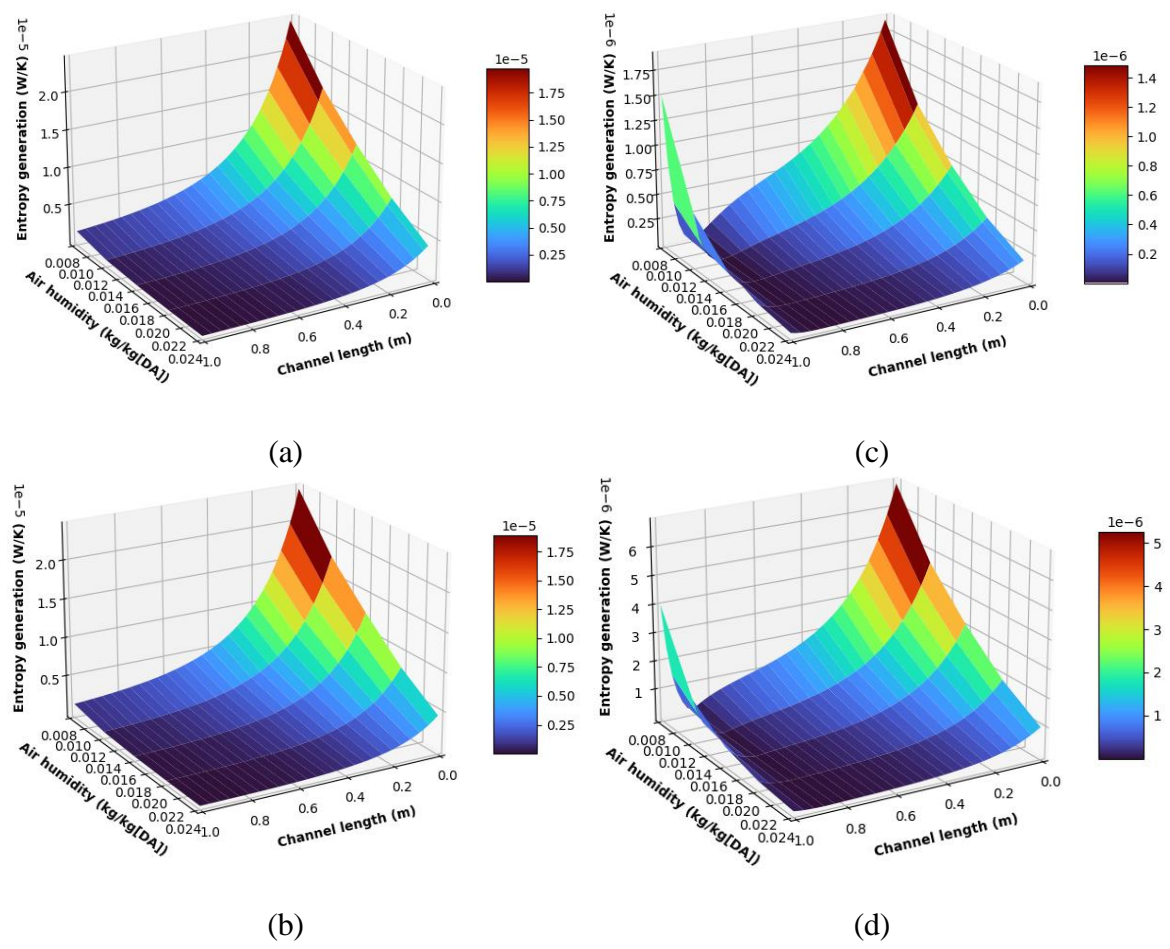
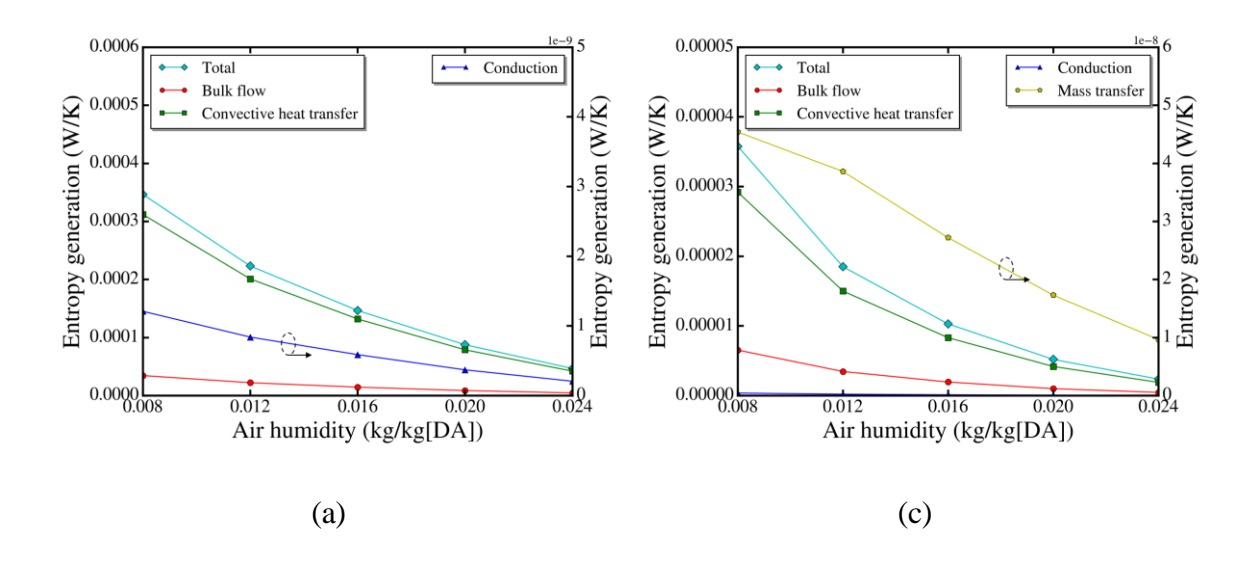


Fig. 2.16. The effects of different inlet humidity on entropy generation: (a) Dry channel air; (b) Channel plate; (c)Wet channel air; (d) Water film.



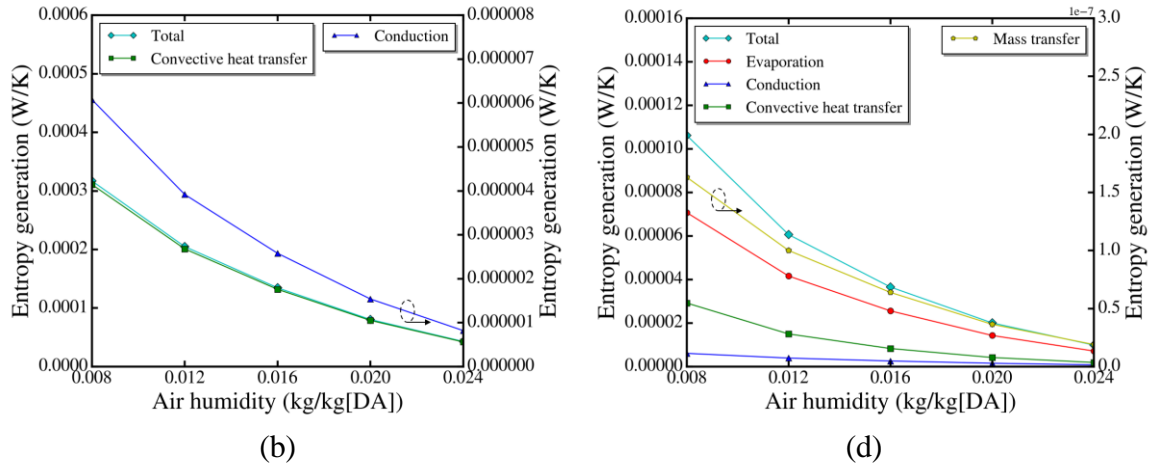


Fig. 2.17. Entropy generation involved in each layer at different inlet air humidity: (a) Dry channel air; (b) Channel plate; (c) Wet channel air; (d) Water film.

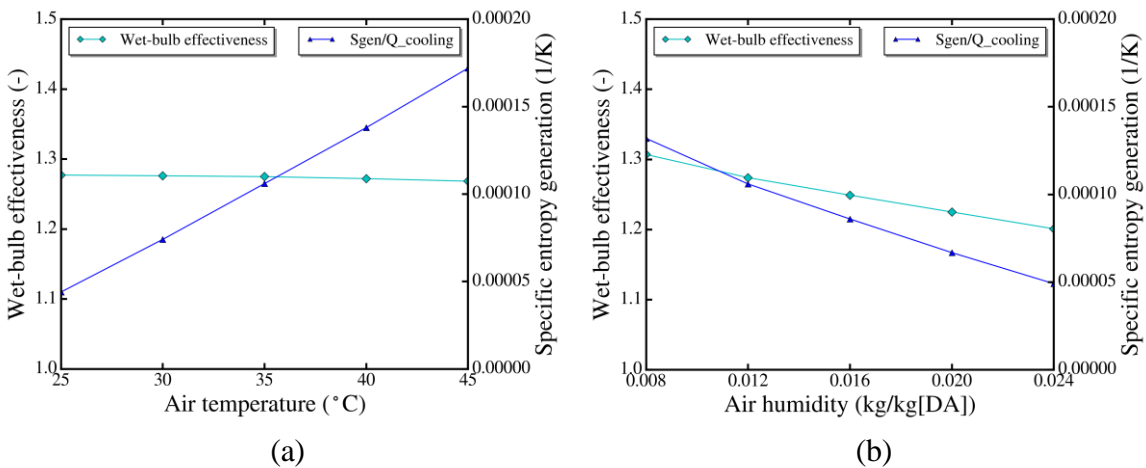


Fig. 2.18. The wet-bulb effectiveness and the specific entropy generation at: (a) different inlet air temperature; (b) different inlet air humidity.

2) Effect of operating condition

For the operating conditions, the primary factors influencing the airflow rate entering each channel are the working ratio and the inlet air velocity. The investigation explores the effects of varying the working ratio from 0.1 to 0.9 on entropy generation across different layers in the DPEC system. The working ratio, which denotes the fraction of intake air directed into the wet channel as working air, significantly affects the temperature and humidity distribution along

Thermodynamic and entropy generation analysis of the counter-flow dew-point evaporative cooling the channel, producing complex outcomes. Fig. 2.19 (a) to (d) illustrates that a higher working ratio corresponds to a larger volume of intake air directed to the wet channel as working air. This increase in working air volume necessitates intensified heat and mass transfer processes, resulting in an overall rise in entropy generation with higher working ratios. When the supply air enters the wet channel at a lower working ratio, the supply air enters the wet channel at a higher temperature, which results in lower relative humidity under identical absolute humidity working conditions. Subsequent interaction with the water film intensifies the mass and heat transfer, consequently leading to elevated entropy generation. Notably, entropy generation peaks at r = 0.1, where limited working air fails to sufficiently cool the dry air, leading to substantial entropy from mass transfer and evaporation processes.

As shown in Fig. 2.20 (a) to (d), increasing the working ratio leads to an upward trend in entropy generation across all layers. For both dry and wet air, the increase in working ratio has minimal impact on entropy generation caused by bulk flow. However, the temperature gradient between the air and channel plates ensures that convective heat transfer remains the dominant contributor to entropy generation. For the water film and channel plates, entropy generation rises with a higher working ratio, though the rate of increase decreases progressively. At r = 0.3, entropy generation linked to heat and mass transfer, as well as evaporation between wet air and water film, reaches a minimum, indicating optimized transfer processes and minimized irreversible heat loss.

At r = 0.1, the limited working air volume induces intense mass transfer evaporation in the wet channel, leading to a marked increase in entropy generation compared to other ratios. This imbalance raises the temperature gradient between the channel plate and air, further increasing convective heat transfer entropy.

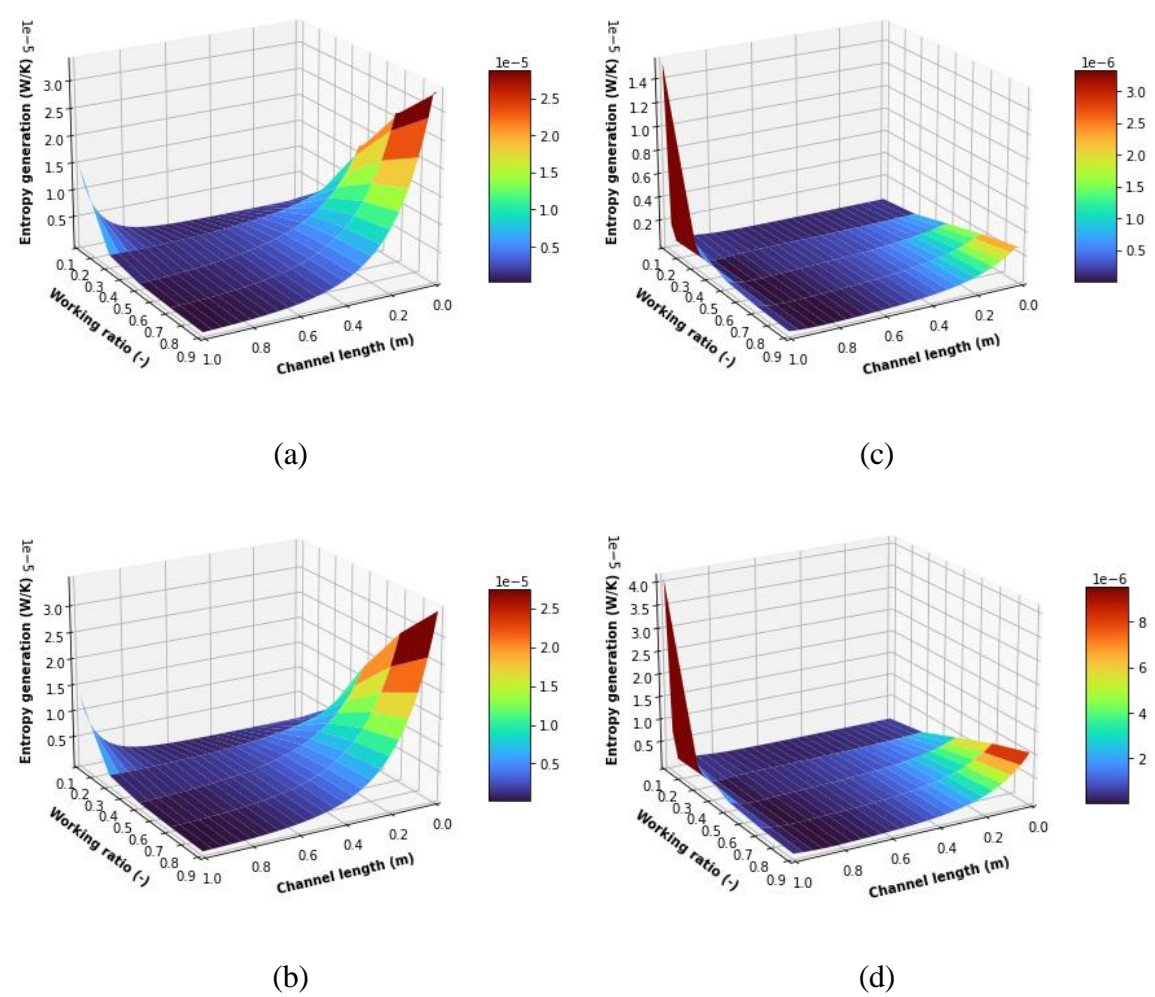
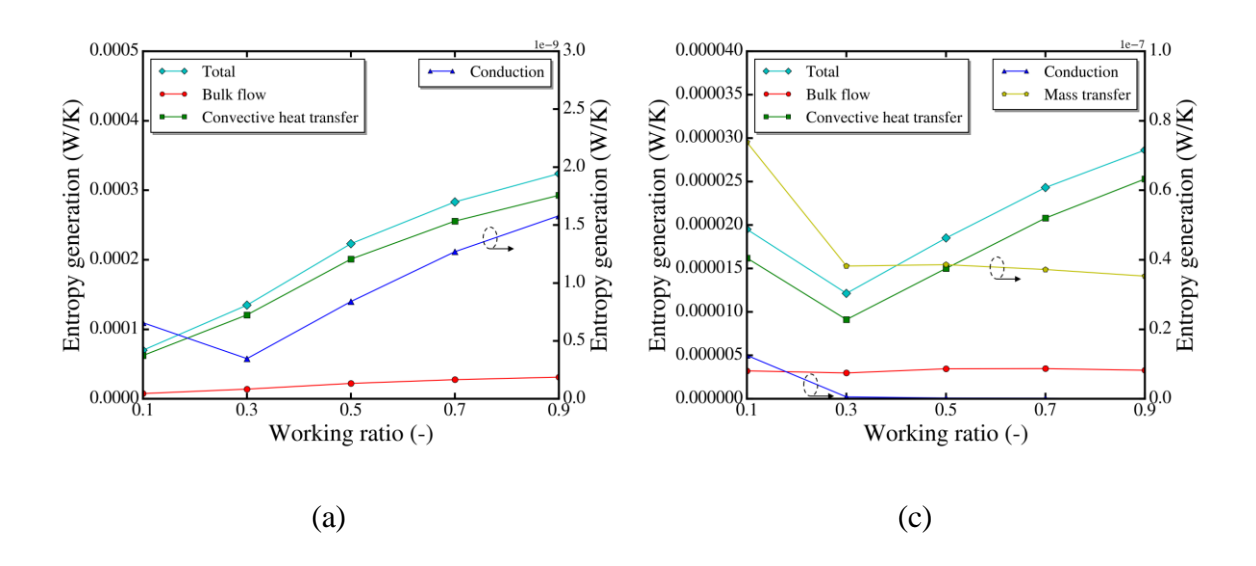


Fig. 2.19. The effects of different working ratio on entropy generation: (a) Dry channel air; (b) Channel plate; (c) Wet channel air; (d) Water film.



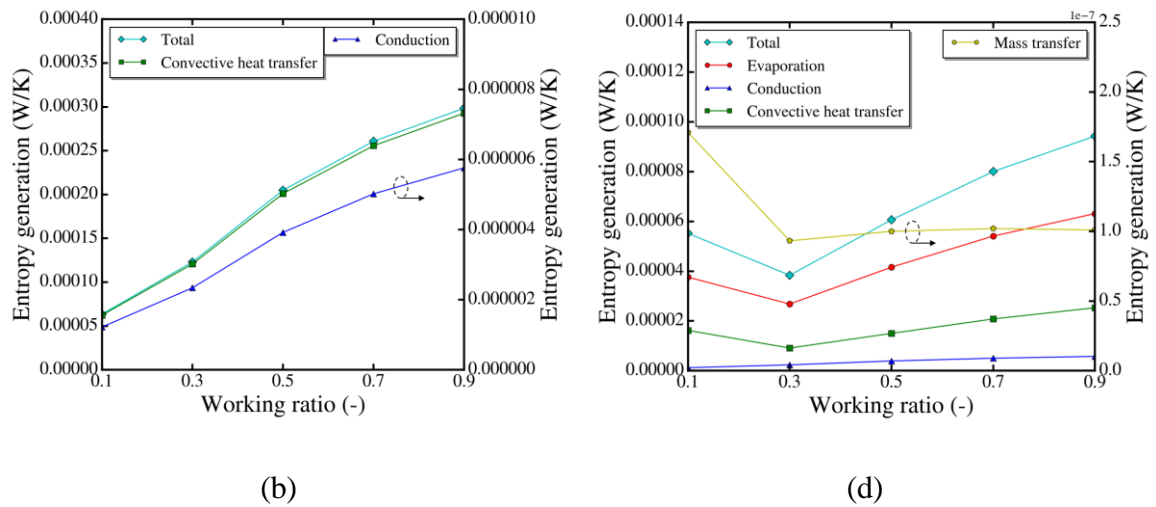


Fig. 2.20. Entropy generation involved in each layer at different working ratio: (a) Dry channel air; (b) Channel plate; (c) Wet channel air; (d) Water film.

In general, indirect evaporative coolers perform optimally at lower air velocities. In this section, the inlet air velocity is adjusted between 0.6 and 2.2 m/s, leading to notable changes in both the Nusselt and Reynolds numbers. As the velocity increases, the entropy generation in each layer of the DPEC also rises. Notably, the entropy generation in the wet air and water film is considerably higher than that in the channel plate and dry air, especially near the wet channel entrance. This observation highlights that the velocity of air entering the wet channel plays a crucial role in enhancing mass transfer processes, as depicted in Fig. 2.21 (a) to (d).

Fig. 2.22 (a) to (d) illustrates that as airflow velocity increases, the heat and mass transfer processes become less effective. This results in reduced heat loss for dry air and less heat gain for wet air, leading to a smaller temperature drop in the dry air and a milder temperature increase in the wet air. The diminished temperature difference between the inlet and outlet air reduces longitudinal heat conduction within the control volume. Conversely, the temperature difference between the air and channel plates within the channel increases, causing a rise in entropy generation from convective heat transfer. Additionally, the higher airflow velocity introduces

Thermodynamic and entropy generation analysis of the counter-flow dew-point evaporative cooling more unsaturated air into the control volume, further enhancing entropy generation due to mass transfer and evaporation processes.

As shown in Fig. 2.23 (a), system efficiency increases steadily with higher working ratios, though the efficiency gains diminish at elevated ratios. Fig. 2.23 (b) demonstrates that as inlet velocity rises, specific entropy generation also increases, leading to a decline in the system's wet-bulb efficiency. These observations underscore the importance of optimizing inlet air velocity to enhance the operational efficiency and performance of the DPEC system.

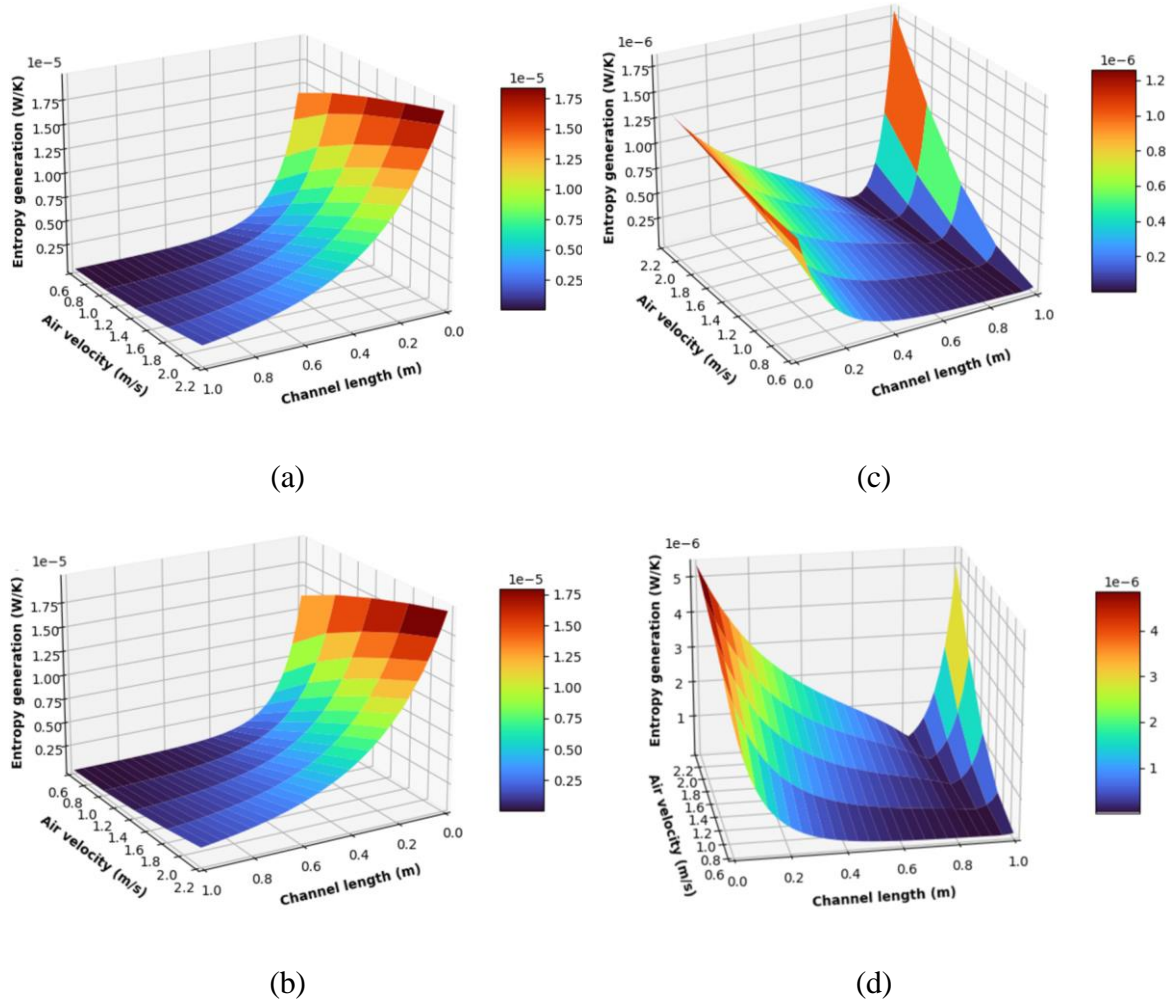


Fig. 2.21. The effects of different air velocity on entropy generation: (a) Dry channel air; (b) Channel plate; (c) Wet channel air; (d) Water film.

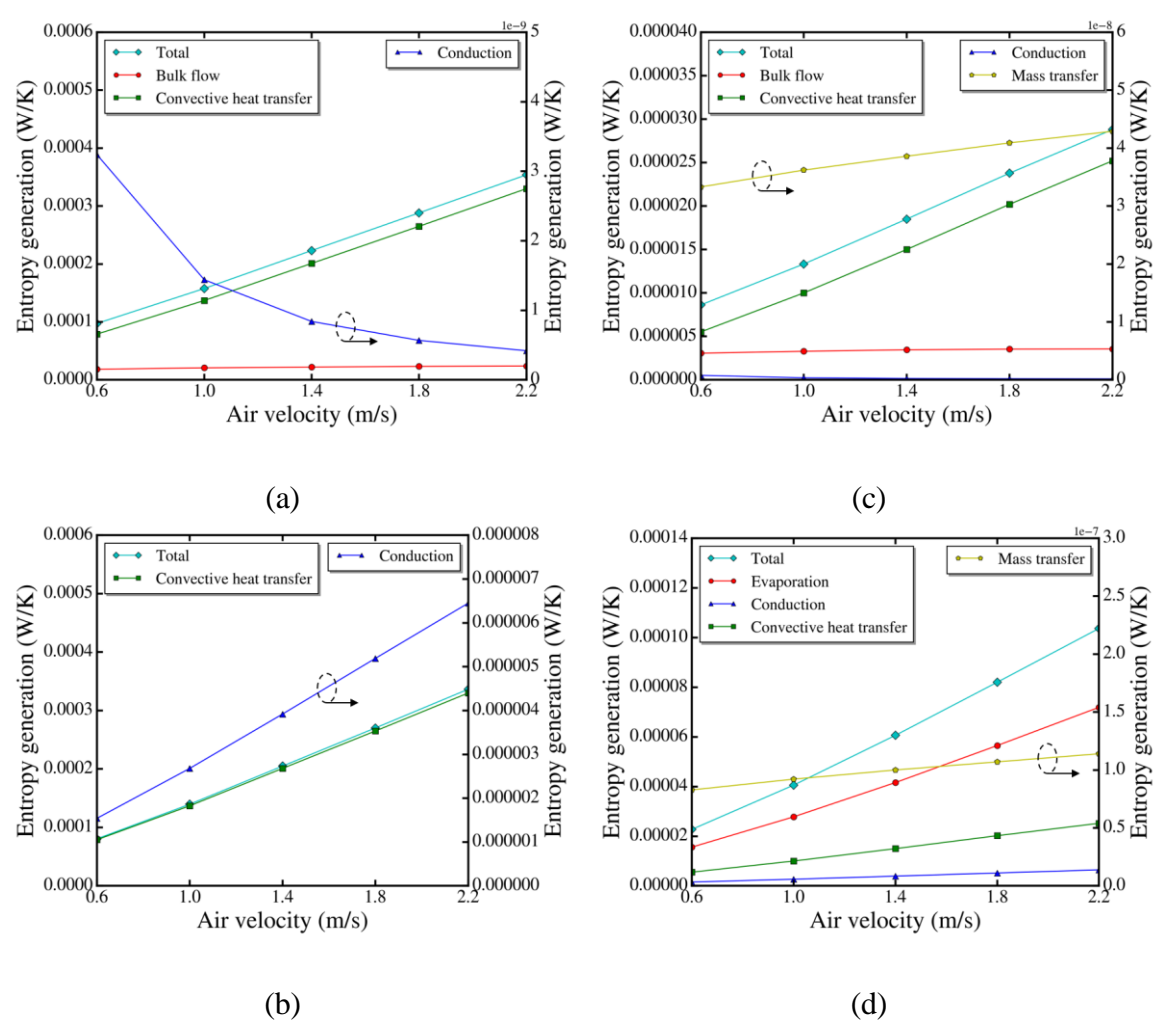


Fig. 2.22. Entropy generation involved in each layer at different inlet air velocity: (a) Dry channel air; (b) Channel plate; (c) Wet channel air; (d) Water film.

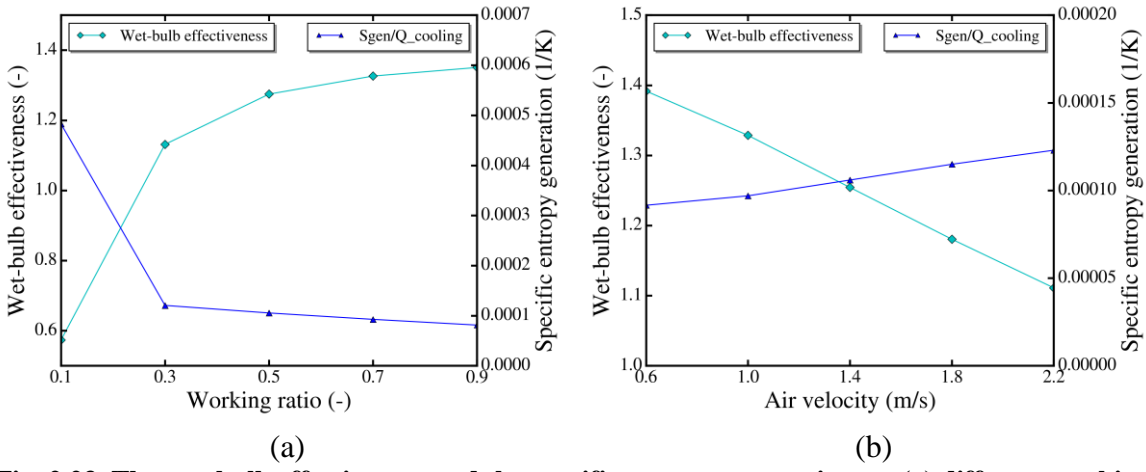
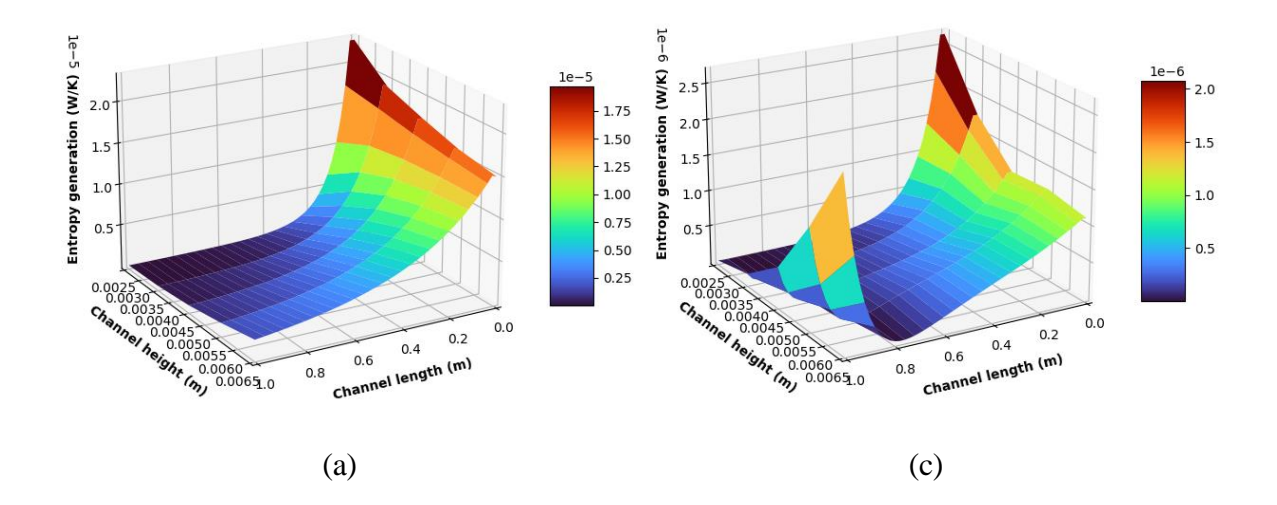


Fig. 2.23. The wet-bulb effectiveness and the specific entropy generation at: (a) different working ratio; (b) different inlet air velocity.

3) Effect of geometry

For the system's geometric dimensions, the effects of channel height and length on system performance are commonly analyzed. The system's entropy generation exhibits a higher sensitivity to variations in channel height, which ranges from 2.5 mm to 6.5 mm in this section. As shown in Fig. 2.24 (a) and (b), a smaller channel height results in a more significant temperature drop in the dry air, promoting stronger convective heat transfer and heat conduction, which leads to an increase in entropy generation. In contrast, as depicted in Fig. 2.24 (c) and (d), a larger channel height enhances the airflow rate, thereby reducing the effectiveness of heat and mass transfer processes within the channel. Consequently, at the entrance of the wet channel, the entropy generation of both wet air and the water film increases significantly with higher channel heights. Fig. 2.25 (a) further illustrates that an increased airflow rate improves convective heat transfer between the air and channel plate, but the reduced temperature gradient diminishes heat conduction in the dry air.



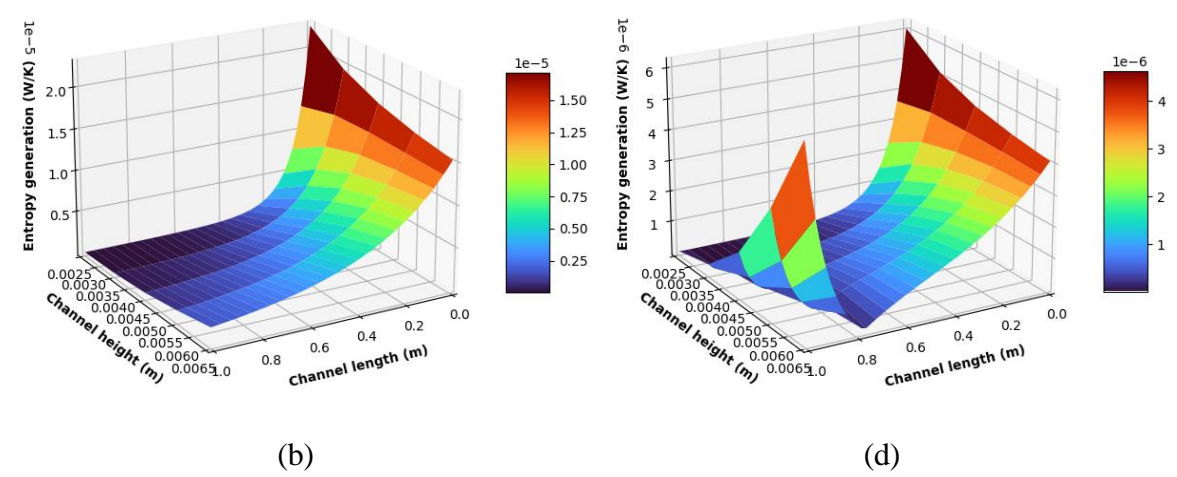


Fig. 2.24. The effects of different channel height on entropy generation: (a) Dry channel air; (b) Channel plate; (c) Wet channel air; (d) Water film.

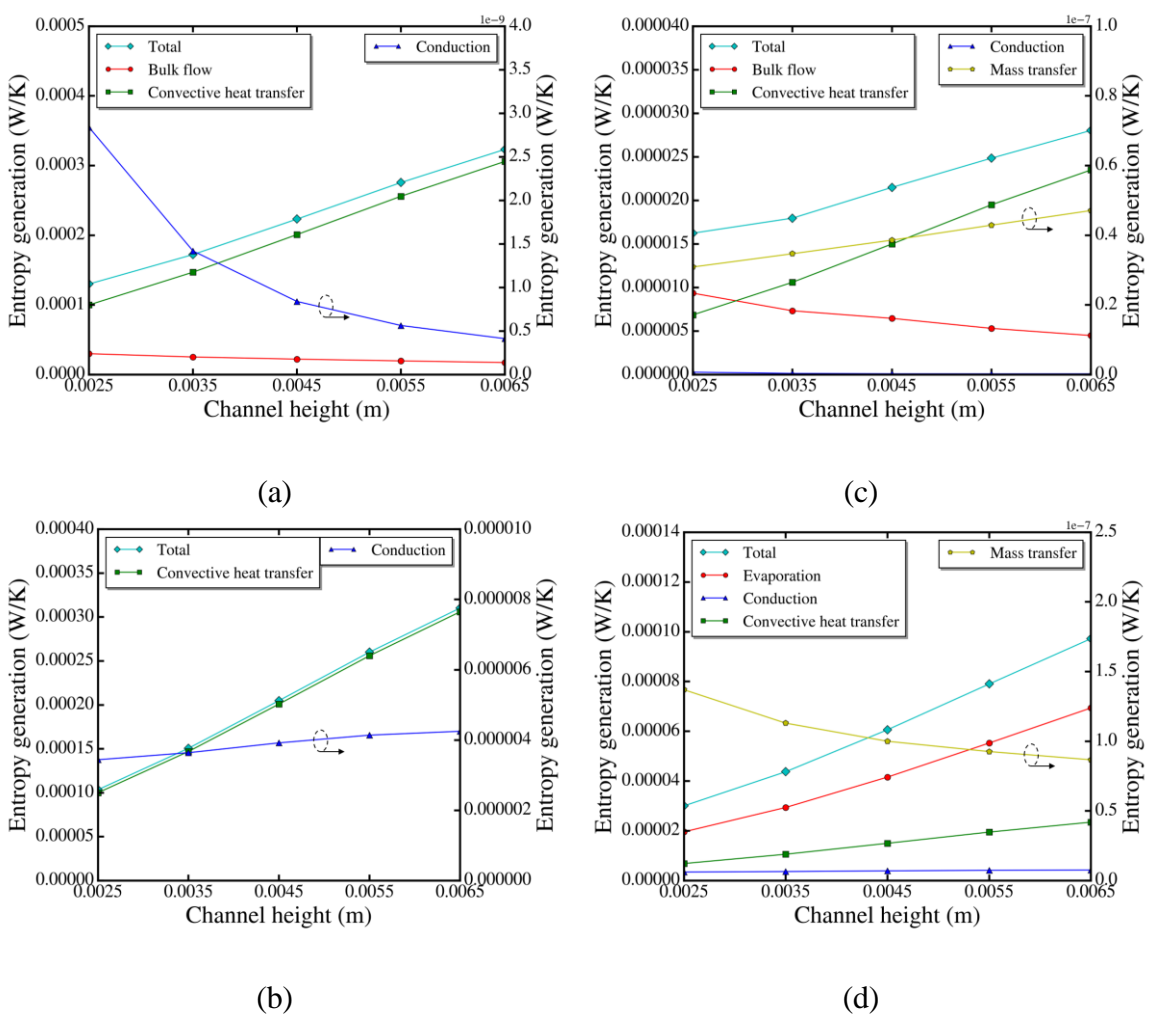


Fig. 2.25. Entropy generation involved in each layer at different channel height: (a) Dry channel air; (b) Channel plate; (c) Wet channel air; (d) Water film.

This section investigates the effect of channel length on system entropy generation, with the length ranging from 0.6 to 1 m. As illustrated in Fig. 2.26 (a) to (d), the influence of channel length on entropy generation across the dry air, plate, wet air, and water film layers is minimal, with no significant deviation in the overall trend. Furthermore, Fig. 2.27 (a) to (d) examines the effect of channel length on entropy generation in relation to the heat flow within each layer. As depicted in Fig. 2.28 (a), within the tested range, a shorter channel length correlates with improved system performance. Conversely, Fig. 2.28 (b) shows that increasing the channel length within the 0.6 to 1 m range leads to enhanced system performance.

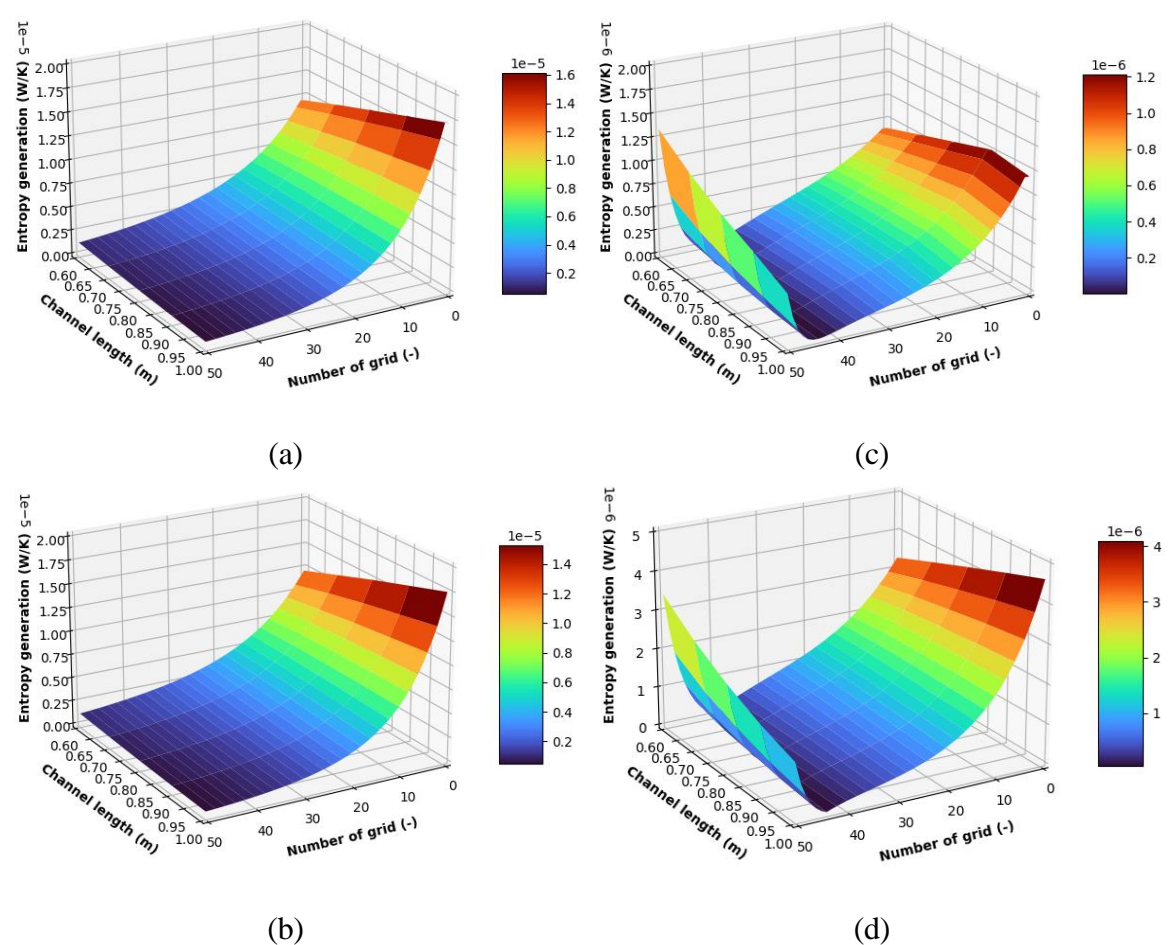


Fig. 2.26. The effects of different channel length on entropy generation: (a) Dry channel air; (b) Channel plate; (c) Wet channel air; (d) Water film.

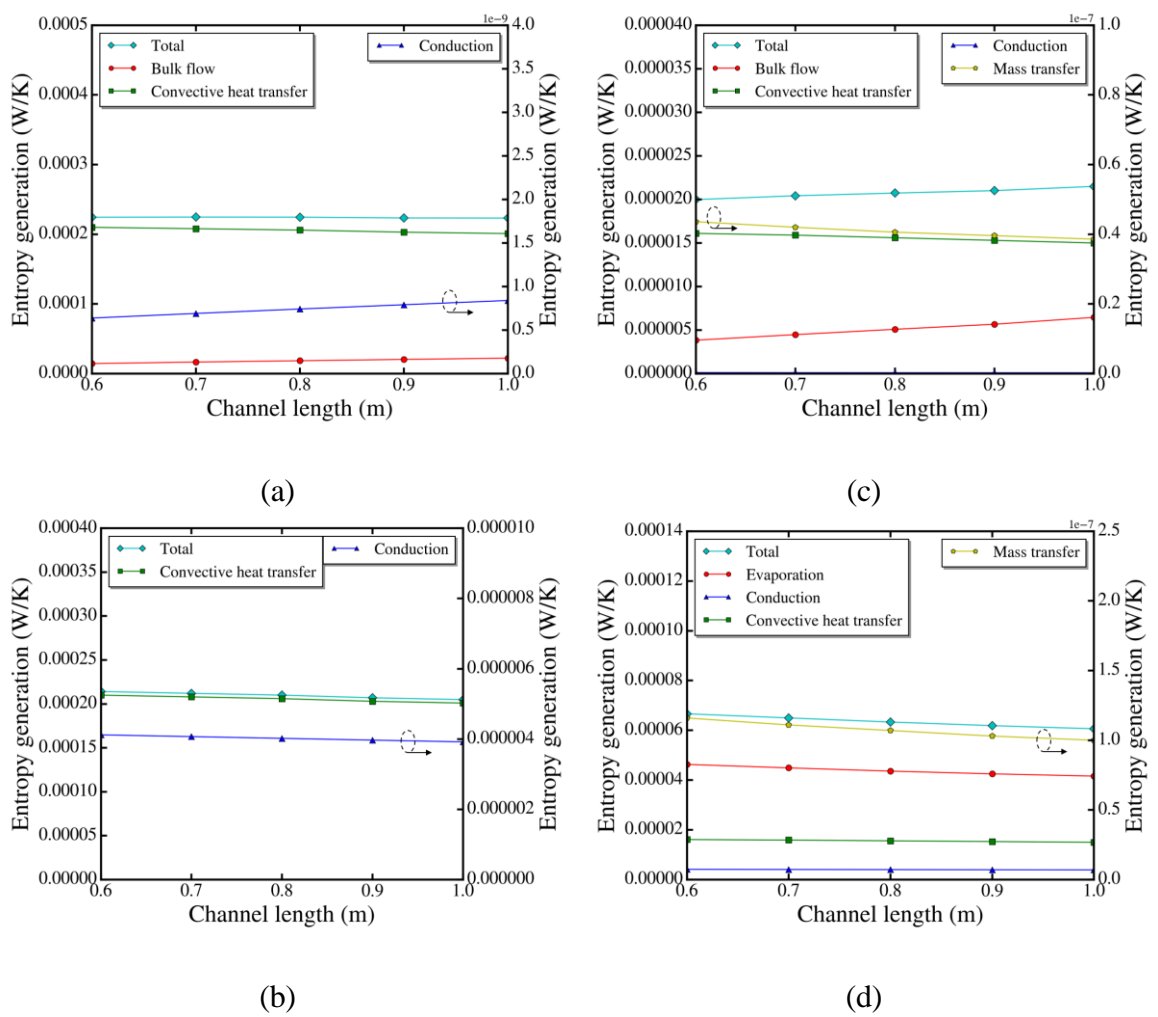


Fig. 2.27. Entropy generation involved in each layer at different channel length: (a) Dry channel air; (b) Channel plate; (c) Wet channel air; (d) Water film.

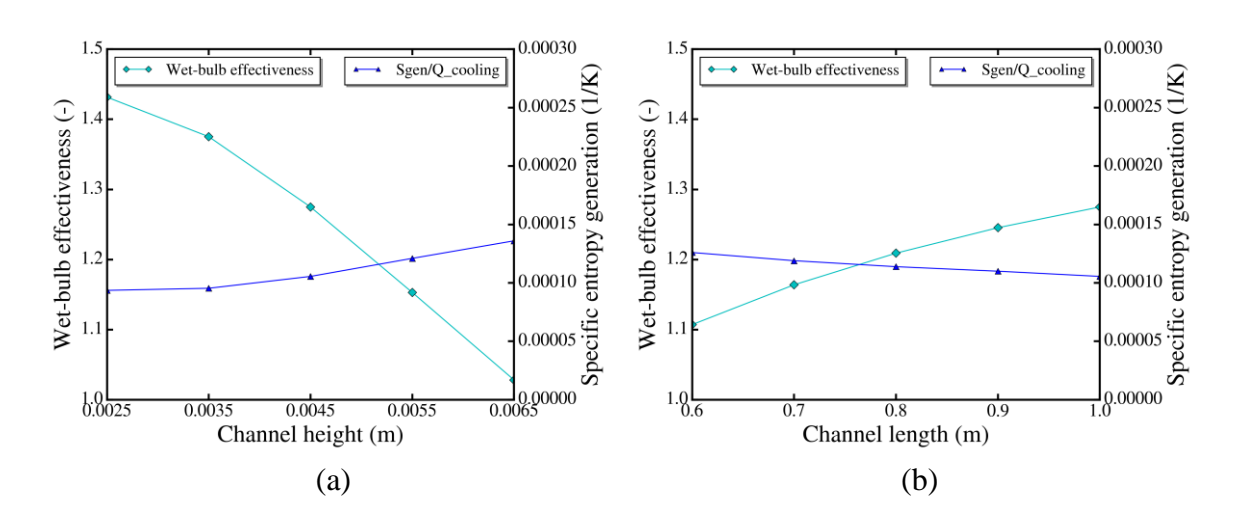


Fig. 2.28. The wet-bulb effectiveness and the specific entropy generation at: (a) different channel height; (b) different channel length.

2.5 Conclusions

A dynamic mathematical model for a counter-flow DPEC system has been developed to comprehensively analyze the mass and heat transfer processes, enabling a detailed second-law thermodynamic analysis. The model is specifically designed to generate transient entropy generation data for dry air, channel plates, wet air, and water film. This capability allows for a thorough assessment of methods to improve system efficiency. The parametric effects on the DPEC system have been systematically explored, offering valuable insights into optimizing the system's performance. Key findings from this study include:

- (1) Higher inlet air temperatures lead to a greater temperature differential across the DPEC system. As the inlet temperature increases from 25°C to 45°C, the wet-bulb efficiency slightly decreases from 1.277 to 1.268. Despite this small decrease, the larger temperature difference results in a significant increase in heat loss. Elevated inlet temperatures notably affect the entropy generation in both dry air and the channel plate, emphasizing the importance of optimizing the inlet temperature to sustain efficient system performance.
- (2) Higher inlet humidity limits the evaporation potential within the wet channel. For instance, at 30°C with 24 g/kg humidity, the wet-bulb temperature reaches 28.4°C, which, despite lower entropy generation, does not satisfy cooling requirements. In contrast, reducing the humidity to 16 g/kg improves the wet-bulb efficiency (1.24) and reduces heat loss, highlighting the importance of aligning humidity levels with cooling needs for optimal system performance.

- (3) An increased working ratio results in higher airflow to the wet channel, enhancing both heat and moisture transfer while lowering the supplied air temperature. However, this also leads to an increase in entropy generation. Optimal system performance was observed at a working ratio of 0.3, which strikes a balance between cooling efficiency and air supply volume, thus preventing excessive heat loss and maintaining a wet-bulb efficiency of 1.13.
- (4) Lower inlet air velocities promote improved mass and heat transfer within the channels, leading to reduced entropy generation. In contrast, higher velocities exacerbate entropy generation and decrease wet-bulb efficiency. A lower velocity (0.6 m/s) enhances system performance and minimizes thermal losses, although it requires more time to reach the desired cooling effect.
- (5) Increasing the channel length from 0.6 m to 1.0 m enhances wet-bulb efficiency from 1.107 to 1.275, improving system performance, albeit at the cost of increasing the system's size. Conversely, channel height has a significant impact on entropy generation. Lower heights, such as 2.5 mm, promote more efficient heat and mass transfer, resulting in a higher wet-bulb efficiency (1.432) and reduced heat loss. However, smaller air volumes may place additional strain on meeting cooling demands.

This section's entropy generation analysis, grounded in the second law of thermodynamics, provides a deeper understanding of the dew point evaporative cooling (DPEC) system. Further efforts could focus on conducting economic analyses to better connect these findings with practical engineering applications.

Chapter 3 Dew-point evaporative cooling of PV panels

3.1 Introduction

The rapid increase in non-renewable energy consumption presents a significant challenge to global energy and environmental sustainability [113–116]. Renewable energy has emerged as a primary approach to addressing these issues, has been developed with the aim of creating a sustainable future [117]. Among these sources, solar energy stands out due to its wide availability, environmental benefits, and versatile applications, offering substantial potential for large-scale utilization [118–121], by two main solar energy technologies: (1) solar thermal collectors which directly transforms solar radiation into thermal energy; (2) photovoltaics (PV) which can convert solar radiation into electrical energy via the photovoltaic effect [122,123]. A significant challenge for PV panels is their low conversion efficiency, which generally remains below 13% [124]. Most of the solar radiation absorbed is dissipated as heat, raising the surface temperature of PV cells and further diminishing their solar-to-electric conversion efficiency. Thus, implementing effective temperature control for PV panels is essential to boost energy conversion efficiency and extend the lifespan of PV cells, ultimately making solar energy more practical and affordable for communities worldwide.

Cooling methods for PV panels are generally categorized into active and passive systems [125,126]. Active cooling uses external fans or pumps to circulate coolant over the PV cells, while passive cooling relies on natural convection and does not require additional power. Studies on air-cooled PV panels have shown temperature reductions of around 15 K, enhancing output efficiency compared to uncooled panels [15–18]. However, the cooling capacity of air-

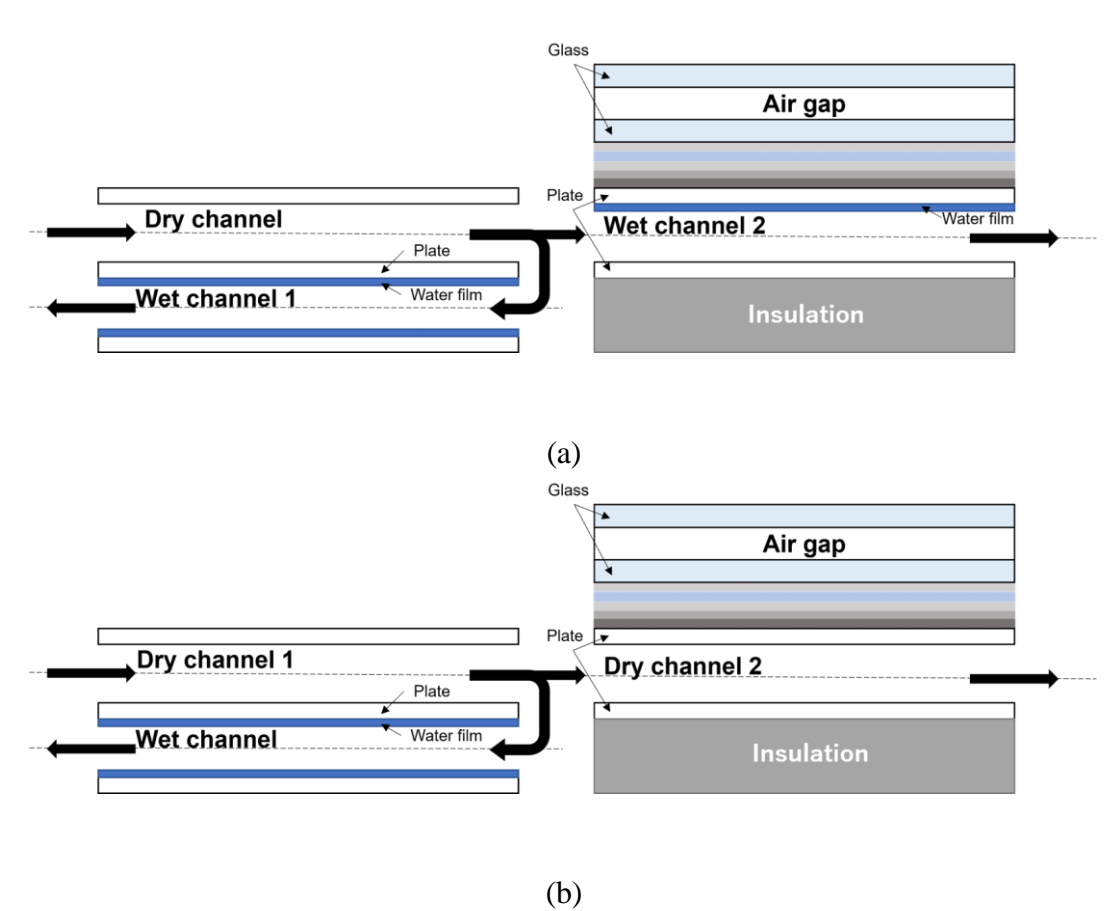
based systems is often insufficient to meet the heat dissipation requirements of PV panels effectively.

The DPEC system, an advanced form of indirect evaporative cooling, is capable of reducing air temperature below the wet-bulb level, demonstrating high performance and promising potential for PV panel cooling applications. Extensive studies have focused on the thermodynamic performance of DPEC systems, yet their application in PV cooling remains unexamined. Most current evaporative cooling designs for PV panels rely on conventional direct evaporative cooling, which provides limited effectiveness and cannot achieve temperatures below the wet-bulb threshold. Therefore, in this chapter, a novel PV panel cooling system using an enhanced DPEC configuration is developed. The proposed system includes a dedicated dew-point evaporative cooler that supplies near-saturated air to wet air channels attached to the back of the PV panels. System performance is compared with that of a PV panel cooled only by sensible air from a standard DPEC outlet. The enhanced system aims to improve cooling efficiency and heat removal from the PV panel. A numerical model is developed to analyze the system's transient performance, investigating dynamic behavior under historical hourly solar irradiance data.

3.2 Description of system

Fig. 3.1(a) illustrates the proposed configuration for cooling a PV panel using an enhanced DPEC. The system features a separate DPEC that supplies near-saturated cooled air to a wet channel attached to the back of the PV panel, where additional evaporative cooling occurs for optimal performance. The system incorporates two wet channels: one within the DPEC and the other at the back of the PV panel. To evaluate its superior cooling efficiency and resulting improvement in PV energy performance, the proposed system was compared with a traditional

DPEC-based PV, which uses air from a DPEC for sensible cooling, as shown in Fig. 3.2(b). The cooling processes of both systems are depicted on the psychrometric chart in Fig. 3.2(c).



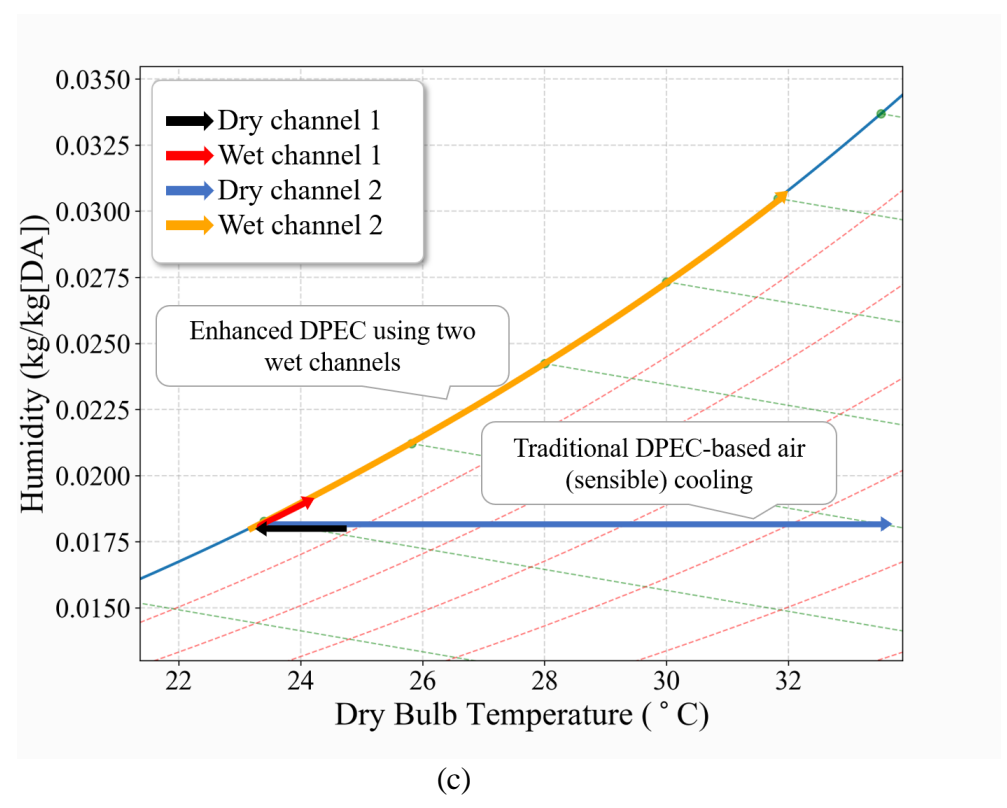


Fig. 3.1. Schematic diagram for solar PV cooling system: (a) enhanced DPEC using two wet channels; (b) traditional DPEC-based air sensible cooling; (c) temperature and humidity profiles for two systems on the psychrometric chart.

3.3 Methodology

3.3.1 Mathematical model

The PV module, comprising multiple layers [127], as shown in Fig. 3.2, is divided into identical elements using the grid meshing technique. Each element consists of a glass layer, PV cell layer, channel plate, water film, and wet channel. A transient model of the PV module with evaporative cooling is developed to analyze its dynamic behavior, based on the following assumptions:

- (5) The thermal properties of each solid layer are assumed to be constant.
- (6) The boundary of wet channel is well insulated thus the boundary thermal loss is negligible.

(7) Water on the wet channel surface is saturated and stagnant.

Environmental parameters, including solar irradiance, ambient air temperature, and wind speed, are obtained from Fukuoka, Japan's weather data with a one-hour temporal resolution. These data are fitted to analytical equations and utilized in the simulations. The proposed system consists of two components: a cooler unit and a PV unit, both of which are modeled in this chapter. The dynamic mathematical model for the DPEC is based on the work of Miyazaki et al [107], while the model for the PV unit follows the framework established by Guarracino et al. [128,129], as outlined below:

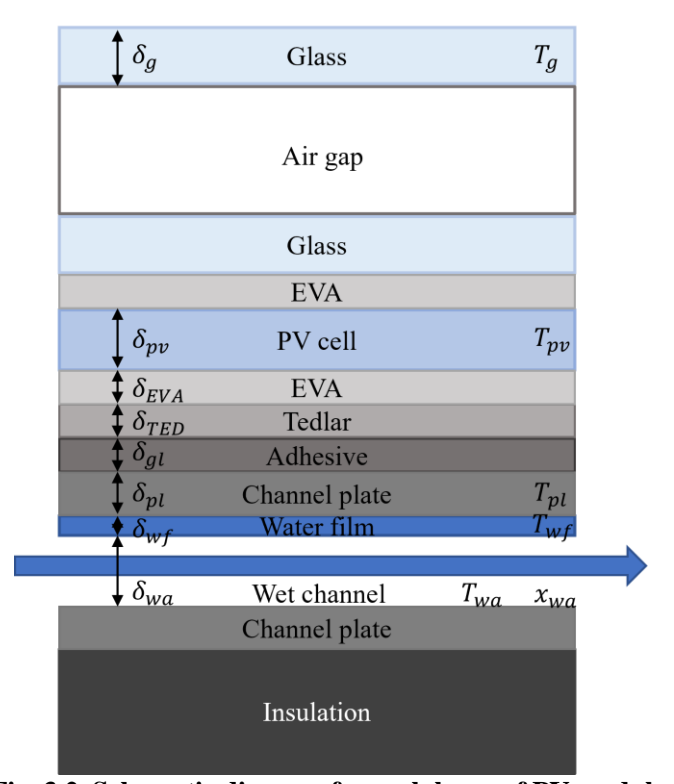


Fig. 3.2. Schematic diagram for each layer of PV module.

(5) Top glass

The energy balance equation for each glass layer element is given as:

Dew-point evaporative cooling of PV panels

$$\rho_{g}c_{g}\frac{dT_{g}}{dt} = k_{g}\frac{\partial^{2}T_{g}}{\partial x^{2}} - \frac{\varepsilon_{g}\sigma}{\delta_{g}}\left(T_{g}^{4} - T_{sky}^{4}\right) - \frac{h_{top}}{\delta_{g}}\left(T_{g} - T_{a}\right)$$

$$+ \left(\frac{1}{\frac{1}{\varepsilon_{g}} + \frac{1}{\varepsilon_{pv}} - 1}\right)\frac{\sigma}{\delta_{g}}\left(T_{pv}^{4} - T_{g}^{4}\right) - \frac{1}{\delta_{g} \cdot R_{gap}}\left(T_{g} - T_{pv}\right)$$

$$+ \frac{\overline{\tau\alpha_{g}}G}{\delta_{g}}$$

$$(1)$$

The terms on the right-hand side of Eq. (1) represent the conductive heat flux, radiative heat loss, convective heat loss to the ambient, convective and radiative heat transfer to the PV cell, and the heat absorbed from solar radiation, respectively. The radiative heat loss term requires the sky temperature, which is calculated using Eq. (2) as [130]:

$$T_{sky} = 0.0522T_a^{1.5} (2)$$

The convective heat loss to the ambient is governed by the surrounding temperature and the convective heat transfer coefficient, h_{top} , as given in Eq. (3) [131]. The heat transfer coefficient for forced air flow, h_w , is determined by the wind speed, as shown in Eq. (4) [132]. The heat transfer coefficient for free convection, h_{free} , is calculated using Eq. (5) which is related to the Nusselt number Nu in Eq. (6), where $Ra_c = 10^8$, $\gamma = 45^\circ$ [133]. Ra is expressed in Eq. (7) with $\beta = 3.22 \times 10^{-3}$ [134].

$$h_{top}^3 = h_w^3 + h_{free}^3 \tag{3}$$

$$h_w = 3v_w + 2.8 (4)$$

$$h_{free} = \frac{Nu_{free}k_a}{L_{PV}} \tag{5}$$

$$Nu_{free} = 0.56 \left(Ra_c cos \gamma^{0.25} + 0.13 \left(Ra^{0.333} - Ra_c^{0.333} \right) \right)$$
 (6)

$$Ra = Pr \frac{g\beta (T_g - T_a)L_{PV}^3}{V^2}$$
 (7)

The thermal resistance R_{gap} between the top glass and PV cell is expressed in Eq. (8) and the convective heat transfer coefficient h_{gap} is calculated in Eq. (9).

$$R_{gap} = \frac{\delta_g}{2k_g} + \frac{1}{h_{gap}} + \frac{\delta_g}{k_g} + \frac{\delta_{EVA}}{k_{EVA}} + \frac{\delta_{PV}}{2k_{PV}} \tag{8}$$

$$h_{gap} = \frac{k_{air}}{\delta_{gap}} \left[1 + 1.44 \left(1 - \frac{1708}{Racos\gamma} \right)^* \left(1 - \frac{1708(sin1.8\gamma)^{1.6}}{Racos\gamma} \right) + \left(\left(\frac{Racos\gamma}{5830} \right)^{0.33} - 1 \right)^* \right]$$
(9)

In Eq. (9), the value of the term with superscript '*' is equal to zero when they are negative.

(6) PV panel

The energy balance for each PV cell element is expressed as:

$$\rho_{PV}c_{PV}\frac{dT_{PV}}{dt} = k_{PV}\frac{\partial^2 T_{PV}}{\partial x^2} - \left(\frac{1}{\frac{1}{\varepsilon_g} + \frac{1}{\varepsilon_{pv}} - 1}\right)\frac{\sigma}{\delta_{PV}}\left(T_{pv}^4 - T_g^4\right) + \frac{1}{\delta_{PV} \cdot R_{gap}}\left(T_g - T_{pv}\right) + \frac{\overline{\tau}\alpha_{PV}G}{\delta_{PV}}$$

$$-\frac{1}{\delta_{PV} \cdot R_{gap}}\left(T_{PV} - T_{pl}\right) - \frac{G\eta_T}{\delta_{PV}}$$
(10)

The right-hand side of the equation accounts for the conductive, radiative, and convective heat transfer to the top glass, the heat absorbed by the top glass, the heat conduction to the channel plate, and the electrical energy conversion. Due to the multiple layers between the PV cell and channel plate, the lumped thermal resistance model for these layers is used, as expressed in Eq. (11).

$$R_{ad} = \frac{\delta_{EVA}}{k_{EVA}} + \frac{\delta_{TED}}{k_{TED}} + \frac{\delta_{gl}}{k_{gl}}$$
(11)

Here, δ_{EVA} , δ_{TED} and δ_{gl} are the thicknesses of encapsulant, tedlar and adhesives layers, respectively. The electricity conversion term in Eq. (10) depends on the conversion efficiency, η_T , which can be commonly calculated as [135,136]:

Dew-point evaporative cooling of PV panels

$$\eta_T = \eta_{ref} \left[1 - \beta_{PV} \left(T_{PV} - T_{ref} \right) \right] \tag{12}$$

The temperature coefficient β_{PV} in Eq. (12) is normally given the value of 0.0045 while the standard solar cell efficiency η_{ref} is around 0.17, and the reference temperature is 25 °C [137].

(7) Channel plate

In the wet channel case (Fig. 2(a)), the conductive heat transfer occurs between the plate and the water film, while in the dry channel case (Fig. 2(b)), the convective heat transfer happens between the channel plate and the air stream. The energy balance equation of the channel plate is expressed as follows.

Wet channel case:

$$\rho_{pl}c_{pl}\frac{\partial T_{pl}}{\partial t} = \frac{1}{\delta_{pl} \cdot R_{ad}} \left(T_{PV} - T_{pl} \right) + \frac{k_e}{\delta_{pl}\delta_e} \left(T_{wf} - T_{pl} \right) \tag{13}$$

Dry channel case:

$$\rho_{pl}c_{pl}\frac{\partial T_{pl}}{\partial t} = \frac{1}{\delta_{pl} \cdot R_{ad}} \left(T_{PV} - T_{pl} \right) - \frac{h_{da}}{\delta_{pl}} \left(T_{pl} - T_{da} \right) \tag{14}$$

Here, ρ is the density, c is the specific heat, Ra is the Rayleigh number, k is the thermal conductivity and h is the convective heat transfer coefficient.

(8) Water film

The energy balance equation of water film is given as:

$$\rho_{wf}c_{wf}\frac{\partial T_{wf}}{\partial t} = \frac{k_e}{\delta_{wf}\delta_e} (T_{pl} - T_{wf}) + \frac{h_{wa}}{\delta_{wf}} (T_{wa} - T_{wf})$$

$$-\frac{\rho_{wa}h_mh_{fg}}{\delta_{wf}} (x_{wf} - x_{wa})$$
(15)

 h_{fg} in Eq. (15) is the latent heat of water evaporation which is calculated by CoolProp library [109].

(9) Channel air

As both heat and mass transfer processes are involved inside the wet channel, the energy and mass balances for the wet air can be given by:

$$\rho_{wa}c_{wa}\frac{\partial T_{wa}}{\partial t} = k_{wa}\frac{\partial^2 T_{wa}}{\partial x^2} + \frac{h_{wa}}{\delta_{wa}}(T_{wf} - T_{wa}) - u_{wa}\rho_{wa}c_{wa}\frac{\partial T_{wa}}{\partial x}$$
(16)

$$\frac{\partial x_{wa}}{\partial t} = D_{ab} \frac{\partial^2 x_{wa}}{\partial x^2} - u_{wa} \frac{\partial x_{wa}}{\partial x} + \frac{h_m}{H} (x_{wf} - x_{wa})$$
(17)

For the mass balance, there is a mass transfer between the water film and the wet air while the humidity of the water film, x_{wf} , is considered saturated and can be obtained from the CoolProp library [109]. The mass transfer coefficient, h_m , is computed using an empirical equation. The heat transfer coefficient, h_{wa} , is calculated by the analogy of Nusselt number and Sherwood number. The latter is related to the mass transfer coefficient.

Heat transfer inside the dry channel case only involves sensible heat and the energy balance equation of dry air is given by:

$$\rho_{da}c_{pda}\frac{\partial T_{da}}{\partial t} = -u_{da}\rho_{da}c_{pda}\frac{\partial T_{da}}{\partial x} + \frac{h_{da}}{\delta_{da}}(T_{pl} - T_{da})$$
(18)

3.3.2 Performance evaluation

The electrical output of the system can be evaluated by the energy conversion efficiency that is given in Eq. (12) and the cooling improvement can be expressed by the air temperature difference of the supply air under two different cooling methods, with the equation given as below:

Dew-point evaporative cooling of PV panels

$$\eta_{th} = \frac{\dot{m}c_{air}(T_{air_ec} - T_{air_ac})}{GA} \tag{19}$$

Here, G represents the solar irradiance and A is the area of the PV panel.

3.3.3 Simulation scheme

Numerical simulations of the evaporative cooling system are performed by solving Eqs. (1), (10), (13), (15), (16), and (17), while the air-cooling system is modeled using Eqs. (1), (10), (14), and (18) as described in Section 3.3.1. The geometric parameters of the PV module are provided in Table 3.1, and the optical and thermal properties are listed in Table 3.2. The following boundary conditions are applied in the simulation:

(4) The inlet conditions of dry channel 2 for air-cooling system:

$$T_{da\ in} = T_{supply}, x_{da} = x_a \tag{20}$$

where the supplied air temperature T_{supply} is the air temperature supplied by the DPEC system.

(5) The inlet condition of wet channel 2 for evaporative cooling system:

$$T_{wa\ in} = T_{sunnly}, x_{wa} = x_a \tag{21}$$

(6) The boundary conditions for other layers of the PV module are given as:

$$\frac{dT_g}{dx}\Big|_{x=0} = \frac{dT_g}{dx}\Big|_{x=L} = \frac{dT_{PV}}{dx}\Big|_{x=0} = \frac{dT_{PV}}{dx}\Big|_{x=L} = \frac{dT_{pl}}{dx}\Big|_{x=0} = \frac{dT_{pl}}{dx}\Big|_{x=L} = \frac{dT_{wf}}{dx}\Big|_{x=0}$$

$$= \frac{dT_{wf}}{dx}\Big|_{x=L} = 0$$
(22)

The finite difference method was employed to solve the partial differential equations in the PV model using a Python-based nonlinear optimization approach. The DPEC model was

validated against experimental data from Miyazaki et al [107] and Yang et al [138]. The length direction was discretized into 50 elements, with the time step determined by the weather data.

Table 3.1 Geometrical parameters of PV module.

-	
Parameters	Value
Glass thickness δ_g (mm)	4
PV cell thickness δ_{PV} (mm)	0.35
EVA thickness δ_{EVA} (mm)	0.5
Tedlar thickness δ_{TED} (mm)	0.05
Adhesive thickness δ_{gl} (mm)	0.05
Channel plate thickness $\delta_{pl}(\text{mm})$	0.125
Wall thickness(mm)	0.45
Channel length(m)	0.6-2.2
Channel width(mm)	83
Channel height(mm)	3.0-9.0
Working air ratio	0.5

Table 3.2 Optical and thermal properties of layers.

Layer	Parameters	Value	Unit	Refs.
Glass	c_g	750	J/kg K	[139]
	k_g	1.8	W/m K	[140]
	$arepsilon_g$	0.9	-	[140]
	$\overline{ aulpha_g}$	0.71	-	[141]
	$ ho_g$	2500	kg/m^3	-
PV cell	c_{PV}	677	J/kg K	[140]
	k_{PV}	149	W/m K	[140]
	$arepsilon_{PV}$	0.9	-	[140]

	$\overline{ aulpha_{PV}}$	0.84	-	[142]
	$ ho_{PV}$	2329	kg/m^3	-
EVA	k_{EVA}	0.35	W/m K	[142]
Tedlar	k_{TED}	0.2	W/m K	[142]
Adhesive	k_{gl}	0.85	W/m K	[142]
Channel plate	c_{pl}	1100	J/kg K	-
	$ ho_{pl}$	1200	kg/m ³	-

3.3.4 Ambient condition

The ambient conditions, including solar irradiance, wind speed and ambient temperature, are inputs to the model. They are based on the weather data of Fukuoka, Japan with one-hour temporal resolution. Several studies [82,143] have highlighted the advantages of using fitted equations: (1) they can be easily modified to accommodate different operating conditions, (2) they help smooth irregular data, making trends more apparent, and (3) they reduce model complexity, saving computation time. Consequently, a set of fitted equations is employed as the initial conditions in this chapter. The hourly data distribution and fitted equations are shown in Fig. 3.3, and an example of the fitted equations for the weather data on the 1st August is as follows:

$$G = \frac{1}{0.0000372(t - 13.3)^2 + 0.000698} - 19t \tag{23}$$

$$u_w = 0.00000114e^{-1.02t + 7.82t^{0.5}} + 2.54 (24)$$

$$T_a = 6.07e^{\frac{(\log t - 2.56)^2}{-0.203}} + 29.7 \tag{25}$$

t in Eq. (23), (24) and (25) represents the current time of 1st August.

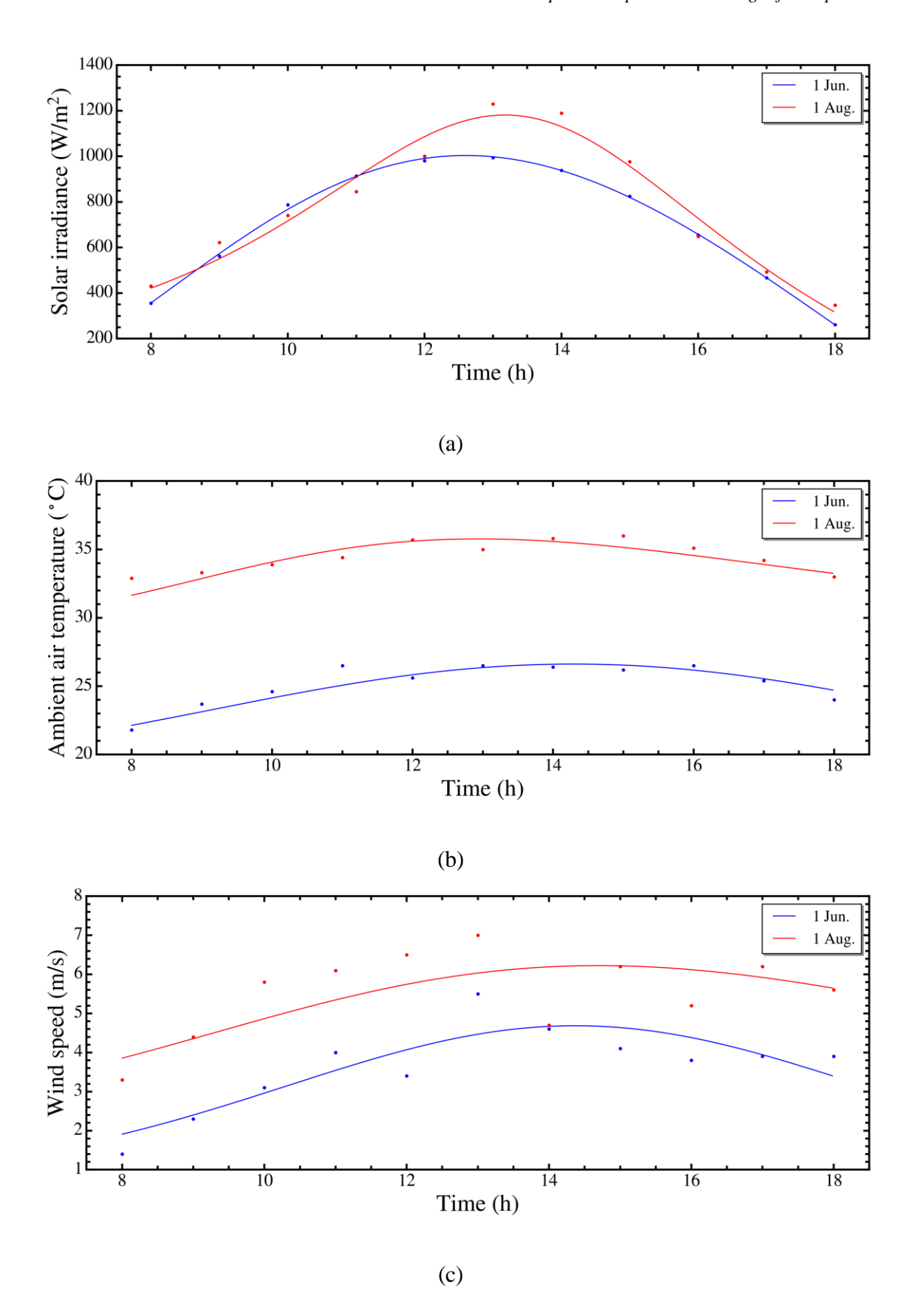
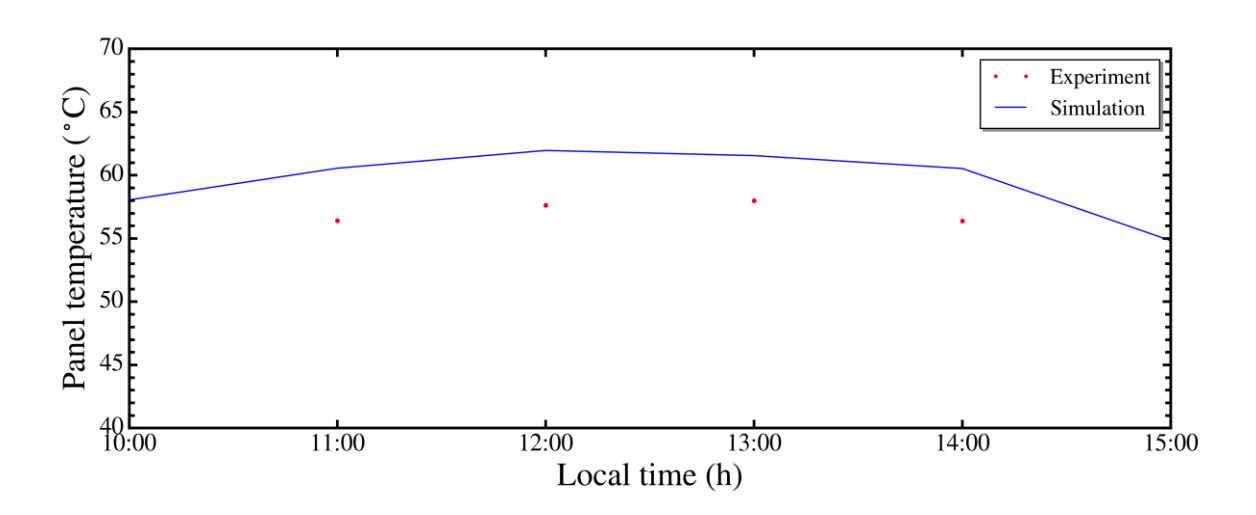


Fig. 3.3. Comparison of local weather data on the 1st June and 1st August with the fitted equations: (a) solar irradiance, (b) ambient air temperature; (c) wind speed.

3.3.5 Model validation

The proposed transient model was validated against experimental data from the literature. Mahmood et al. [82] conducted an experimental study on a hybrid photovoltaic evaporative cooling system utilizing a cellulose cooling pad. Various local weather parameters, including solar irradiance, ambient temperature, wind speed, and supply air temperature, were used to assess the system's cooling performance. The model was validated using their experimental data from July 2nd and 3rd, as shown in Fig. 3.4. The results indicate that the model predicts PV panel temperature with a discrepancy ranging from 2.6% to 7.8%. However, several challenges remain for this model, such as: (1) reliance on simplified assumptions regarding the physical system, (2) potential inconsistencies in the boundary conditions for the partial differential equations, and (3) the lack of experimental data for the proposed system, despite validation of the DPEC and direct evaporative cooling models. Nevertheless, the model demonstrates reasonable accuracy in predicting PV panel performance.



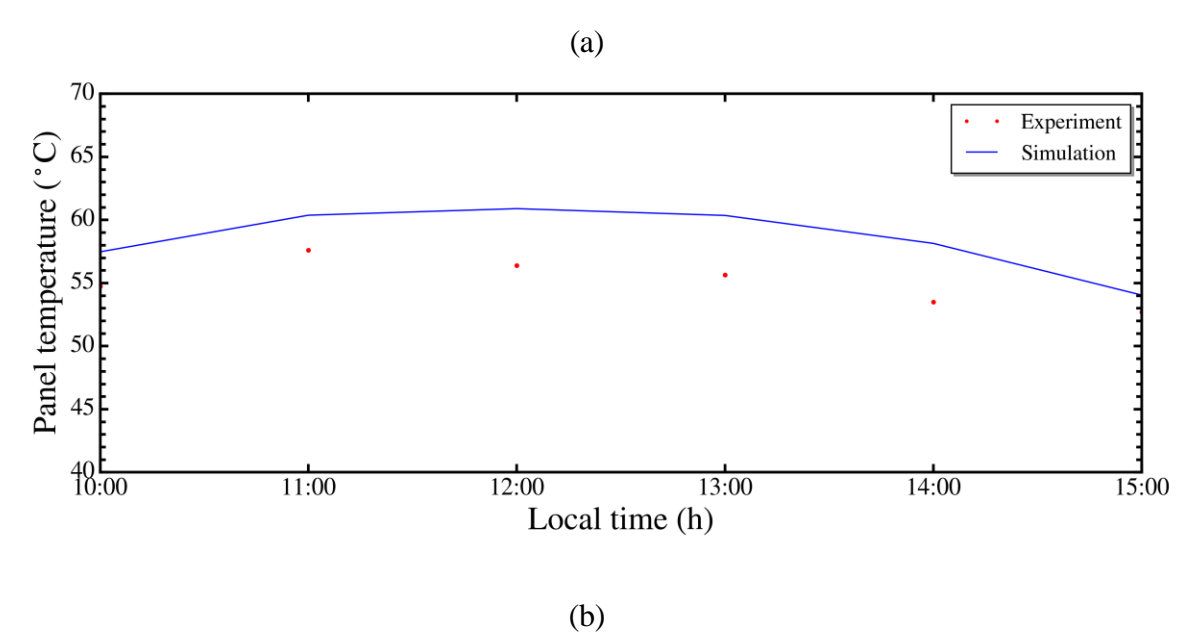


Fig. 3.4. Model validation with local weather data from Mahmood et al. [82]: (a) July 2nd; (b) July 3rd.

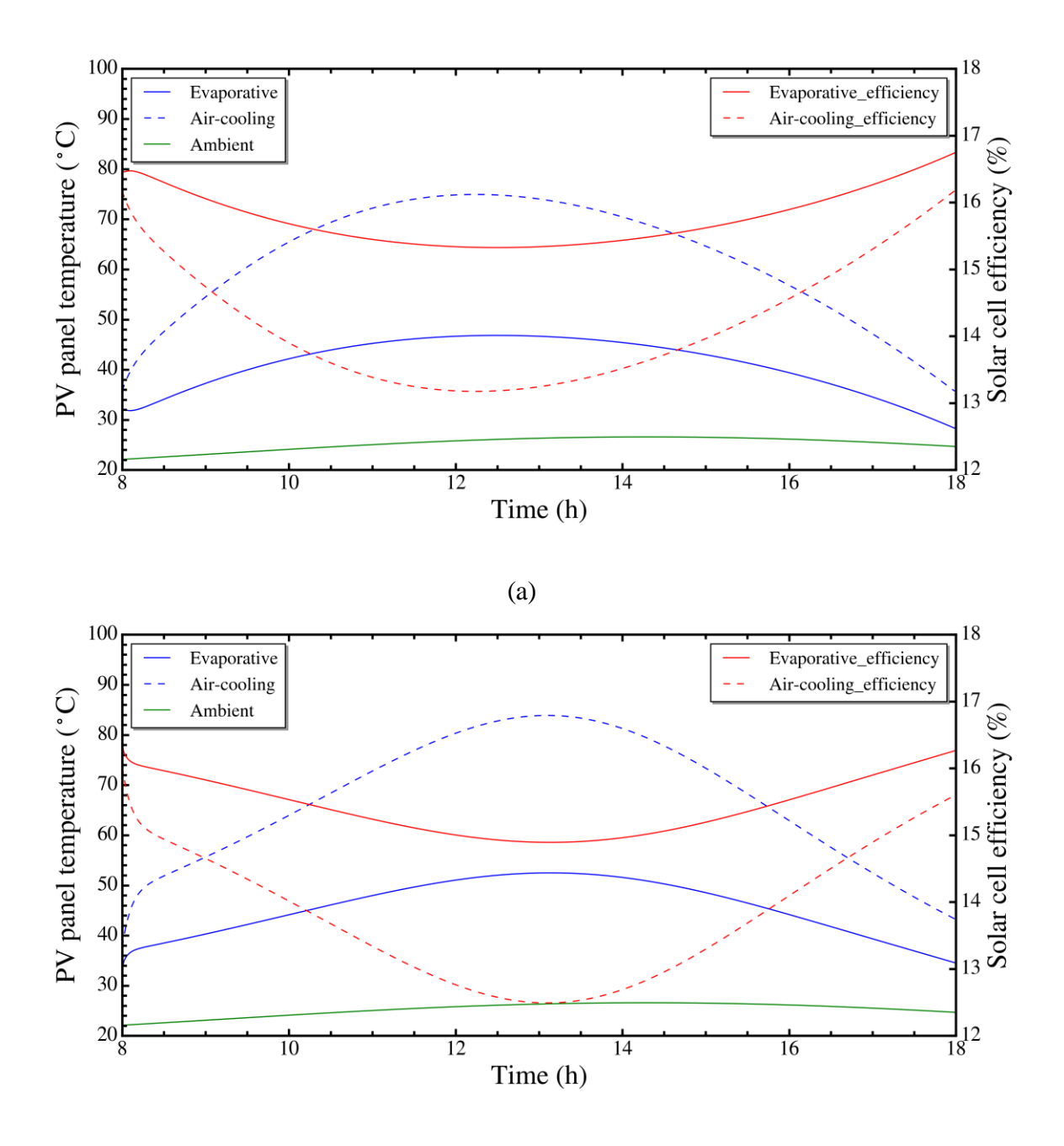
3.4 Results and discussion

3.4.1 Comparison of evaporative cooling and air-cooling system

The dynamic behaviors of the PV panels with two different cooling configurations are shown in Fig. 3.5. Based on the hourly data from 1st June from 8:00 to 18:00 h, The temperature distribution of the PV panel generally follows the solar irradiance pattern. With the proposed cooling system (enhanced DPEC with two wet channels), the PV panel achieves higher efficiency than with the sensible DPEC cooling (using air from a DPEC), as its maximum temperature remains at 47 °C, compared to 75 °C in the latter. Minimum temperatures are 28 °C and 36 °C for the enhanced and sensible DPEC systems, respectively.

Efficiency curves show a maximum solar cell efficiency of 16.7% on June 1st, approximately 16.4% higher than with sensible air cooling. The minimum efficiency is 15.3%, 1.9% higher than that of the sensible air-cooled case. Enhanced evaporative cooling improves PV efficiency, as illustrated in Fig. 3.6, where efficiency is plotted against the reduced

temperature $T_r = \frac{T_{air_in} - T_{ambient}}{G}$. As the value of Tr increases, the temperature difference between inlet air and ambient narrows, resulting in reduced heat transfer effectiveness and lower efficiency. However, the enhanced DPEC cooling shows less efficiency drop compared to sensible cooling, indicating superior performance. Additionally, PV efficiency is higher in June, driven by lower surface temperatures associated with reduced solar irradiance.



(b)

Fig. 3.5. Comparison of temperature and solar cell efficiency of PV based on hourly irradiance data with evaporative cooling and air cooling: (a) 1st June; (b) 1st August.

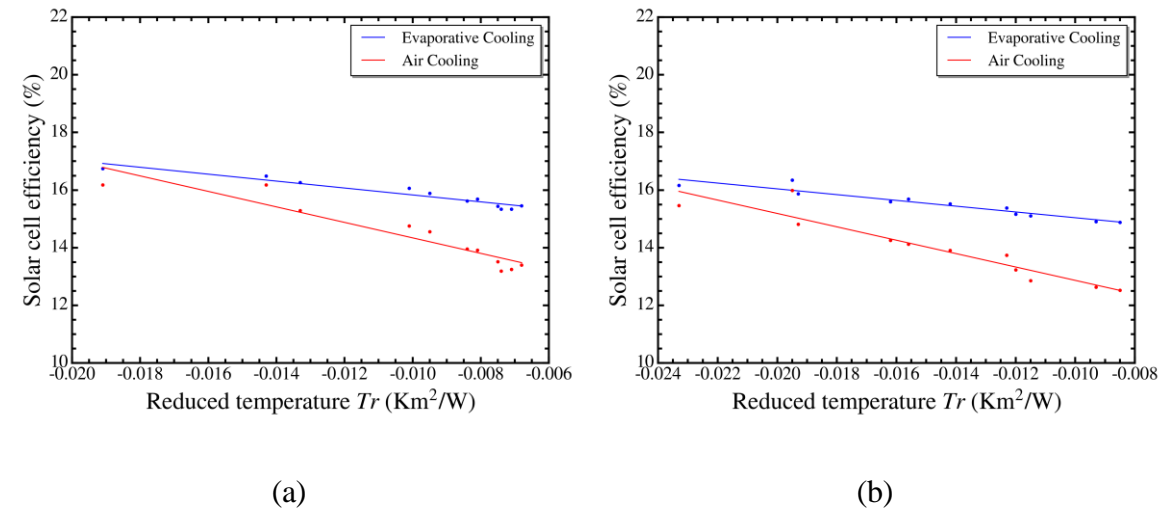


Fig. 3.6. Solar cell efficiency of two cooling configurations based on: (a) 1st June; (b) 1st August.

Fig. 3.7 illustrates the thermal efficiency gains when replacing sensible air cooling with the proposed evaporative cooling. The key distinction between the two systems lies in the air temperature within the PV panel's air channel. Thermal efficiency improvement is defined as the difference in heat removal between evaporative and sensible cooling, relative to the panel's heat gain from solar energy. Using data of 1st June (from Fig. 3.5), he maximum and minimum temperature differences between the cooling methods reach 25.45 °C and 3.96 °C, respectively. Under evaporative cooling, air temperature ranges from 26.73 °C to 40.24 °C throughout the day. This results in a thermal efficiency increase of up to 19.9%, with a minimum improvement of 13.7%, demonstrating that the proposed DPEC system provides notable efficiency enhancements.

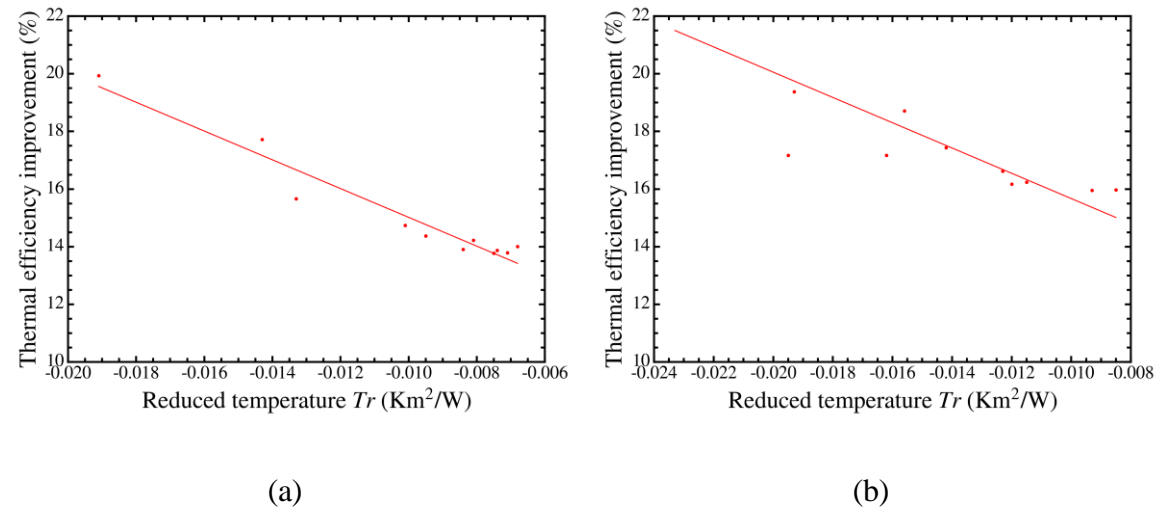
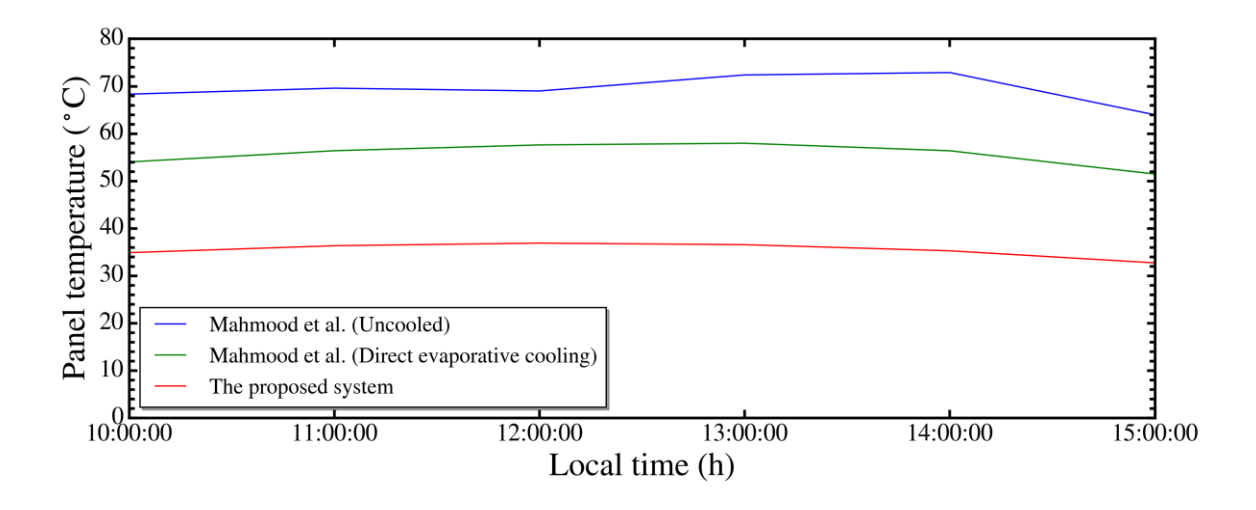


Fig. 3.7. Thermal efficiency improvement based on the weather data of: (a) 1st June; (b) 1st August.

Additionally, the performance of the proposed enhanced DPEC system with dual wet channels is compared with two other cooling methods: direct evaporative cooling and no cooling, based on Mahmood et al. [82] as shown Fig. 3.8. The enhanced DPEC system achieves a PV panel temperature reduction of approximately 15 °C compared to direct evaporative cooling and around 30 °C relative to the uncooled system, demonstrating the DPEC's superior cooling effectiveness for PV panels.



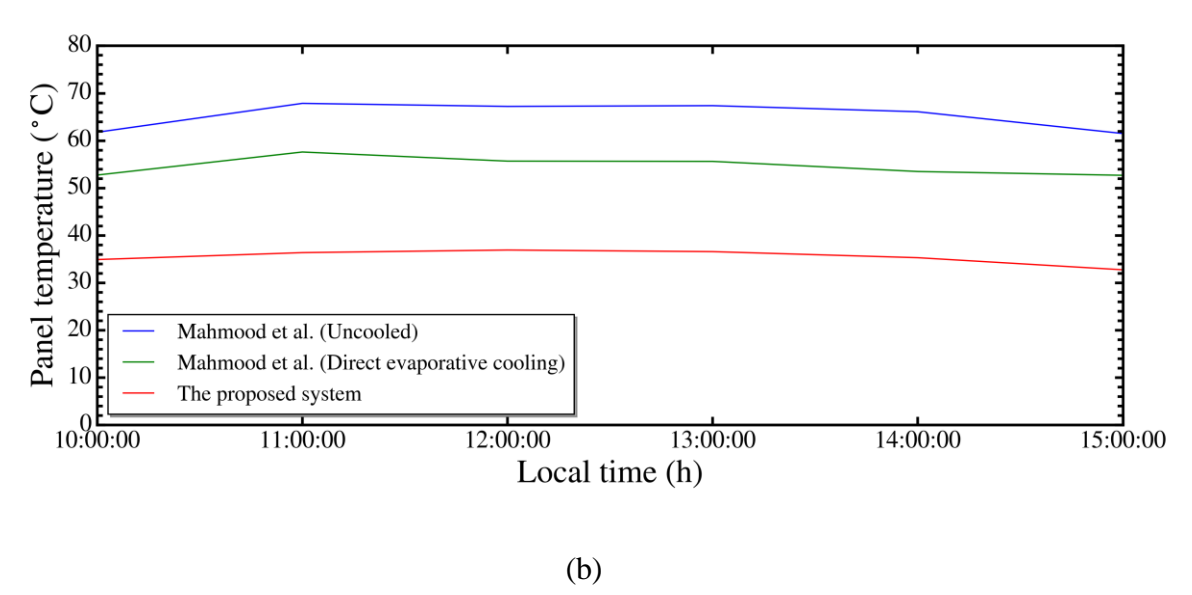


Fig. 3.8. Comparison of the PV temperature with different cooling methods and the weather data of: (a) July 2^{nd} ; (b) July 3^{rd} .

3.4.2 Temperature distribution along the air channels

Fig. 3.9 (a) and (b) show the temperature profiles along the channel length of the DPEC and PV module. The PV panel's temperature decreases significantly upon activation of the cooling system, especially near the panel's air inlet, where cool air from the DPEC unit enters. A notable temperature gradient between layers occurs at the panel inlet, diminishing along the channel as heat transfer balances the temperatures across layers.

Fig. 3.9 (c) and (d) present the humidity distribution along wet channels 1 and 2. Continuous heat transfer from the dry channel to wet channel 1 and from the PV panel to wet channel 2 drives water evaporation, raising air humidity. In wet channel 2, where substantial heat transfer from the PV panel intensifies evaporation, air humidity increases from 0.018 to 0.13 kg/kg [DA]. Another point worth noting is the system's water consumption due to the intense evaporation occurring in wet channel 2. Water consumption is calculated based on the humidity difference between the inlet and outlet of the wet channels. As shown in Fig. 3.9 (c) and (d), the humidity difference in the DPEC unit (for air saturation) is 0.008 kg/kg [DA], while in the

wet channel behind the PV panel, it reaches 0.11 kg/kg DA. For a 10-hour daily operation, the DPEC unit consumes approximately 0.07 kg of water, and the wet channel at the PV panel's back requires an additional 0.72 kg, totaling around 0.79 kg of water consumption for the proposed system.

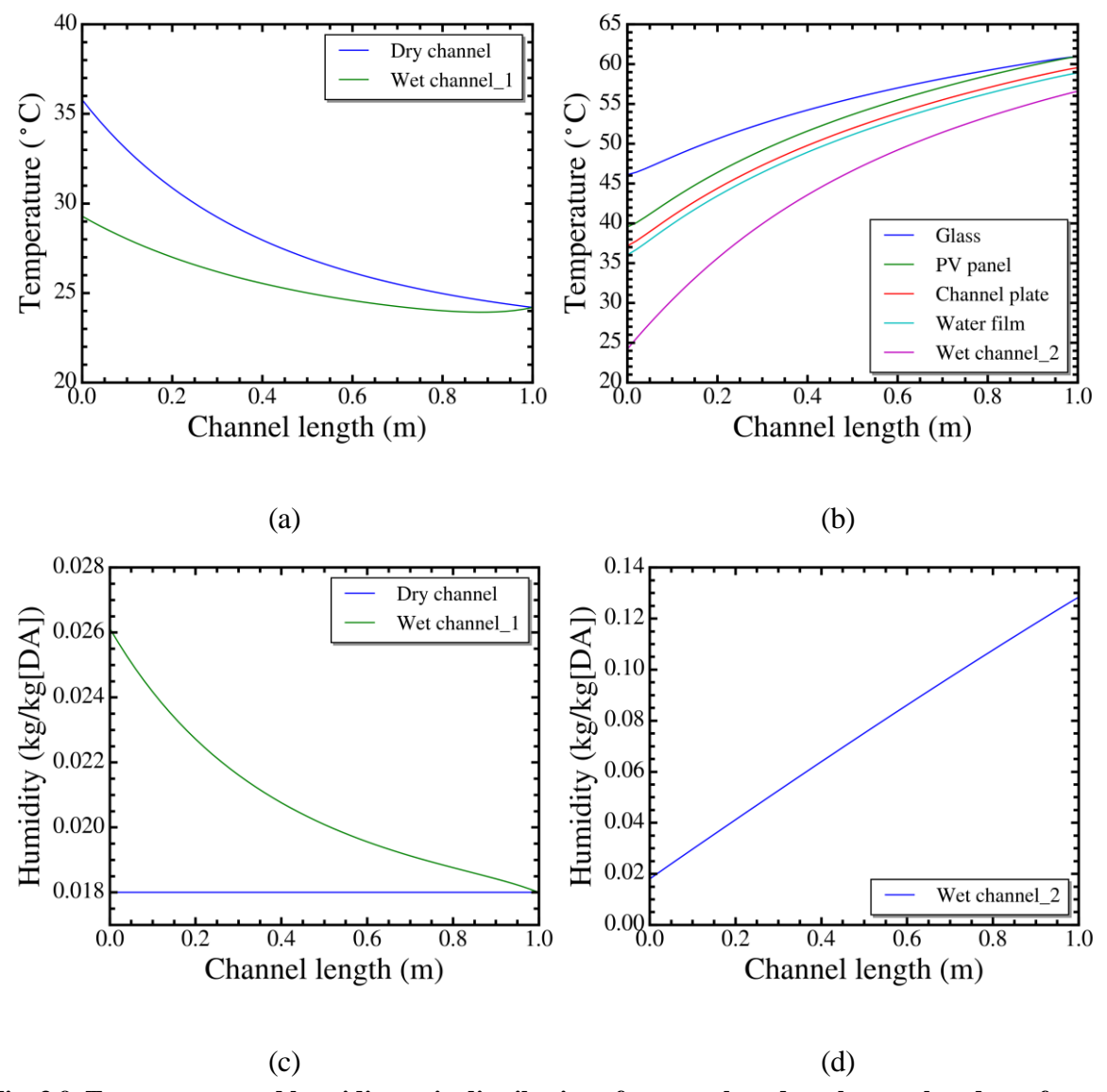


Fig. 3.9. Temperature and humidity ratio distribution of systems based on the weather data of 13:00, 1st June: (a) DPEC; (b) temperature of each layer of PV module; (c) humidity distribution for DPEC dry channel and wet channel 1; (d) humidity distribution for wet channel 2 in PV module.

3.4.3 Effect of cooling system parameters

This section examines the impact of varying input parameters (channel length, height, inlet air velocity, and working air ratio) on system performance, which is critical for system design optimization. The analysis is based on weather data at 13:00, 1st June 2022. Table 3.3 lists the nominal parameter values, serving as the reference case. Identical channel lengths and heights are used for both the DPEC and PV panel. Solar cell efficiency is calculated using Eq. (12), and thermal efficiency improvement is defined as the difference in heat removal between the modified and reference systems relative to the heat gained from solar energy.

Table 3.3 Nominal parameters of the reference system.

Parameters	Value
Channel length(m)	1.0
Channel height(mm)	4.5
Inlet air velocity(m/s)	1.4
Working air ratio	0.5

1) The effect of channel length

Channel length, varied from 0.6 to 2.2 m, has a notable impact on operating temperature, as shown in Fig. 3.10, due to changes in the contact surface area for heat and mass transfer. Longer channels result in higher PV operating temperatures; for instance, at a length of 2.2 m, the temperature reaches 64 °C, which is 15 °C higher than at 0.6 m. Both solar cell efficiency and thermal efficiency improvement decrease as channel length increases. While the channel length may be limited by the PV panel dimensions in practice, desired channel dimensions could still be achieved by optimizing cooler design parameters.

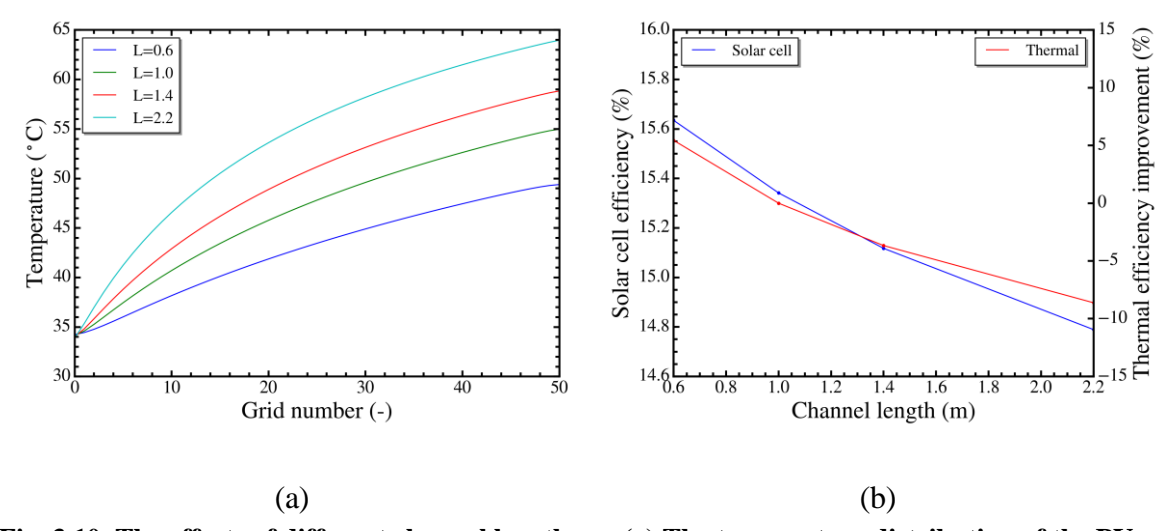


Fig. 3.10. The effects of different channel lengths on (a) The temperature distribution of the PV panel; (b) The solar cell efficiency and the thermal efficiency improvement.

2) The effect of channel height

The impact of channel height on system performance is evaluated by varying it from 3 to 9 mm. As shown in Fig. 3.11, temperature variation along the channel is more pronounced at smaller channel heights. However, the minimum temperature at the channel entrance rises with increasing channel height. In general, greater channel height enhances solar cell efficiency, though this improvement diminishes beyond a certain height. Channel height significantly influences system performance by directly affecting the heat and mass transfer coefficients. Increasing channel height allows more unsaturated air into the PV panel, enhancing heat and mass transfer, reducing operating temperature, and thus improving solar cell efficiency.

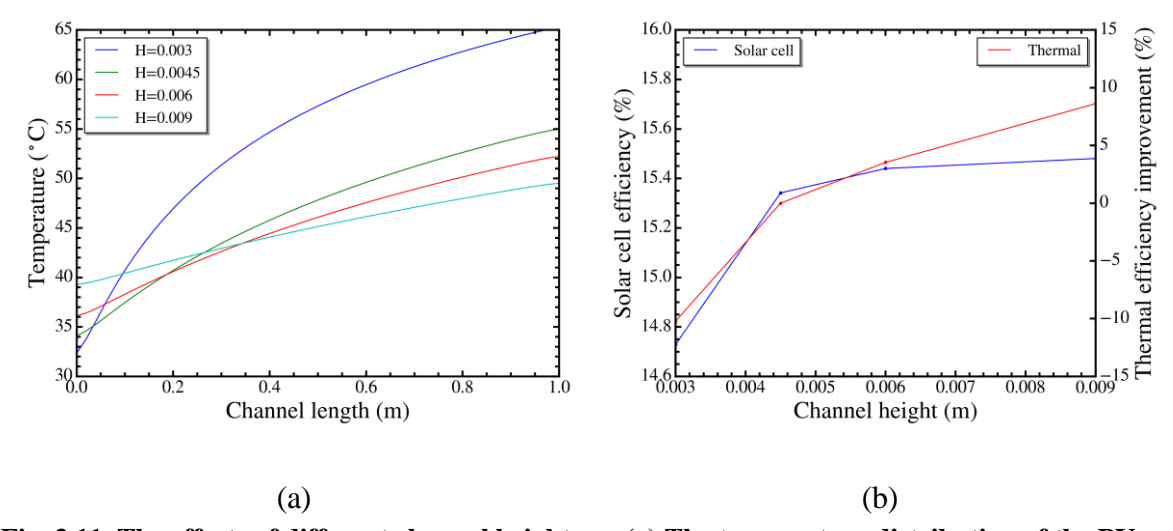


Fig. 3.11. The effects of different channel heights on (a) The temperature distribution of the PV panel; (b) The solar cell efficiency and the thermal efficiency improvement.

3) The effect of inlet air velocity

For indirect evaporative coolers, lower air velocities are generally preferred when the dry channel outlet air is considered the useful effect. In this part, the inlet air velocity to the cooler varies from 1.0 to 3.0 m/s, affecting both Reynolds and Nusselt numbers. With increasing velocity, the DPEC supply air temperature rises, while the wet air temperature in the wet channel of the PV panel decreases, maintaining a lower PV panel temperature. As shown in Fig. 3.12, higher inlet velocity lowers the PV panel's operating temperature and enhances solar cell efficiency. Increasing inlet air velocity can reduce PV temperature by up to 12 °C, though the effect is less significant compared to changes in geometric parameters.

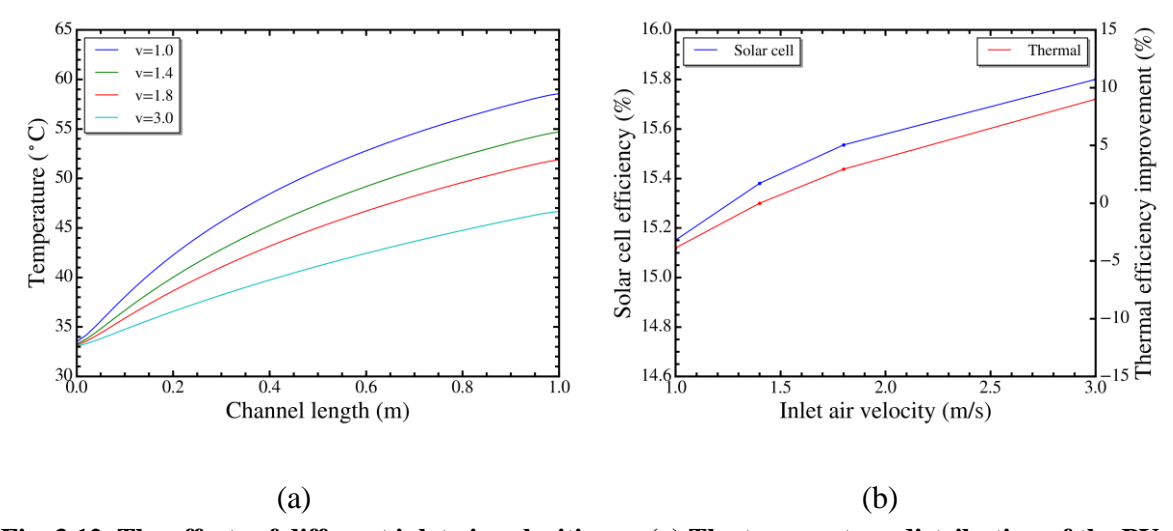


Fig. 3.12. The effects of different inlet air velocities on (a) The temperature distribution of the PV panel; (b) The solar cell efficiency and the thermal efficiency improvement.

4) The effect of working air ratio

The working air ratio of the DPEC, r, is defined as the ratio of the mass flow rate of air entering wet channel 1 to that entering the dry channel. Consequently, (1-r) represents the percentage of air directed to wet channel 2 in the PV panel. As shown in Fig. 3.13, increasing the working air ratio reduces the airflow to wet channel 2, leading to a lower mass transfer rate within the PV panel. This results in decreased solar cell efficiency and thermal efficiency improvement.

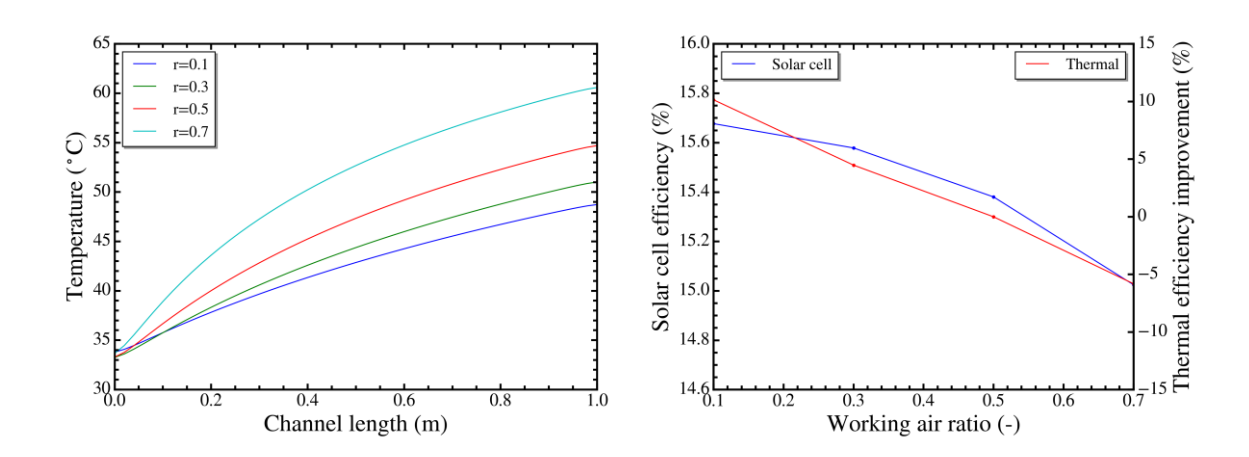


Fig. 3.13. The effects of different working air ratios on (a) The temperature distribution of the PV panel; (b) The solar cell efficiency and the thermal efficiency improvement.

3.5 Conclusions

This chapter presents a novel cooling approach for PV panels utilizing an enhanced Dew Point Evaporative Cooling (DPEC) system. In addition to the conventional DPEC, the proposed system further improves evaporative cooling by incorporating an additional wet channel at the rear of the PV panel. A comparative analysis between the proposed system and a conventional sensible cooling system with DPEC was performed. The results demonstrate that the proposed system offers superior cooling performance, maintaining higher solar cell efficiency in the PV panel. The impact of the enhanced DPEC system on solar efficiency was investigated, along with the influence of geometric parameters on the system's performance, providing valuable insights for optimizing the system design. Key findings from this study are summarized as follows:

- (6) Under various climatic conditions, the proposed enhanced cooling system demonstrated superior cooling performance and maintained higher PV panel efficiency compared to uncooled, direct evaporative cooling, and DPEC-based sensible cooling systems.
- (7) The proposed system maintained an efficiency exceeding 15% under two summer environmental conditions. The maximum solar cell efficiency reached 16.7%, representing a 16.4% improvement compared to the sensible DPEC system. The cooling performance improvement between the two systems ranged from a maximum increase of 16.5% to a minimum of 11.4%.
- (8) The cooling performance of the system is influenced by various geometric parameters. A shorter channel length and larger channel height enhance cooling performance, leading to

higher PV panel efficiency. Conversely, a higher inlet air velocity and working air ratio further optimize system performance.

However, the proposed system has some limitations: (1) the addition of a second wet channel increases water consumption. In a 10-hour operation, the traditional sensible cooling system requires 0.07 kg of water, while the proposed system consumes 0.79 kg, with 0.72 kg used by the second wet channel; (2) being based on evaporative cooling, the system's performance is limited by the humidity of the surrounding air. Under high humidity conditions, cooling potential may be reduced, requiring pre-dehumidification. Further experimental studies will assess the feasibility of the enhanced cooling system.

Chapter 4 Combined Dew-point evaporative cooling system for winter heating

4.1 Introduction

Winter indoor heating remains a critical energy demand due to the harsh cold conditions in many regions, leading to significant challenges in maintaining comfortable indoor temperatures while managing energy efficiency[144–146]. During winter, people's thermal comfort needs are shaped by the desire to maintain a balance between body heat production and environmental heat loss to achieve a comfortable indoor environment[147–149]. Thermal comfort is determined by factors such as air temperature, humidity, air velocity, clothing insulation, and metabolic activity. HVAC systems enhance winter comfort by optimizing these parameters to maintain a balanced and efficient indoor environment[150,151]. Traditional heating systems, such as electric and gas heaters or air conditioners, are energy-intensive and often fall short in sustainability due to their reliance on fossil fuels. These systems generally offer limited adaptability for optimizing energy consumption, frequently resulting in overheated spaces or uneven temperature distribution. Such inefficiencies not only increase operational costs but also contribute to higher greenhouse gas emissions, exacerbating environmental concerns. This underscores the need for innovative solutions that address both the energy efficiency of heating systems and their environmental impact[152,153].

Current research highlights gaps in conventional heating technologies, particularly their inability to integrate renewable energy sources efficiently or to address thermal comfort comprehensively under diverse conditions.

Many researchers have begun to explore the development of novel DPEC systems integrated with desiccant technology. These efforts aim to enhance the versatility of this highly efficient cooling method and expand its applications across broader cooling domains. However, limited research focuses on the year-round operational feasibility of these systems. Most studies emphasize their cooling performance while neglecting potential heating applications. To date, Anisimov et al. [154] is among the few researchers to address the dual functionality of DPEC systems. His study proposed a cross-flow system that functions as an evaporative cooler during summer and a heat recovery unit in winter. Simulation-based analyses conducted in his work provided insights into the heat and mass transfer mechanisms underpinning year-round operation. These findings highlight the potential for all-season systems to achieve energyefficient performance, aligning with global sustainability goals and environmental imperatives. Building on these developments, this chapter introduces an innovative system that combines desiccant technology, photovoltaic modules, and a DPEC unit. The focus is on evaluating its feasibility for winter heating, with the goal of maintaining high cooling efficiency in summer while ensuring indoor thermal comfort during winter. This analysis is performed using detailed simulation modeling, targeting a balanced and sustainable approach to year-round thermal management.

4.2 Description of system

Fig 4.1 illustrates the proposed configuration for heating a working space using a hybrid system that integrates a PV panel, DPEC, and desiccant unit. The system operates with a standalone DPEC where outdoor is cooled to near its dew point temperature. The cooled, dry air is then directed into a wet channel situated behind the PV panel. Here, an additional evaporative cooling process occurs, allowing the air to absorb latent heat and become nearly

saturated, which raises its temperature due to heat exchange with the PV panel. The humidified air then enters the desiccant unit, where dehumidification occurs as moisture is adsorbed by the desiccant material. This adsorption process releases heat, raising the air's temperature. Upon exiting the desiccant unit, the air is both dehumidified and moderately warmed, achieving a balanced temperature and humidity level. This conditioned air is subsequently delivered to the working space, ensuring a stable and comfortable indoor environment.

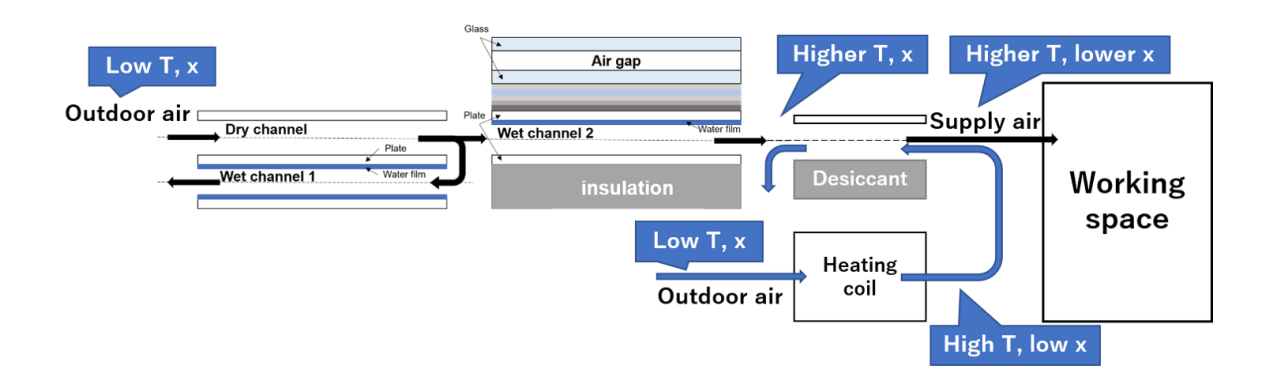


Fig. 4.1. Schematic diagram for the hybrid system for winter heating: the DPEC with PV panel and desiccant.

4.3 Methodology

4.3.1 Mathematical model

The proposed system comprises three main components: the DPEC unit, PV unit, and desiccant unit, each requiring detailed modeling in this study. The dynamic mathematical models for the DPEC and PV units were developed in Chapter 3, where each element was analyzed from the perspective of air and water vapor interactions within the desiccant material, as shown in Fig. 4.2. To capture the transient behavior of the desiccant module, a time-

dependent model incorporating both adsorption and regeneration processes was developed based on the following assumptions:

- (8) The thermal properties of each desiccant layer are assumed to be constant.
- (9) The boundary thermal loss is negligible.

Ambient parameters, including air temperature, humidity, and wind speed, are derived from weather data for Fukuoka, Japan. The proposed system integrates three main components: a cooler unit, PV unit, and desiccant unit. Dynamic mathematical models for the DPEC and PV modules were developed in Chapter 3, while the desiccant unit model follows the framework established by Miyazaki et al.[155], as outlined below:

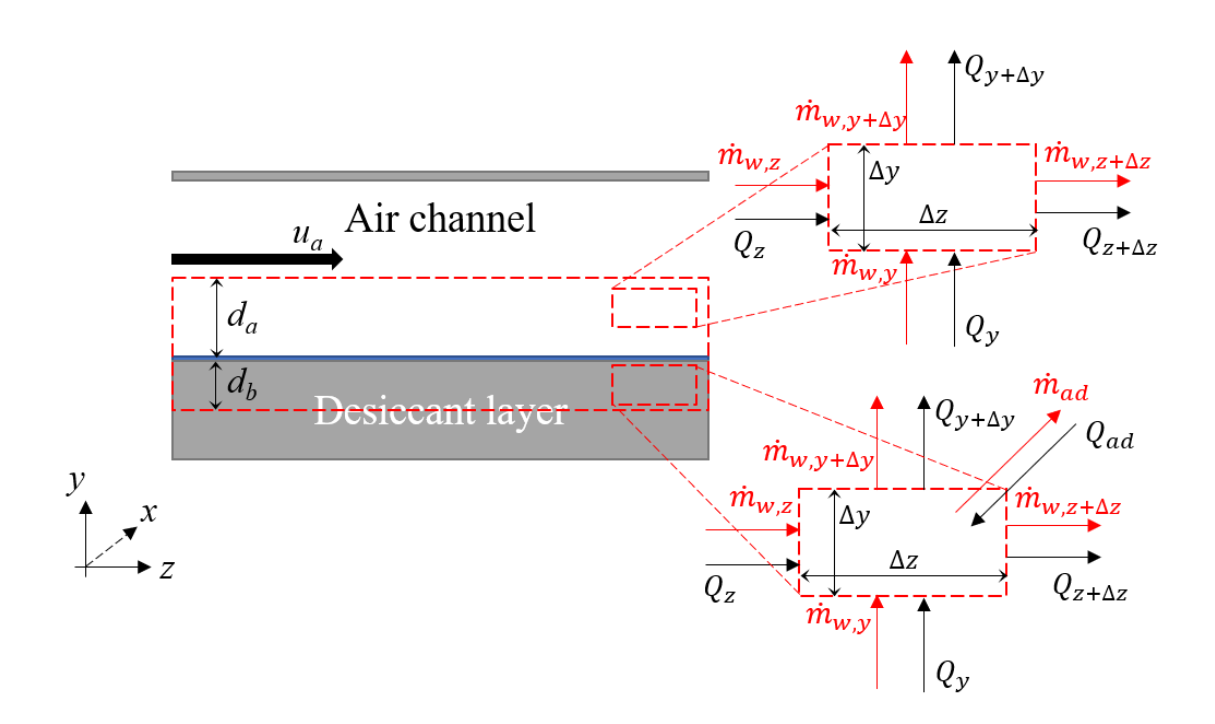


Fig. 4.2. Schematic diagram each control volume for air and desiccant.

(10) Air channel

Based on the mass balance, the stored water vapor in each element within air channel can be calculated by:

$$\rho_a \Delta y \Delta z \frac{\partial x_a}{\partial t} = \dot{m}_{w,z} - \dot{m}_{w,z+\Delta z} + \dot{m}_{w,y} - \dot{m}_{w,y+\Delta y} \tag{1}$$

By writing into mass flow term:

$$\rho_{a}\Delta y \Delta z \frac{\partial x_{a}}{\partial t} = -\rho_{a} u_{a} \Delta y \Delta z \frac{\partial x_{a}}{\partial z} + \rho_{a} D_{w} \Delta y \Delta z \frac{\partial^{2} x_{a}}{\partial y^{2}}$$
 (2)

The terms on the right-hand side of Eq. (2) represent the mass flow alone z-direction, and the mass diffusion in y-direction. The average of air humidity $\overline{x_a}$ in y-direction was defined by integral form: $\overline{x_a} = \frac{1}{d_a} \int_0^{d_a} x_a dy$. The eq. (2) can be transformed into:

$$\frac{\partial \overline{x_a}}{\partial t} = -u_a \frac{\partial \overline{x_a}}{\partial z} + \frac{D_w}{d_a} \int_0^{da} \frac{\partial^2 x_a}{\partial y^2} dy \tag{3}$$

The diffusion behavior in eq. (3) can be simplified by mass transfer coefficient h_m term, thus the eq. (3) can be expressed as:

$$\frac{\partial \overline{x_a}}{\partial t} = -u_a \frac{\partial \overline{x_a}}{\partial z} + \frac{h_m}{d_a} (x_i - \overline{x_a}) \tag{4}$$

Here, x_i represents the interfacial value of water vapor humidity.

The energy conservation of the air in the air channel is influenced by flow in the z-direction and diffusion in the y-direction. Thus, the energy balance can be expressed as follows:

$$\rho_a c_{p,a} \Delta y \Delta z \frac{\partial T_a}{\partial t} = Q_z - Q_{z+\Delta z} + Q_y - Q_{y+\Delta y}$$
 (5)

In terms of the heat flow term:

$$\rho_{a}c_{p,a}\Delta y\Delta z\frac{\partial T_{a}}{\partial t} = -\rho_{a}c_{p,a}u_{a}\Delta y\Delta z\frac{\partial T_{a}}{\partial z} + k_{a}\Delta y\Delta z\frac{\partial^{2}T_{a}}{\partial v^{2}}$$
(6)

Similarly, the average of air temperature $\overline{T_a}$ in y-direction was defined by integral form: $\overline{T_a} = \frac{1}{d_a} \int_0^{d_a} T_a dy$. The eq. (6) can be transformed into:

$$\frac{\partial \overline{T_a}}{\partial t} = -u_a \frac{\partial \overline{T_a}}{\partial z} + \frac{h_a}{\rho_a c_{p,a} d_a} (T_i - \overline{T_a})$$
 (7)

Here, T_i represents the interfacial value of air temperature.

(11) Desiccant layer

Based on the mass balance, the stored water vapor in each element within desiccant layer was:

$$\varepsilon \Delta y \Delta z \frac{\partial \rho_w}{\partial t} = \dot{m}_{w,y} - \dot{m}_{w,y+\Delta y} + \dot{m}_{w,z} - \dot{m}_{w,z+\Delta z} - \dot{m}_{ad}$$
 (8)

The right-hand side of the equation accounts for the diffusion of water vapor in the y-direction, diffusion in the z-direction, and water vapor gain/release due to the adsorption/desorption process.

The adsorption behavior was described by linear driving force model as:

$$\frac{\partial w_b}{\partial t} = k_m(\overline{W} - w_b) \tag{9}$$

Here, k_m is the mass transfer coefficient of adsorption, which can be calculated by $\frac{15D_s}{r_p^2}$. The mass transfer by adsorption can be expressed as:

$$\dot{m}_{ad} = \rho_s (1 - \varepsilon) \Delta y \Delta z \frac{\partial w_b}{\partial t} \tag{10}$$

From the mass flow perspective, Eq. (8) can be written as:

$$\varepsilon \Delta y \Delta z \frac{\partial \rho_w}{\partial t} = -u \Delta y \Delta z \frac{\partial \rho_w}{\partial y} + D_b \Delta y \Delta z \frac{\partial^2 \rho_w}{\partial z^2} - \rho_s (1 - \varepsilon) \Delta y \Delta z \frac{\partial w_b}{\partial t}$$
 (11)

The water vapor flow inside the porous media can be described by Darcy's law and the calculation of partial pressure can be defined by ideal gas law:

$$u = -\frac{k}{\mu} \frac{dP}{dx} \tag{12}$$

$$P = \rho RT \tag{13}$$

Thus, by applying eqs. (12), (13), eq. (11) can be shown as:

$$\varepsilon \Delta y \Delta z \frac{\partial \rho_w}{\partial t} = \frac{\rho_w kRT_b}{\mu} \Delta y \Delta z \frac{\partial^2 \rho_w}{\partial y^2} + D_b \Delta y \Delta z \frac{\partial^2 \rho_w}{\partial z^2} - \rho_s (1 - \varepsilon) \Delta y \Delta z \frac{\partial w_b}{\partial t}$$
(14)

Here, the diffusion coefficient of water vapor in desiccant layer can be defined as $D_b = \frac{\rho_w k_R T_b}{\mu}$.

The average of the density of water vapor in desiccant layer ρ_w in y-direction was defined by integral form: $\overline{\rho_w} = \frac{1}{d_b} \int_0^{d_b} \rho_w dy$. The eq. (14) can be transformed into:

$$\frac{\partial \overline{\rho_w}}{\partial t} = \frac{D_b}{\varepsilon d_b} \int_0^{d_b} \frac{\partial^2 \rho_w}{\partial y^2} dy + \frac{D_b}{\varepsilon} \frac{\partial^2 \overline{\rho_w}}{\partial z^2} - \frac{\rho_s (1 - \varepsilon)}{\varepsilon} \frac{\partial w_b}{\partial t}$$
(15)

The distribution of ρ_w in y-direction was assumed as parabolic. The eq. (15) can be simplified as:

$$\frac{\partial \overline{\rho_w}}{\partial t} = \frac{3D_b}{\varepsilon d_b^2} (\rho_i - \overline{\rho_w}) + \frac{D_b}{\varepsilon} \frac{\partial^2 \overline{\rho_w}}{\partial z^2} - \frac{\rho_s (1 - \varepsilon)}{\varepsilon} \frac{\partial w_b}{\partial t}$$
(16)

For water vapor within the adsorbent material, as illustrated in Fig. 4.2. Energy conservation is governed by three factors: diffusion of water vapor in the z-direction, diffusion in the y-direction, and heat release/gain due to the adsorption/desorption process. Therefore, the energy balance equation can be formulated as follows:

$$\rho_s(1-\varepsilon)c_{p,b}\Delta y\Delta z\frac{\partial T_b}{\partial t} = Q_z - Q_{z+\Delta z} + Q_y - Q_{y+\Delta y} + Q_{ad}$$
(17)

The heat flow inside desiccant layer element was described by heat conduction. Thus the eq. (17) can be transformed into:

$$\rho_{s}(1-\varepsilon)c_{p,b}\Delta y\Delta z\frac{\partial T_{b}}{\partial t} = k_{b}\Delta y\Delta z\left(\frac{\partial^{2}T_{b}}{\partial y^{2}} + \frac{\partial^{2}T_{b}}{\partial z^{2}}\right) + q_{ad}\rho_{s}(1-\varepsilon)\Delta y\Delta z\frac{\partial w_{b}}{\partial t} \quad (18)$$

The average of the temperature of desiccant layer T_b in y-direction was defined by integral form: $\overline{T_b} = \frac{1}{d_b} \int_0^{d_b} T_b dy$, and the distribution of T_b in y-direction was assumed as parabolic. The eq. (18) can be transformed into:

$$\frac{\partial \overline{T_b}}{\partial t} = \frac{3k_b}{\rho_s c_{p,b} (1 - \varepsilon) d_b^2} (T_i - \overline{T_b}) + \frac{k_b}{\rho_s c_{p,b} (1 - \varepsilon)} \frac{\partial^2 \overline{T_b}}{\partial z^2} + \frac{q_{ad}}{c_{p,b}} \frac{\partial w_b}{\partial t}$$
(19)

By applying the definition of thermal diffusivity of desiccant layer $\alpha_b = \frac{k_b}{\rho_s c_{p,b}(1-\varepsilon)}$, the eq. (1) can be simplified as:

$$\frac{\partial \overline{T_b}}{\partial t} = \frac{3\alpha_b}{{d_b}^2} (T_i - \overline{T_b}) + \alpha_b \frac{\partial^2 \overline{T_b}}{\partial z^2} + \frac{q_{ad}}{c_{p,b}} \frac{\partial w_b}{\partial t}$$
 (20)

The calculation of the interfacial value T_i, x_i, ρ_i is carried by the conservation of energy and mass:

$$-k_b \frac{\partial T_b}{\partial y}\Big|_{y=db} = -k_a \frac{\partial T_a}{\partial y}\Big|_{y=0}$$
(21)

$$-D_b \frac{\partial \rho_w}{\partial y} \bigg|_{y=db} = -\rho_a D_w \frac{\partial x_a}{\partial y} \bigg|_{y=0}$$
 (22)

4.3.2 Simulation scheme

Numerical simulations of the evaporative cooling system are performed by solving Eqs. (4), (7), (9), (16), and (20), as described in Section 4.3.1. The geometric parameters of the desiccant module are provided in Table 4.1, and the ambient properties are listed in Table 4.2. The following boundary conditions in z-direction is applied in the simulation:

$$\left. \frac{dT_b}{dx} \right|_{z=0} = \frac{dT_b}{dx} \bigg|_{z=L} = \frac{d\rho_w}{dx} \bigg|_{z=0} = \frac{d\rho_w}{dx} \bigg|_{z=L} = 0 \tag{24}$$

The finite difference method was applied to solve the partial differential equations in the desiccant model, utilizing a Python-based nonlinear optimization approach. The channel length was discretized into 50 elements, with a time step spanning 3600 intervals. The simulation algorithm is shown in Fig. 4.3.

Table 4.1 Input parameters of desiccant module

Parameters	Value
Desiccant thickness d_b (mm)	0.3
Porosity of desiccant $\varepsilon(-)$	0.9
Density of desiccant $\rho_s(kg/m^3)$	1500
Specific heat of desiccant	805
$c_{p,b}(J/kg K)$	
Thermal conductivity of	0.33
desiccant $k_b(W/m K)$	
Diffusion coefficient of	0.0001
desiccant $D_b(\text{m}^2/\text{s})$	
Air channel length(m)	0.4
Air channel height(mm)	1.7

Table 4.2 Input winter weather parameters used in simulation

Parameters	Values
Ambient temperature (°C)	13.2
Solar irradiance (W/m ²)	586
Wind velocity (m/s)	2.5
Relative humidity (%)	45
Inlet air humidity (kg/kg DA)	0.0042

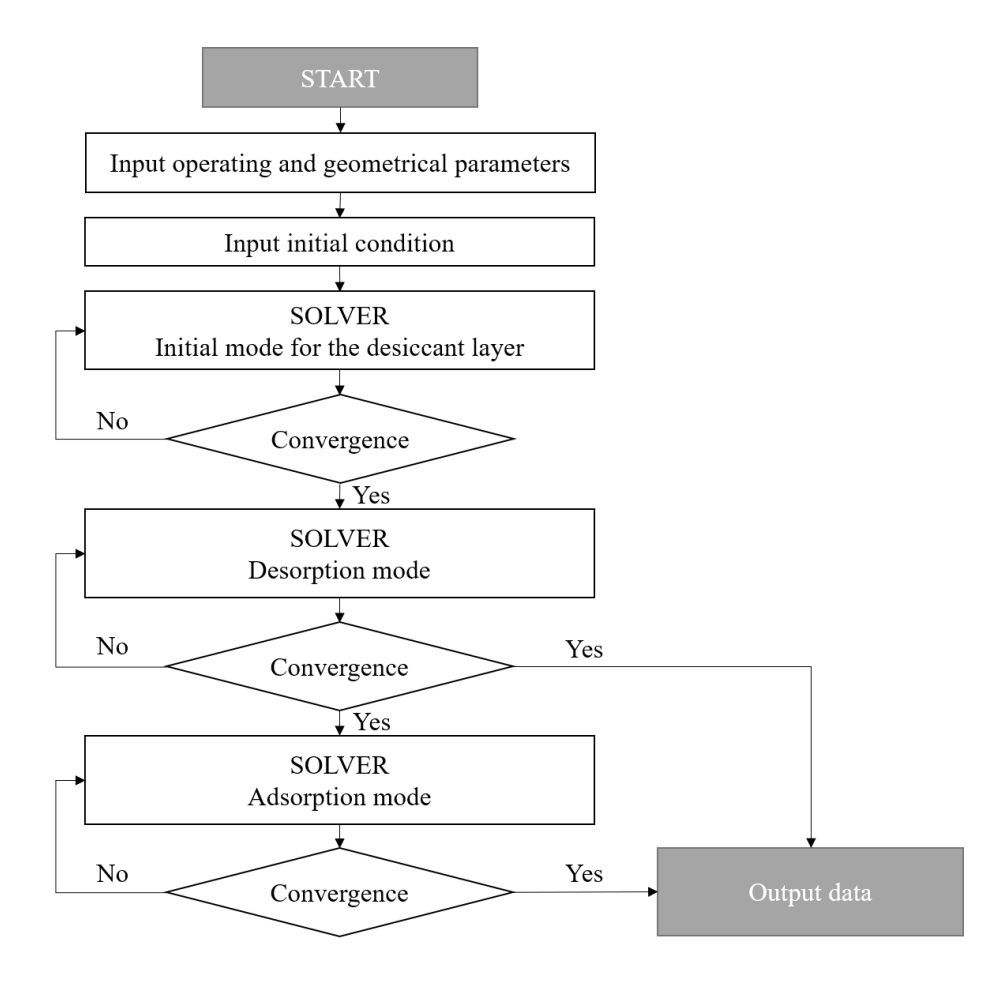


Fig. 4.3. Simulation flowchart.

4.3.3 Model validation

The proposed transient model was validated against experimental data from the literature. Priyadarshi et al. [156] coated the heat exchanger tubes with desiccant material (silica gel) and experimentally investigated its performance, obtaining outlet air temperature data. This data serves to validate the accuracy of the desiccant unit's simulation model presented in this chapter. As shown in Fig. 4.4, the results indicate that the current model accurately predicts the temporal variation of outlet air temperature from the desiccant unit. The maximum discrepancy between the simulation and experimental data is 6.2%, with an average error of 1.24%. However, the validation of the current model faces several challenges, requiring further experimental studies to verify its accuracy. This is particularly important as the system comprises three components,

with dynamic environmental conditions influencing the DPEC, PV, and desiccant units. Comprehensive experiments on the entire system are necessary. Overall, at this stage, the desiccant unit provides reasonably accurate predictions for the adsorption/desorption processes.

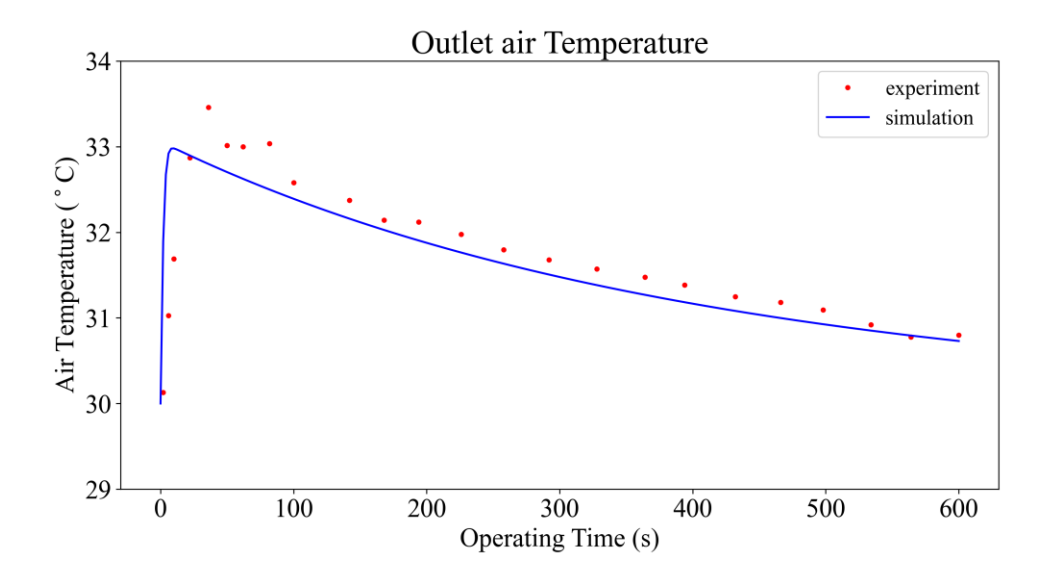


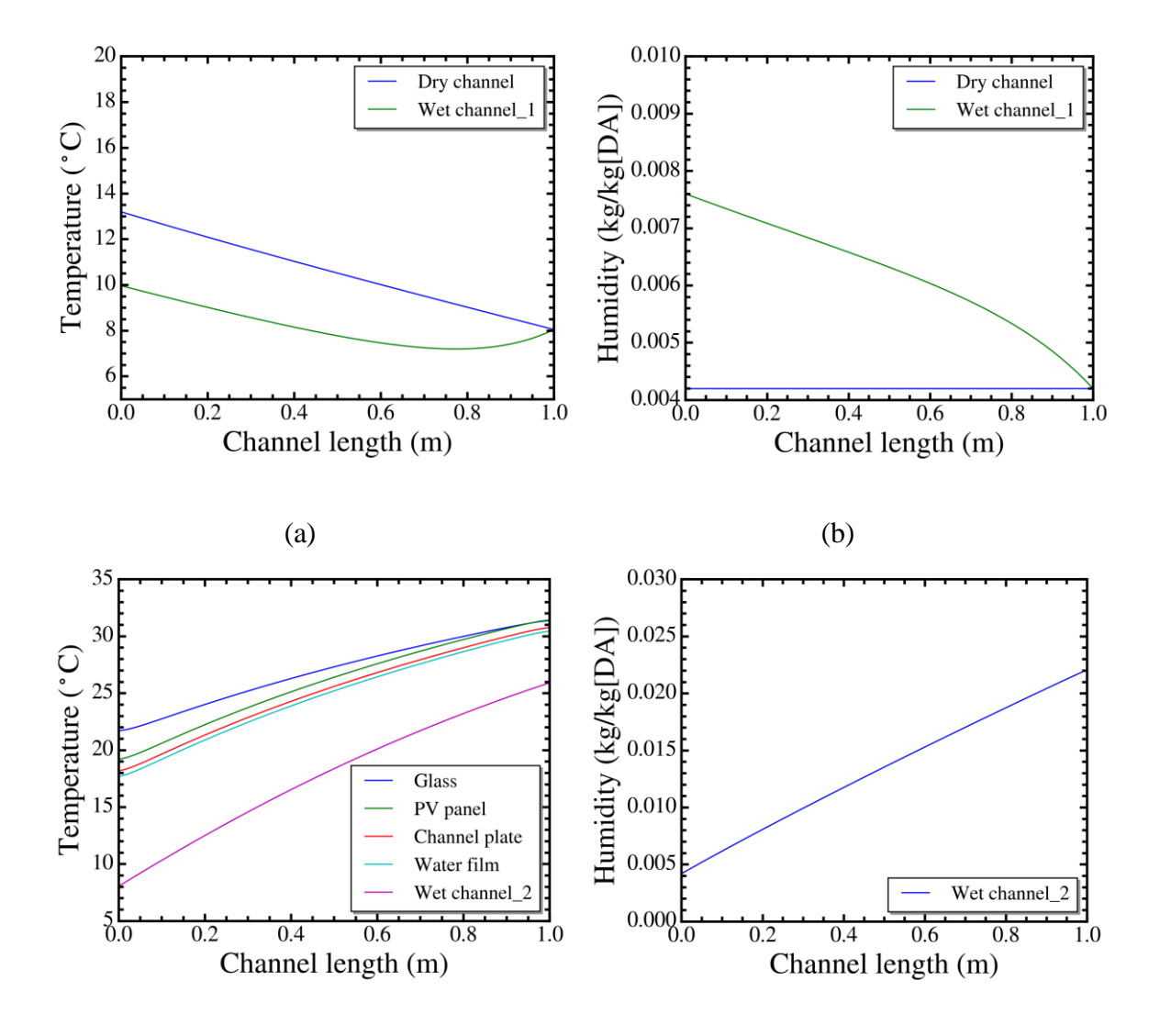
Fig. 4.4. Model validation with experimental data from Priyadarshi et al. [156].

4.4 Results and discussion

4.4.1 Comparison of evaporative cooling and air-cooling system

Fig. 4.5 presents the temperature and humidity profiles of air within the channels of the various components in the proposed system under winter operating conditions. The weather data used for the analysis were obtained from Fukuoka, Japan, between 12:00 and 13:00 on December 12, 2022. Figs. 4.5 (a) to (d) highlight the thermal and humidity performance of the integrated DPEC and PV system. During winter conditions, ambient air, characterized by low temperature and low humidity, is initially cooled by the DPEC to 8°C, which is below the wetbulb temperature, as shown in Fig. 4.5 (a). Upon entering the air channel of the PV unit, the air undergoes an additional dew point evaporative cooling process, absorbing substantial heat from

the PV panel. As a result, the air temperature rises to 26°C, while the surface temperature of the PV panel is maintained at 31.2°C, as depicted in Fig. 4.5 (c). At this point, the air exiting the PV unit has its humidity increased to 22 g/kg[DA], reaching saturation under the given conditions. The warm, moisture-laden air exiting the PV unit subsequently flows into the desiccant unit. Within this unit, the air undergoes an adsorption process, during which air moisture is removed and adsorption heat is released. As shown in Figs. 4.5 (e) and (f), this process further elevates the air temperature to 28°C and reduces its humidity to 13 g/kg[DA], preparing it for delivery to the working space.



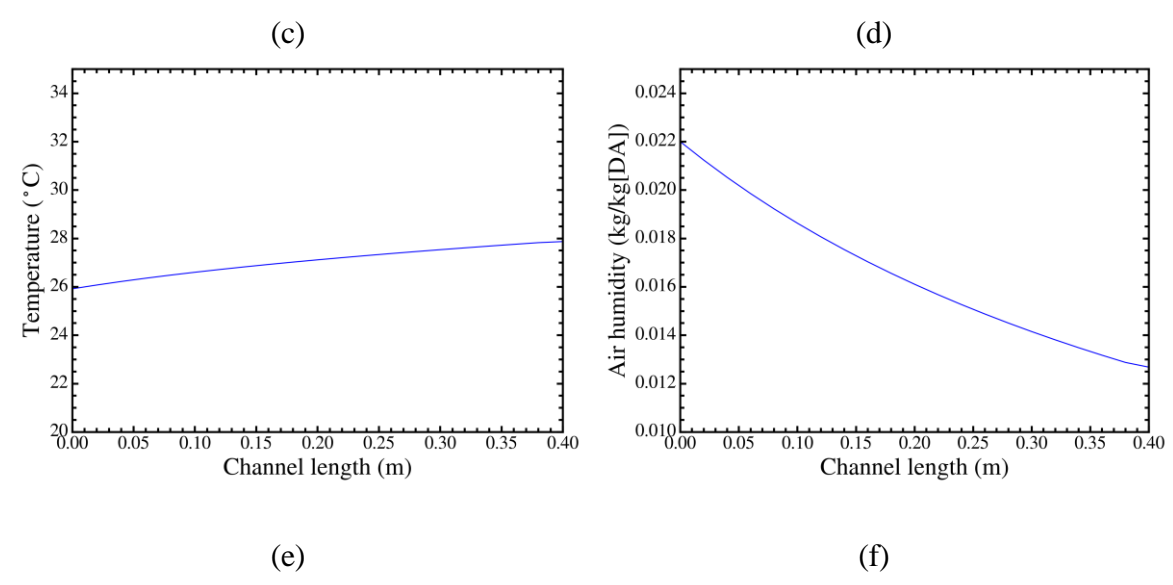


Fig. 4.5. Air temperature and humidity distribution of each unit: (a) temperature of DPEC; (b) humidity of DPEC; (c) temperature of PV panel; (d) humidity of PV panel; (e) temperature of desiccant unit; (f) humidity of desiccant unit.

Fig. 4.6 (a) illustrates the configuration of the PV panel system with natural air cooling, while Fig. 4.6 (b) depicts the temperature distribution of the PV panel surface and the cooling air under this setup. Under winter conditions, ambient air appears capable of meeting the cooling requirements of the PV panel. However, simulation results reveal that in the natural air cooling system, the surface temperature of the PV panel exceeds 30°C near the air inlet and rises above 50°C at the air outlet. Similarly, the cooling air used for the PV panel reaches a temperature exceeding 50°C at the outlet.

Fig. 4.7 compares the temperature and humidity changes of supply air across different components in the proposed system and the natural air cooling system using a psychrometric chart. From the perspective of PV panel efficiency, the excessively high surface temperature under natural air cooling significantly hinders efficiency retention. On the other hand, from a thermal comfort standpoint, as indicated by the dashed box in Fig. 4.7, this represents the indoor thermal comfort range for winter conditions under some studies [1,157]: a metabolic rate of 1–1.2, clothing insulation of 0.3–0.6, and an air velocity of 0–0.5 m/s. While natural air cooling

can raise the air temperature to over 50°C, its heating-only approach drastically reduces the relative humidity to around 5%. In contrast, the proposed system increases the air temperature to 28°C and maintains a relative humidity of 45% after passing through the desiccant unit, placing it well within the thermal comfort range. These results demonstrate the potential of the proposed system to deliver thermally comfortable air under winter conditions.

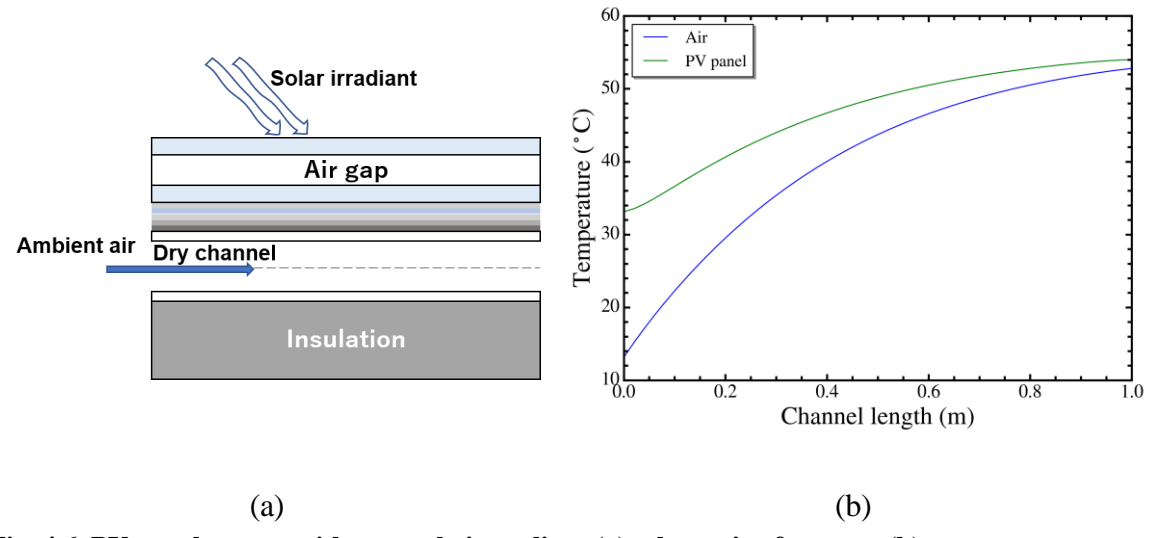


Fig. 4.6. PV panel system with natural air cooling: (a) schematic of system; (b) temperature distribution.

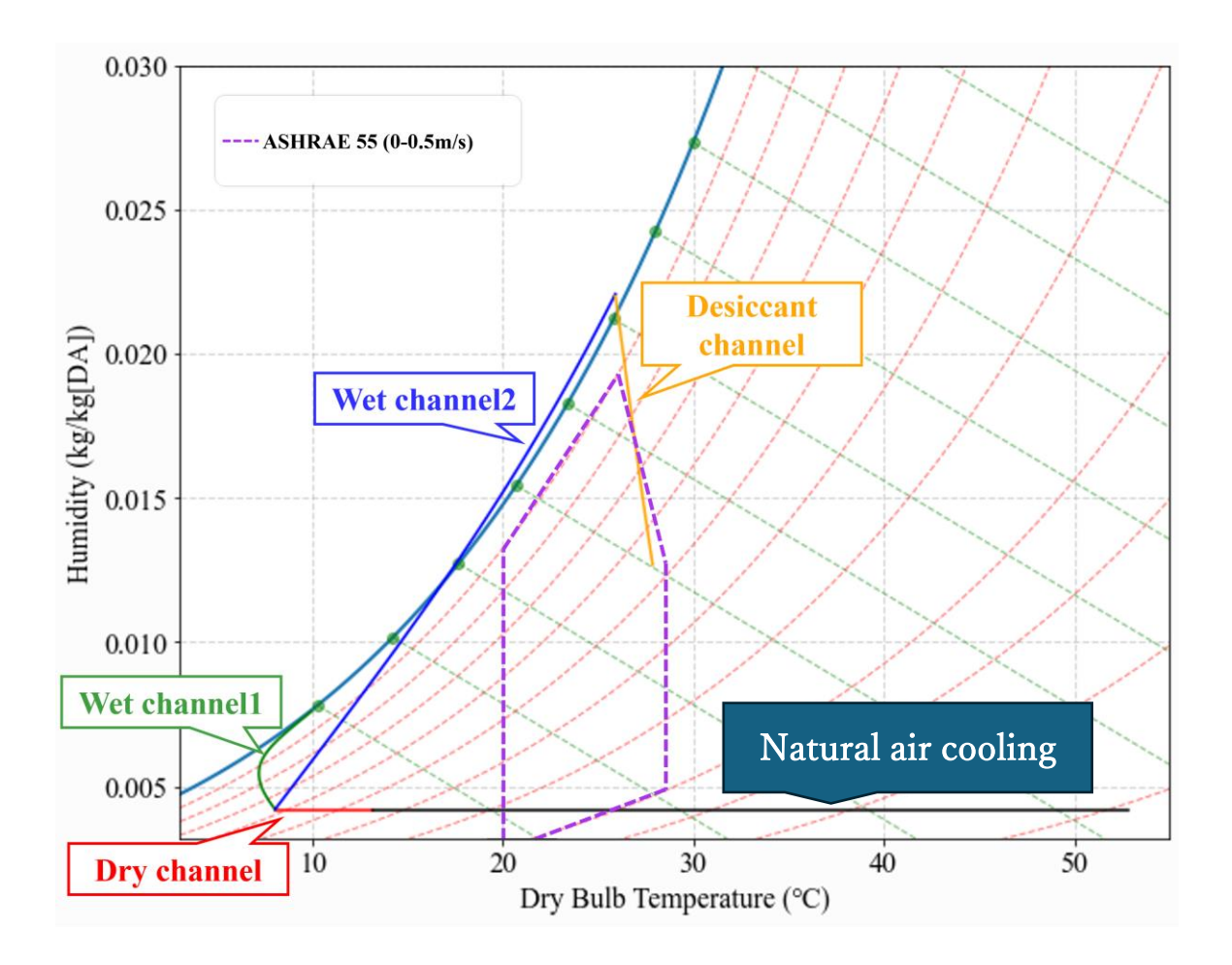


Fig. 4.7. Comparison of the air temperature and humidity change with different system.

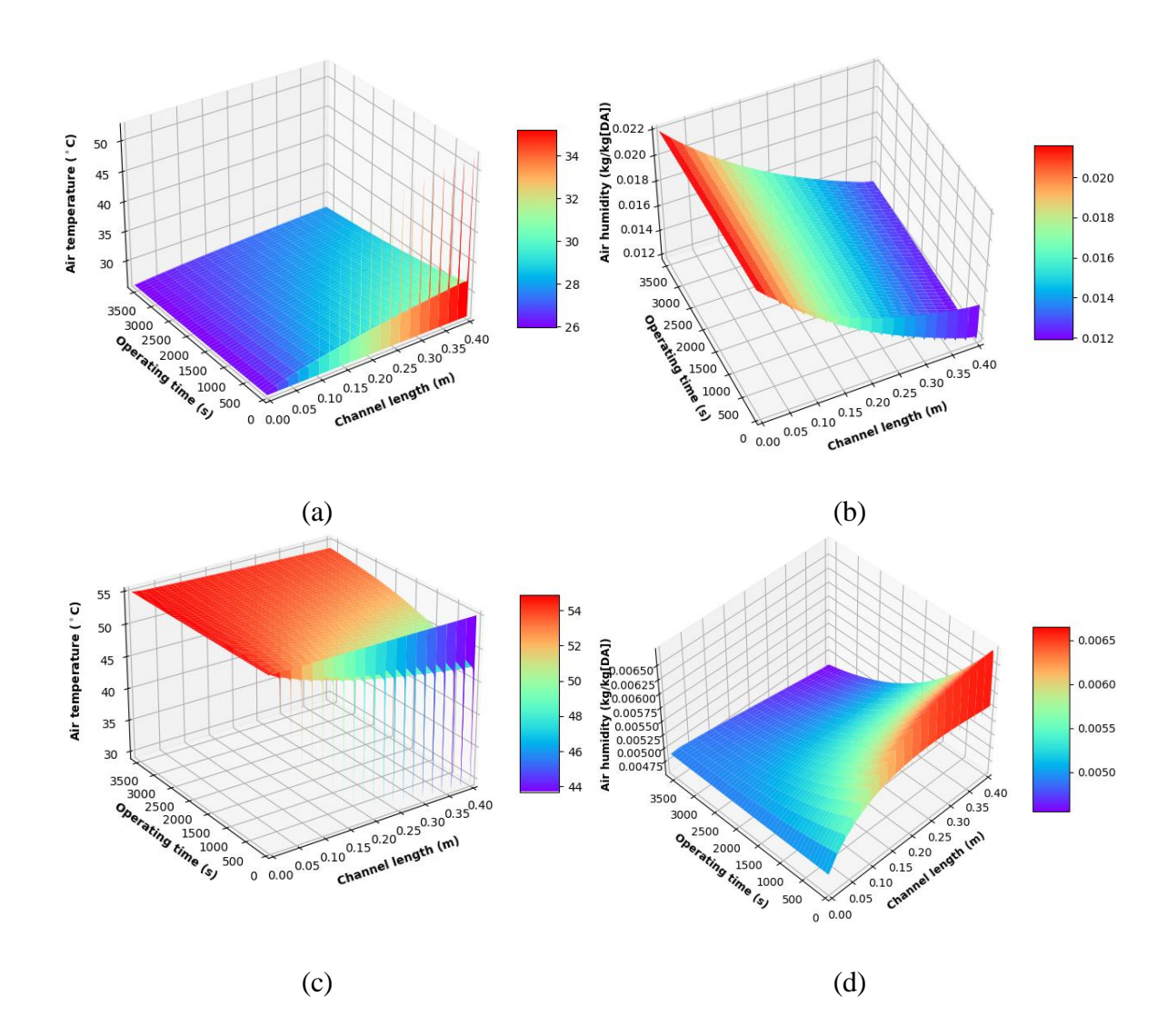
4.4.2 Temperature and humidity behavior of air during the adsorption/desorption process

Fig. 4.8 illustrates the dynamic temperature and humidity profiles of inlet air along the channel under both adsorption and desorption modes. As shown in Figs. 4.8(a) and (b), during the adsorption process, air absorbs adsorption heat from the desiccant material, resulting in an increasing temperature trend along the channel. This increase is particularly rapid during the initial 100 s, as the air temperature rises sharply. Over time, as the water content in the desiccant material increases, its adsorption capacity diminishes, leading to a reduced heat release. Consequently, the temperature rise along the channel becomes less pronounced, while the

temporal trend shows a rapid initial increase followed by a gradual decline. In terms of humidity distribution, the air exhibits an overall decreasing trend along the channel, with a slower reduction in the latter half. Temporally, the humidity first drops sharply and then gradually increases. Figs. 4.8(c) and (d) depict the temperature and humidity profiles during the desorption process. Ambient air is first heated to 55°C by a heat coil, achieving an absolute humidity of 4.2 g/kgDA and a relative humidity of approximately 5%. This heated air is then used for regeneration. Initially, the desiccant material rapidly releases moisture, but as its water content decreases, the rate of moisture release declines. Accordingly, Fig. 4.8(c) shows a sharp drop in air temperature during the first 100 s, after which the temperature remains relatively high. Fig. 4.8(d) demonstrates that the air gains significant moisture during the initial 100 s, followed by a gradual reduction in the rate of moisture uptake. Fig. 4.8(e) illustrates the dynamic changes in water uptake by the desiccant material. The first 3600 s correspond to the desorption process, followed by the adsorption process. Temporally, water uptake initially decreases and then increases. Along the channel direction, the uptake consistently declines due to the increasing or decreasing moisture content in the desiccant material, which directly affects its ability to absorb or release water.

Fig. 4.9 shows the dynamic temperature and humidity profiles of air at the outlet of the air channel. During desorption, the air removes heat from the system. As the process progresses and high-temperature air is no longer required to supply heat to the desiccant material, the temperature exhibits a rapid initial decrease, followed by a gradual stabilization. For humidity, the air initially absorbs a significant amount of moisture, but the rate of moisture absorption decreases over time. After 3600 s, the adsorption process begins, where the saturated air at 26°C exiting the PV unit enters the desiccant unit. Here, the air loses moisture and gains adsorption

heat, resulting in a sharp initial increase in temperature followed by a slower rise, while the humidity first decreases rapidly and then gradually declines.



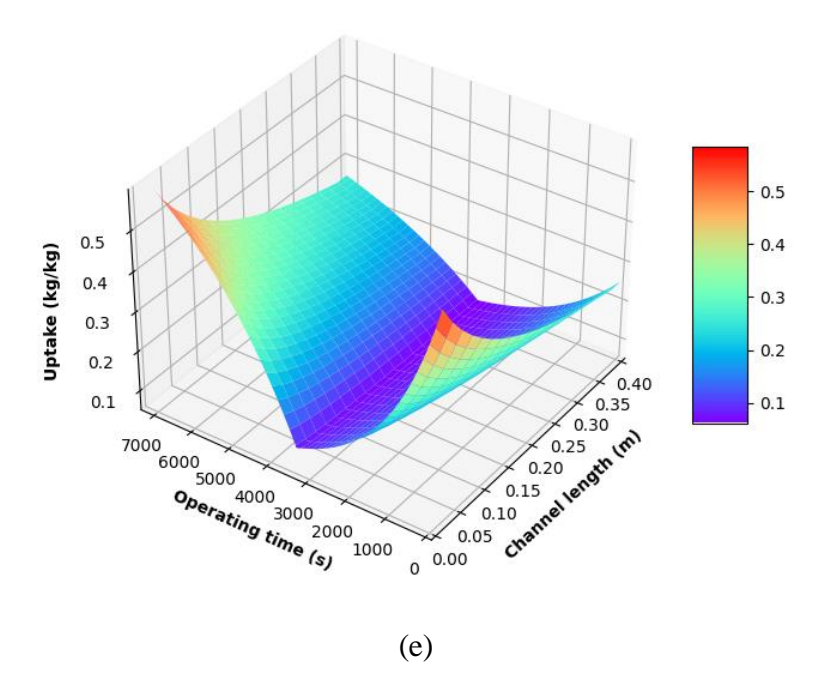
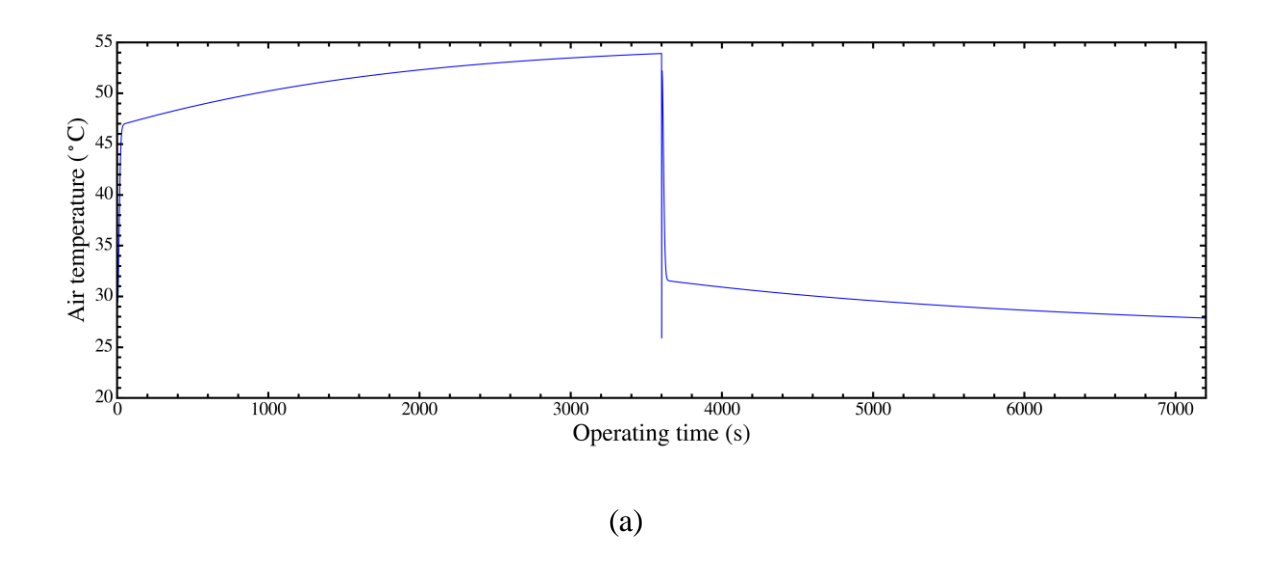


Fig. 4.8. Temperature and humidity behavior of air during the adsorption/desorption process: (a) adsorption mode temperature profile; (b) adsorption mode humidity profile; (c) desorption mode temperature profile; (d) desorption mode humidity profile; (e) uptake of the adsorbent.



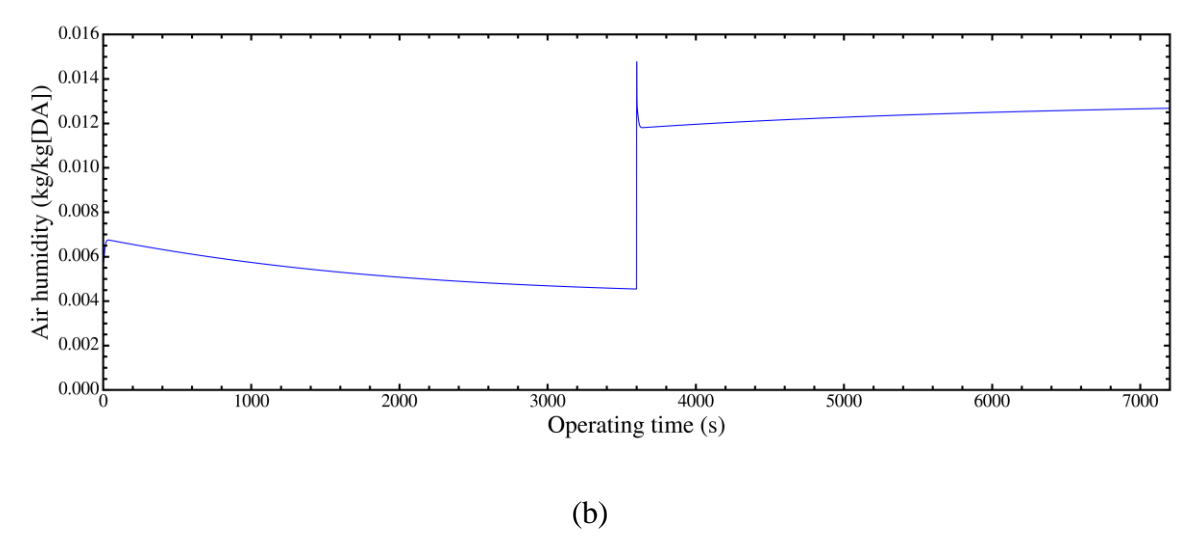


Fig. 4.9. Temperature and humidity distribution of air channel outlet: (a) temperature; (b) humidity.

4.5 Conclusions

This section investigated the performance of a proposed hybrid system integrating DPEC, PV, and desiccant units under winter conditions, focusing on its potential to enhance thermal comfort and energy efficiency. On the other hand, the system demonstrated the capability to warm and dehumidify air effectively while maintaining the PV panel's efficiency in the winter season. Simulations revealed that the DPEC unit initially cooled ambient air to below wet-bulb temperature, which then absorbed heat from the PV panel, increasing its temperature to 26°C and stabilizing the PV panel surface at 31.2°C. The desiccant unit further processed the high-humidity air, raising its temperature to 28°C and reducing its humidity to 13 g/kg[DA], thus delivering air within the comfort range defined for winter conditions.

Compared to a naturally ventilated PV system, the proposed system maintained a stable PV surface temperature and produced supply air with balanced temperature and humidity. While natural ventilation increased air temperature to over 50°C, it reduced relative humidity to below 5%, leading to discomfort. In contrast, the hybrid system produced air at 28°C with a relative humidity of 45%, aligning with thermal comfort standards. Dynamic modeling and analysis of

adsorption/desorption processes validated the system's ability to manage temperature and humidity effectively. Results indicated the proposed system's significant potential to provide energy-efficient and thermally comfortable air in winter, with room for further optimization through experimental validation.

At this stage, the key findings of the chapter can be highlighted as below:

- 1. A hybrid DPEC-PV-desiccant system effectively balances air temperature and humidity, achieving thermal comfort under winter conditions.
- 2. The proposed system enhances PV efficiency by stabilizing surface temperature and delivers energy-efficient air at 28°C and 45% relative humidity.

Chapter 5 Conclusions and future prospects

5.1 Conclusions

This study has systematically explored the potential and performance of dew-point evaporative cooling (DPEC) systems and their integration into advanced energy systems under various operational scenarios. The findings highlight the versatility and efficiency of DPEC technology in addressing cooling and heating challenges, offering significant implications for sustainable energy solutions. The following key insights have been derived from the comprehensive investigations:

- In the context of entropy generation analysis, a comprehensive dynamic model was developed to investigate the thermodynamic behavior of a counter-flow DPEC system. Key insights from this analysis demonstrated the critical influence of inlet air conditions, working ratios, airflow velocities, and channel geometries on system performance. Higher inlet air temperatures and reduced humidity levels enhanced the system's cooling potential but increased entropy generation in specific components, necessitating careful optimization. The study revealed that an optimal working ratio and lower air velocities improved heat and mass transfer efficiency, striking a balance between cooling performance and system entropy. This foundational understanding lays the groundwork for further optimizing DPEC systems for energy-efficient cooling.
- 2) The application of an enhanced DPEC system for photovoltaic (PV) panel cooling was evaluated. By introducing an additional wet channel, the system achieved superior thermal management compared to conventional cooling methods. It maintained PV panel efficiencies exceeding 15% under extreme summer conditions, with notable

improvements in cooling performance. However, the study also acknowledged the trade-offs, such as increased water consumption and limited efficacy under high humidity conditions. These findings emphasize the need for integrated strategies, including pre-dehumidification, to overcome climatic constraints.

3) The hybrid DPEC-PV-desiccant system was analyzed for its winter heating performance. The system demonstrated the capability to effectively warm and dehumidify air while stabilizing the PV panel surface temperature, ensuring thermal comfort. The integration of desiccant units facilitated precise humidity control, delivering supply air at optimal conditions of 28°C and 45% relative humidity. Comparative analysis highlighted the system's advantages over natural ventilation, including enhanced energy efficiency and improved thermal comfort under winter scenarios.

Overall, this research underscores the adaptability of DPEC systems in diverse applications, from cooling PV panels to hybrid heating systems for winter. By leveraging thermodynamic principles and advanced modeling techniques, it offers valuable insights into system design and operational strategies.

5.2 Future prospects

Future work in the field of dew-point evaporative cooling (DPEC) systems should address several key areas to enhance their applicability and performance in real-world settings. First, experimental validations are essential to confirm the theoretical findings and model predictions. While simulations offer valuable insights, experimental setups provide real-world data that can refine system design and ensure that the models accurately represent the complexities of operational environments. Second, economic analyses are crucial for assessing the cost-

effectiveness of DPEC systems in commercial applications. While DPEC offers energy-efficient cooling solutions, factors such as installation, maintenance, and water consumption need to be evaluated in terms of operational costs and energy savings over time. A cost-benefit analysis can guide decision-makers in industries such as data centers, solar panel cooling, or even residential applications. Finally, innovative integrations of DPEC with other technologies hold significant promise. For instance, combining DPEC systems with renewable energy sources, such as solar thermal collectors or wind energy, could lead to highly efficient, low-carbon cooling and heating solutions. Furthermore, integrating DPEC with desiccant materials for hybrid systems can improve both the cooling efficiency and humidity control, particularly in applications requiring both temperature and moisture regulation. These future research directions will be critical to advancing DPEC systems from laboratory settings to widespread practical applications, ultimately optimizing energy usage and environmental sustainability.

References

- [1] ASHRAE-55, Thermal Environmental Conditions for Human Occupancy-2017, ANSI/ASHRAE Standard 55 7 (2017) 60.
- [2] Y. Geng, W. Ji, B. Lin, Y. Zhu, The impact of thermal environment on occupant IEQ perception and productivity, Build Environ 121 (2017) 158–167. https://doi.org/10.1016/j.buildenv.2017.05.022.
- [3] W. Liu, T. (Tim) Zhang, D. Lai, Inverse design of a thermally comfortable indoor environment with a coupled CFD and multi-segment human thermoregulation model, Build Environ 227 (2023) 109769. https://doi.org/10.1016/j.buildenv.2022.109769.
- [4] S.G.L. Persiani, B. Kobas, S.C. Koth, T. Auer, Biometric Data as Real-Time Measure of Physiological Reactions to Environmental Stimuli in the Built Environment, Energies (Basel) 14 (2021) 232. https://doi.org/10.3390/en14010232.
- [5] X. Shan, E.H. Yang, Supervised machine learning of thermal comfort under different indoor temperatures using EEG measurements, Energy Build 225 (2020) 110305. https://doi.org/10.1016/j.enbuild.2020.110305.
- [6] A. Aryal, B. Becerik-Gerber, Thermal comfort modeling when personalized comfort systems are in use: Comparison of sensing and learning methods, Build Environ 185 (2020) 107316. https://doi.org/10.1016/j.buildenv.2020.107316.
- [7] M. Lind, S. Holøs, K. Thunshelle, A. Yang, M. Mysen, How Does Low Relative Humidity Affect Perceived Air Quality, Thermal Comfort and Symptoms in Modern Office Buildings in Cold Climates?, (2019) 899–909. https://doi.org/10.1007/978-3-030-00662-4_76.
- [8] A. Sekatia, E. Setyowati, G. Hardiman, On the comparison of thermal comfort performances in dutch style churches with low ventilation in hot-humid tropical region, Civil Engineering and Architecture 8 (2020) 1419–1435. https://doi.org/10.13189/cea.2020.080625.
- [9] B. Chenari, J. Dias Carrilho, M. Gameiro Da Silva, Towards sustainable, energy-efficient and healthy ventilation strategies in buildings: A review, Renewable and

- Sustainable Energy Reviews 59 (2016) 1426–1447. https://doi.org/10.1016/j.rser.2016.01.074.
- [10] Y. Yu, T. Xiang, D. Wang, L. Yang, Optimization control strategy for mixed-mode buildings based on thermal comfort model: A case study of office buildings, Appl Energy 358 (2024) 122627. https://doi.org/10.1016/j.apenergy.2024.122627.
- [11] F. Savanti, E. Setyowati, G. Hardiman, The Impact of Ventilation on Indoor Air Quality and Air Change Rate, Evergreen 9 (2022) 219–225. https://doi.org/10.5109/4774237.
- [12] A. Remizov, S.A. Memon, J.R. Kim, Novel building energy performance-based climate zoning enhanced with spatial constraint, Appl Energy 355 (2024) 122238. https://doi.org/10.1016/j.apenergy.2023.122238.
- [13] International Energy Agency (IEA), "The Future of Cooling Opportunities for energy- efficient air conditioning" International Energy Agency Website: www.iea.org, 2018, (2018). www.iea.org.
- [14] I.E. Agency, Energy Technology Perspectives, OECD Publishing, 2023. https://doi.org/10.1787/9789264109834-en.
- [15] O.M. Zaki, O. Abdelaziz, Minimizing annual energy consumption using innovative cooling system architecture for diverse climatic conditions, International Journal of Refrigeration 159 (2024) 147–162. https://doi.org/10.1016/j.ijrefrig.2023.12.037.
- [16] S. Feng, L. Yao, M. Feng, H. Cai, X. He, M. He, X. Bu, Y. Zhou, T. Zhang, Sustainable regeneration of waste polystyrene foam as cooling coating: Building cooling energy saving, CO2 emission reduction and cost-benefit prospective, J Clean Prod 434 (2024). https://doi.org/10.1016/j.jclepro.2023.140361.
- [17] T. Abergel, B. Dean, J. Dulac, Towards a zero-emission, efficient, and resilient buildings and construction sector: Global Status Report 2017, UN Environment and International Energy Agency: Paris, France 22 (2017).
- [18] A. Standard, Performance rating of unitary air-conditioning & air-source heat pump equipment, AHRI Standard 210 (2008) 240.
- [19] M.T. Kibria, M.A. Islam, B.B. Saha, T. Nakagawa, S. Mizuno, Assessment of environmental impact for air-conditioning systems in Japan using HFC based refrigerants, Evergreen 6 (2019) 246–253. https://doi.org/10.5109/2349301.
- [20] K. Zhao, X.H. Liu, T. Zhang, Y. Jiang, Performance of temperature and humidity

- independent control air-conditioning system in an office building, Energy Build 43 (2011) 1895–1903. https://doi.org/10.1016/j.enbuild.2011.03.041.
- [21] P. Tanadecha, K. Khaothong, Thermoeconomic analysis of duct works for air-conditioned building in Thailand, Energy and Built Environment 6 (2025) 80–95. https://doi.org/10.1016/j.enbenv.2023.09.002.
- [22] Q. Zhang, T. Alexis Salazar Sazon, F. Skaug Fadnes, X. Peng, N. Ahmed, H. Nikpey, M. Mansouri, M. Assadi, Design optimization of the cooling systems with PCM-to-air heat exchanger for the energy saving of the residential buildings, Energy Conversion and Management: X 23 (2024) 100630. https://doi.org/10.1016/j.ecmx.2024.100630.
- [23] B. Sandong Omgba, F. Lontsi, M.K. Ndame, S.M. Thierry Olivier, I. Ndoh Mbue, Development and energy analysis of a solar-assisted air conditioning system for energy saving, Energy Conversion and Management: X 19 (2023) 100390. https://doi.org/10.1016/j.ecmx.2023.100390.
- [24] M. Elhelw, W.M. El-Maghlany, A.H. Abdelaziz, Experimental and theoretical study of hybrid electric solar driven vapour compression system, Renew Energy 182 (2022) 452–466. https://doi.org/10.1016/j.renene.2021.10.035.
- [25] P. Martínez, M. Lucas, F.J. Aguilar, J. Ruiz, P. V. Quiles, Experimental study of an on-grid hybrid solar air conditioner with evaporative pre-cooling of condenser inlet air, Appl Therm Eng 248 (2024) 123335. https://doi.org/10.1016/j.applthermaleng.2024.123335.
- [26] X. Li, C. Shen, C.W.F. Yu, Building energy efficiency: Passive technology or active technology?, Indoor and Built Environment 26 (2017) 729–732. https://doi.org/10.1177/1420326X17719157.
- [27] C. Liang, X. Li, G. Zheng, Optimizing air conditioning systems by considering the grades of sensible and latent heat loads, Appl Energy 322 (2022) 119458. https://doi.org/10.1016/j.apenergy.2022.119458.
- [28] M. Rampazzo, M. Lionello, A. Beghi, E. Sisti, L. Cecchinato, A static moving boundary modelling approach for simulation of indirect evaporative free cooling systems, Appl Energy 250 (2019) 1719–1728. https://doi.org/10.1016/j.apenergy.2019.04.087.
- [29] B. Tashtoush, M. Tahat, A. Al-Hayajneh, V.A. Mazur, D. Probert, Thermodynamic

- behavior of an airconditioning system employing combined evaporative-water and air coolers, Appl Energy 70 (2001) 305–319. https://doi.org/10.1016/S0306-2619(01)00039-3.
- [30] H. Yan, Y. Xia, S. Deng, Simulation study on a three-evaporator air conditioning system for simultaneous indoor air temperature and humidity control, Appl Energy 207 (2017) 294–304. https://doi.org/10.1016/j.apenergy.2017.05.125.
- [31] J. Chen, X. Wang, X. Wu, C. Ding, D. Han, W. He, Experimental investigation on the thermal and flow performance of a thermodynamically-balanced packed bed humidification system, Appl Therm Eng 236 (2024). https://doi.org/10.1016/j.applthermaleng.2023.121771.
- [32] R. Mao, H. Wu, C. Li, Z. Zhang, X. Liang, J. Zhou, J. Chen, Experimental investigation on the application of cold-mist direct evaporative cooling in data centers, International Journal of Thermal Sciences 208 (2025) 109500. https://doi.org/10.1016/j.ijthermalsci.2024.109500.
- [33] I. Khan, W. Khalid, H.M. Ali, M. Sajid, Z. Ali, M. Ali, An experimental investigation on the novel hybrid indirect direct evaporative cooling system, International Communications in Heat and Mass Transfer 155 (2024) 107503. https://doi.org/10.1016/j.icheatmasstransfer.2024.107503.
- [34] W. Gao, M. Yang, Y. Wang, L. Yang, Q. Miao, R. Yan, Y. Hu, Numerical study on parametric correlations and regional applicability of a cross-flow indirect evaporative cooler, Journal of Building Engineering 97 (2024) 110876. https://doi.org/10.1016/j.jobe.2024.110876.
- [35] G. Zhu, T. Wen, Q. Wang, X. Xu, A review of dew-point evaporative cooling: Recent advances and future development, Appl Energy 312 (2022) 118785. https://doi.org/10.1016/j.apenergy.2022.118785.
- [36] P. Glanville, A. Kozlov, V. Maisotsenko, Dew Point Evaporative Cooling: Technology Review and Fundamentals, n.d.
- [37] X. Zhao, J.M. Li, S.B. Riffat, Numerical study of a novel counter-flow heat and mass exchanger for dew point evaporative cooling, Appl Therm Eng 28 (2008) 1942–1951. https://doi.org/10.1016/j.applthermaleng.2007.12.006.
- [38] Z. Duan, Investigation of a novel dew point indirect evaporative air conditioning system for buildings, Phd Dissertation (2011).

- http://etheses.nottingham.ac.uk/12200/.
- [39] S. Anisimov, D. Pandelidis, Numerical study of the Maisotsenko cycle heat and mass exchanger, Int J Heat Mass Transf 75 (2014) 75–96. https://doi.org/10.1016/j.ijheatmasstransfer.2014.03.050.
- [40] S. Anisimov, D. Pandelidis, J. Danielewicz, Numerical analysis of selected evaporative exchangers with the Maisotsenko cycle, Energy Convers Manag 88 (2014) 426–441. https://doi.org/10.1016/j.enconman.2014.08.055.
- [41] S. Anisimov, D. Pandelidis, A. Jedlikowski, V. Polushkin, Performance investigation of a M (Maisotsenko)-cycle cross-flow heat exchanger used for indirect evaporative cooling, Energy 76 (2014) 593–606. https://doi.org/10.1016/j.energy.2014.08.055.
- [42] D. Pandelidis, S. Anisimov, W.M. Worek, Comparison study of the counter-flow regenerative evaporative heat exchangers with numerical methods, Appl Therm Eng 84 (2015) 211–224. https://doi.org/10.1016/j.applthermaleng.2015.03.058.
- [43] A. Hasan, Indirect evaporative cooling of air to a sub-wet bulb temperature, Appl Therm Eng 30 (2010) 2460–2468. https://doi.org/10.1016/j.applthermaleng.2010.06.017.
- [44] A. Hasan, Going below the wet-bulb temperature by indirect evaporative cooling: Analysis using a modified ε-NTU method, Appl Energy 89 (2012) 237–245. https://doi.org/10.1016/j.apenergy.2011.07.005.
- [45] J. Lee, D.Y. Lee, Experimental study of a counter flow regenerative evaporative cooler with finned channels, Int J Heat Mass Transf 65 (2013) 173–179. https://doi.org/10.1016/j.ijheatmasstransfer.2013.05.069.
- [46] J. Lin, K. Thu, T.D. Bui, R.Z. Wang, K.C. Ng, K.J. Chua, Study on dew point evaporative cooling system with counter-flow configuration, Energy Convers Manag 109 (2016) 153–165. https://doi.org/10.1016/j.enconman.2015.11.059.
- [47] S.K. Gupta, Thermodynamic Performance Enhancement of an Air Conditioner With Dew Point Evaporative Cooler, (2023) 1–9. https://doi.org/10.1115/1.4063498.
- [48] B. Riangvilaikul, S. Kumar, Numerical study of a novel dew point evaporative cooling system, Energy Build 42 (2010) 2241–2250. https://doi.org/10.1016/j.enbuild.2010.07.020.
- [49] B. Riangvilaikul, S. Kumar, An experimental study of a novel dew point evaporative cooling system, Energy Build 42 (2010) 637–644.

- https://doi.org/10.1016/j.enbuild.2009.10.034.
- [50] A. Pakari, S. Ghani, Comparison of 1D and 3D heat and mass transfer models of a counter flow dew point evaporative cooling system: Numerical and experimental study, International Journal of Refrigeration 99 (2019) 114–125. https://doi.org/10.1016/j.ijrefrig.2019.01.013.
- [51] K. Thu, Y.D. Kim, A. Myat, W.G. Chun, K.C. Ng, Entropy generation analysis of an adsorption cooling cycle, Int J Heat Mass Transf 60 (2013) 143–155. https://doi.org/10.1016/j.ijheatmasstransfer.2012.12.055.
- [52] L.A. Al-Azez Mahdi, M.A. Fayad, M.T. Chaichan, Analysis of Entropy Generation for Horizontal Heated Cylinder by Natural Convection and Radiation, Evergreen 10 (2023) 888–896. https://doi.org/10.5109/6792884.
- [53] G. Sachdeva, B. Sharma, P. Anuradha, S. Verma, Irreversibility Analysis of an Ejector Refrigeration Cycle by Modified Gouy-Stodola Formulation, Evergreen 10 (2023) 252–271. https://doi.org/10.5109/6781075.
- [54] R. Kumar, S.K. Verma, N.K. Gupta, S.K. Singh, Performance Enhancement of TSAH using Graphene and Graphene/CeO2 -Black Paint Coating on Absorber: A Comparative Study, Evergreen 9 (2022) 673–681. https://doi.org/10.5109/4843098.
- [55] L. Wang, C. Zhan, J. Zhang, X. Zhao, Optimization of the counter-flow heat and mass exchanger for M-Cycle indirect evaporative cooling assisted with entropy analysis, Energy 171 (2019) 1206–1216. https://doi.org/10.1016/j.energy.2019.01.099.
- [56] M.A. Aziz, J. Lin, F. Mikšík, T. Miyazaki, K. Thu, The second law analysis of a humidification-dehumidification desalination system using M-cycle, Sustainable Energy Technologies and Assessments 52 (2022). https://doi.org/10.1016/j.seta.2022.102141.
- [57] J. Lin, D.T. Bui, R. Wang, K.J. Chua, On the exergy analysis of the counter-flow dew point evaporative cooler, Energy 165 (2018) 958–971. https://doi.org/10.1016/j.energy.2018.10.042.
- [58] J. Lin, K. Thu, S. Karthik, M.W. Shahzad, R. Wang, K.J. Chua, Understanding the transient behavior of the dew point evaporative cooler from the first and second law of thermodynamics, Energy Convers Manag 244 (2021) 114471. https://doi.org/10.1016/j.enconman.2021.114471.

- [59] H. Caliskan, I. Dincer, A. Hepbasli, A comparative study on energetic, exergetic and environmental performance assessments of novel M-Cycle based air coolers for buildings, Energy Convers Manag 56 (2012) 69–79. https://doi.org/10.1016/j.enconman.2011.11.007.
- [60] H. Caliskan, A. Hepbasli, I. Dincer, V. Maisotsenko, Thermodynamic performance assessment of a novel air cooling cycle: Maisotsenko cycle, International Journal of Refrigeration 34 (2011) 980–990. https://doi.org/10.1016/j.ijrefrig.2011.02.001.
- [61] Y. Duan, Y. Zhou, Z. Dou, Q. Dai, Y. Yu, Q. Li, Performance study of a novel indirect evaporative/air-cooled thermoelectric cooling air conditioning system, Build Environ 265 (2024). https://doi.org/10.1016/j.buildenv.2024.111977.
- [62] A. Urso, E. Velasco-Gómez, A. Tejero-González, M. Andrés-Chicote, F. Nocera, Experimental study of the optimal design and performance of a mixed-flow dewpoint indirect evaporative cooler, Appl Therm Eng 257 (2024). https://doi.org/10.1016/j.applthermaleng.2024.124294.
- [63] D. Pandelidis, W. Worek, S. Cetin, Analysis of heat and mass transfer potential of a dew-point cooling tower in different climatic conditions, International Communications in Heat and Mass Transfer 156 (2024) 107671. https://doi.org/10.1016/j.icheatmasstransfer.2024.107671.
- [64] B.C. Wang, Z. Chen, G.L. You, J.N. Ding, G.G. Cheng, T.D. Bui, Improving indoor air quality and cooling efficiency: Indirect dew-point evaporative cooling in South China summers, Energy Build 324 (2024). https://doi.org/10.1016/j.enbuild.2024.114908.
- [65] B.C. Wang, Z. Chen, G.L. You, J.N. Ding, G.G. Cheng, T.D. Bui, Performance assessment of a high-efficiency indirect dew-point evaporative cooler through threedimensional modeling, Energy 312 (2024) 133422. https://doi.org/10.1016/j.energy.2024.133422.
- [66] Y.E. Güzelel, U. Olmuş, O. Büyükalaca, Performance evaluation of different types of indirect evaporative coolers: A CFD-based comparative study, Journal of Building Engineering 96 (2024). https://doi.org/10.1016/j.jobe.2024.110399.
- [67] K. Wu, S. Wang, J. Lin, Y. Shao, F. Gao, K.J. Chua, The enhanced dew-point evaporative cooling with a macro-roughened structure, Int J Heat Mass Transf 219 (2024) 124898. https://doi.org/10.1016/j.ijheatmasstransfer.2023.124898.

- [68] P. Xu, X. Mu, H. Chen, X. Ma, X. Zhao, Experimental and numerical investigation of the temperature and humidity distribution inside the channels for a regenerative indirect evaporative cooler, Appl Therm Eng 236 (2024) 121586. https://doi.org/10.1016/j.applthermaleng.2023.121586.
- [69] S. Chakraborty, D. Vernon, A. Jha, V. Narayanan, Performance characterization of M-cycle indirect evaporative cooler and heat recovery ventilator for commercial buildings – Experiments and model, Energy Build 281 (2023) 112762. https://doi.org/10.1016/j.enbuild.2022.112762.
- [70] B.C. Wang, M. Garcia, C.D. Wei, G.G. Cheng, W. Pang, T. Bui, Development and performance analysis of a compact counterflow dew-point cooler for tropics, Thermal Science and Engineering Progress 46 (2023) 102218. https://doi.org/10.1016/j.tsep.2023.102218.
- [71] A. Pacak, K. Sierpowski, B. Baran, Z. Malecha, W. Worek, S. Cetin, D. Pandelidis, Impact of air distribution on dew point evaporative cooler thermal performance, Appl Therm Eng 224 (2023). https://doi.org/10.1016/j.applthermaleng.2023.120137.
- [72] G. Zhu, W. Chen, D. Zhang, T. Wen, Performance evaluation of counter flow dewpoint evaporative cooler with a three-dimensional numerical model, Appl Therm Eng 219 (2023) 119483. https://doi.org/10.1016/j.applthermaleng.2022.119483.
- [73] F. Gao, K. Thu, S. Wang, F. Zhao, J. Lin, K. Wu, Numerical investigation of a novel tubular dew-point evaporative cooler, Appl Therm Eng 223 (2023) 120064. https://doi.org/10.1016/j.applthermaleng.2023.120064.
- [74] F. Comino, M.J. Romero-Lara, M. Ruiz de Adana, Experimental and numerical study of dew-point indirect evaporative coolers to optimize performance and design, International Journal of Refrigeration 142 (2022) 92–102. https://doi.org/10.1016/j.ijrefrig.2022.06.006.
- [75] M. Puglia, N. Morselli, M. Cossu, S. Pedrazzi, G. Allesina, A. Muscio, Recovered water from fuel cells as a supply for Maisotsenko evaporative cooling systems in a hydrogen-powered urban bus, Appl Therm Eng 256 (2024) 124053. https://doi.org/10.1016/j.applthermaleng.2024.124053.
- [76] Q. Chen, K. Yang, M. Wang, N. Pan, Z.-Y. Guo, A new approach to analysis and optimization of evaporative cooling system I: Theory, Energy 35 (2010) 2448–2454. https://doi.org/https://doi.org/10.1016/j.energy.2010.02.037.

- [77] Q. Chen, N. Pan, Z.-Y. Guo, A new approach to analysis and optimization of evaporative cooling system II: Applications, Energy 36 (2011) 2890–2898. https://doi.org/https://doi.org/10.1016/j.energy.2011.02.031.
- [78] C. Sheng, A.G. Agwu Nnanna, Empirical correlation of cooling efficiency and transport phenomena of direct evaporative cooler, Appl Therm Eng 40 (2012) 48–55. https://doi.org/https://doi.org/10.1016/j.applthermaleng.2012.01.052.
- [79] M. Lucas, F.J. Aguilar, J. Ruiz, C.G. Cutillas, A.S. Kaiser, P.G. Vicente, Photovoltaic Evaporative Chimney as a new alternative to enhance solar cooling, Renew Energy 111 (2017) 26–37. https://doi.org/10.1016/j.renene.2017.03.087.
- [80] Z.A. Haidar, J. Orfi, Z. Kaneesamkandi, Experimental investigation of evaporative cooling for enhancing photovoltaic panels efficiency, Results Phys 11 (2018) 690–697. https://doi.org/10.1016/j.rinp.2018.10.016.
- [81] Z.A. Haidar, COOLING OF SOLAR PV PANELS USING EVAPORATIVE COOLING, (2016).
- [82] D.M. Noori Mahmood, I.M. Ali Aljubury, Experimental investigation of a hybrid photovoltaic evaporative cooling (PV/EC) system performance under arid conditions, Results in Engineering 15 (2022) 100618. https://doi.org/10.1016/j.rineng.2022.100618.
- [83] T. Žižak, S. Domjan, S. Medved, C. Arkar, Efficiency and sustainability assessment of evaporative cooling of photovoltaics, Energy 254 (2022). https://doi.org/10.1016/j.energy.2022.124260.
- [84] M. Alktranee, B. Péter, Energy and exergy analysis for photovoltaic modules cooled by evaporative cooling techniques, Energy Reports 9 (2023) 122–132. https://doi.org/10.1016/j.egyr.2022.11.177.
- [85] D. Kumar Sharma, A. Saikiran Pegallapati, M. Ramgopal, Performance of a CO2 based transcritical air conditioning system under summer and winter conditions, Thermal Science and Engineering Progress 41 (2023) 101847. https://doi.org/10.1016/j.tsep.2023.101847.
- [86] M. Qu, X. Yan, X. Sang, Y. Bai, W. Chu, X. Zhu, Field studies on indoor thermal environment and start-stop characteristics of the radiant air conditioning system during intermittent heating, Journal of Building Engineering 76 (2023) 107121. https://doi.org/10.1016/j.jobe.2023.107121.

- [87] M. Qu, X. Sang, X. Yan, P. Huang, B. Zhang, X. Bai, A simulation study on the heating characteristics of residential buildings using intermittent heating in Hot-Summer/Cold-Winter areas of China, Appl Therm Eng 241 (2024) 122360. https://doi.org/10.1016/j.applthermaleng.2024.122360.
- [88] J. Dong, W. Zheng, Z. Ran, B. Zhang, Experimental investigation on heating performance of a novel radiant-convective heating terminal, Renew Energy 164 (2021) 804–814. https://doi.org/10.1016/j.renene.2020.09.100.
- [89] Y. Yang, C. Ren, M. Tu, B. Luo, J. Fu, Theoretical performance analysis of a new hybrid air conditioning system with two-stage energy recovery in cold winter, International Journal of Refrigeration 117 (2020) 1–11. https://doi.org/10.1016/j.ijrefrig.2020.03.028.
- [90] Y. Li, G. Zhang, G.Z. Lv, A.N. Zhang, R.Z. Wang, Performance study of a solar photovoltaic air conditioner in the hot summer and cold winter zone, Solar Energy 117 (2015) 167–179. https://doi.org/10.1016/j.solener.2015.04.015.
- [91] M.A. Said, H. Hassan, Impact of energy storage of new hybrid system of phase change materials combined with air-conditioner on its heating and cooling performance, J Energy Storage 36 (2021) 102400. https://doi.org/10.1016/j.est.2021.102400.
- [92] H. Zhang, Z. Fang, X. Zhang, S. Yang, Z. Qian, Z. Chen, A novel dual-wheel air-conditioning system operating strategy in different seasons, Energy Build 323 (2024) 114812. https://doi.org/10.1016/j.enbuild.2024.114812.
- [93] T.S. Ge, Y.J. Dai, R.Z. Wang, Performance study of desiccant coated heat exchanger air conditioning system in winter, Energy Convers Manag 123 (2016) 559–568. https://doi.org/10.1016/j.enconman.2016.06.075.
- [94] J.Y. Zhang, T.S. Ge, Y.J. Dai, Y. Zhao, R.Z. Wang, Experimental investigation on solar powered desiccant coated heat exchanger humidification air conditioning system in winter, Energy 137 (2017) 468–478. https://doi.org/10.1016/j.energy.2017.02.164.
- [95] S. Nain, A. Parinam, S. Kajal, Experimental study and analysis of solar based winter air conditioning system using desiccant coated heat exchanger, Mater Today Proc 46 (2019) 9938–9943. https://doi.org/10.1016/j.matpr.2021.02.705.
- [96] R. Raad, M. Itani, N. Ghaddar, K. Ghali, A novel M-cycle evaporative cooling vest

- for enhanced comfort of active human in hot environment, International Journal of Thermal Sciences 142 (2019) 1–13. https://doi.org/10.1016/j.ijthermalsci.2019.04.010.
- [97] J. Lin, H.N. Chu, K. Thu, M. Wojtala, F. Gao, K.J. Chua, Novel battery thermal management via scalable dew-point evaporative cooling, Energy Convers Manag 283 (2023) 116948. https://doi.org/10.1016/j.enconman.2023.116948.
- [98] H.S. Dizaji, E. Hu, L. Chen, S. Pourhedayat, M. Wae-hayee, Proposing the concept of mini Maisotsenko cycle cooler for electronic cooling purposes; experimental study, Case Studies in Thermal Engineering 27 (2021) 101325. https://doi.org/10.1016/j.csite.2021.101325.
- [99] X. Ma, C. Zeng, Z. Zhu, X. Zhao, X. Xiao, Y.G. Akhlaghi, S. Shittu, Real life test of a novel super performance dew point cooling system in operational live data centre, Appl Energy 348 (2023) 121483. https://doi.org/10.1016/j.apenergy.2023.121483.
- [100] W. Yan, X. Cui, M. Zhao, X. Meng, C. Yang, Y. Zhang, Y. Liu, L. Jin, Multi-objective optimization of dew point indirect evaporative coolers for data centers, Appl Therm Eng 241 (2024) 122425.
 https://doi.org/10.1016/j.applthermaleng.2024.122425.
- [101] Y.E. Güzelel, U. Olmuş, O. Büyükalaca, Simulation of a desiccant air-conditioning system integrated with dew-point indirect evaporative cooler for a school building, Appl Therm Eng 217 (2022) 119233. https://doi.org/10.1016/j.applthermaleng.2022.119233.
- [102] A. Pacak, A. Jurga, B. Kaźmierczak, D. Pandelidis, Experimental verification of the effect of air pre-cooling in dew point evaporative cooler on the performance of a solid desiccant dehumidifier, International Communications in Heat and Mass Transfer 142 (2023) 106651.
 https://doi.org/10.1016/j.icheatmasstransfer.2023.106651.
- [103] M.J. Romero-Lara, F. Comino, M. Ruiz de Adana, Experimental assessment of the energy performance of a renewable air-cooling unit based on a dew-point indirect evaporative cooler and a desiccant wheel, Energy Convers Manag 310 (2024) 118486. https://doi.org/10.1016/j.enconman.2024.118486.
- [104] L. Lai, X. Wang, G. Kefayati, E. Hu, K.C. Ng, Optimisation of cooling performance and water consumption of a solid desiccant-assisted indirect evaporative cooling

- system using response surface methodology, International Journal of Refrigeration 168 (2024) 376–388. https://doi.org/10.1016/j.ijrefrig.2024.09.023.
- [105] L. Chun, Z. Liao, G. Wang, Y. Xiao, J. Huo, D. Liu, B. Jiang, Operational characteristics and controlling strategies of a novel dual-return-air dehumidification evaporative cooling system (DDEC), Energy 309 (2024) 133173. https://doi.org/10.1016/j.energy.2024.133173.
- [106] W. Chen, X. Cui, Z.F. Huang, Y.L. Shao, K.J. Chua, Developing an integrated solid desiccant dehumidifier and dew-point evaporative cooler for green air conditioning, Journal of Building Engineering 96 (2024) 110404. https://doi.org/10.1016/j.jobe.2024.110404.
- [107] T. Miyazaki, I. Nikai, A. Akisawa, Simulation analysis of an open-cycle adsorption air conditioning system-numeral modeling of a fixed bed dehumidification unit and the maisotsenko cycle cooling unit, International Journal of Energy for a Clean Environment 12 (2011) 341–354.

 https://doi.org/10.1615/InterJEnerCleanEnv.2012005977.
- [108] J. Lin, K. Thu, T.D. Bui, R.Z. Wang, K.C. Ng, M. Kumja, K.J. Chua, Unsteady-state analysis of a counter-flow dew point evaporative cooling system, Energy 113 (2016) 172–185. https://doi.org/10.1016/j.energy.2016.07.036.
- [109] I.H. Bell, J. Wronski, S. Quoilin, V. Lemort, Pure and Pseudo-pure Fluid Thermophysical Property Evaluation and the Open-Source Thermophysical Property Library CoolProp, Ind Eng Chem Res 53 (2014) 2498–2508. https://doi.org/10.1021/ie4033999.
- [110] M.J. Moran, H.N. Shapiro, D.D. Boettner, M.B. Bailey, Fundamentals of Engineering Thermodynamics, Wiley, 2010.
- [111] A. Sciacovelli, V. Verda, E. Sciubba, Entropy generation analysis as a design tool A review, Renewable and Sustainable Energy Reviews 43 (2015) 1167–1181. https://doi.org/10.1016/j.rser.2014.11.104.
- [112] J. Lin, D.T. Bui, R. Wang, K.J. Chua, On the fundamental heat and mass transfer analysis of the counter-flow dew point evaporative cooler, Appl Energy 217 (2018) 126–142. https://doi.org/10.1016/j.apenergy.2018.02.120.
- [113] T. Ghazouani, Dynamic impact of globalization on renewable energy consumption: Non-parametric modelling evidence, Technol Forecast Soc Change 185 (2022)

- 122115. https://doi.org/https://doi.org/10.1016/j.techfore.2022.122115.
- [114] T. Kober, H.-W. Schiffer, M. Densing, E. Panos, Global energy perspectives to 2060
 WEC's World Energy Scenarios 2019, Energy Strategy Reviews 31 (2020)
 100523. https://doi.org/https://doi.org/10.1016/j.esr.2020.100523.
- [115] D.S. Timmons, K. Elahee, M. Lin, Energy efficiency and conservation values in a variable renewable electricity system, Energy Strategy Reviews 43 (2022) 100935. https://doi.org/https://doi.org/10.1016/j.esr.2022.100935.
- [116] International Energy Agency, International Energy Agency (IEA) World Energy Outlook 2022, Https://Www.Iea.Org/Reports/World-Energy-Outlook-2022/Executive-Summary (2022) 524.
- [117] C.N. Markides, The role of pumped and waste heat technologies in a high-efficiency sustainable energy future for the UK, Appl Therm Eng 53 (2013) 197–209. https://doi.org/https://doi.org/10.1016/j.applthermaleng.2012.02.037.
- [118] N. Kannan, D. Vakeesan, Solar energy for future world: A review, Renewable and Sustainable Energy Reviews 62 (2016) 1092–1105. https://doi.org/https://doi.org/10.1016/j.rser.2016.05.022.
- [119] E. Kabir, P. Kumar, S. Kumar, A.A. Adelodun, K.-H. Kim, Solar energy: Potential and future prospects, Renewable and Sustainable Energy Reviews 82 (2018) 894–900. https://doi.org/10.1016/j.rser.2017.09.094.
- [120] R. Prăvălie, C. Patriche, G. Bandoc, Spatial assessment of solar energy potential at global scale. A geographical approach, J Clean Prod 209 (2019) 692–721. https://doi.org/10.1016/j.jclepro.2018.10.239.
- [121] M. Adaramola, Solar energy: application, economics, and public perception, CRC Press, 2014.
- [122] P.G.V. Sampaio, M.O.A. González, Photovoltaic solar energy: Conceptual framework, Renewable and Sustainable Energy Reviews 74 (2017) 590–601. https://doi.org/10.1016/j.rser.2017.02.081.
- [123] G. Li, M. Li, R. Taylor, Y. Hao, G. Besagni, C.N. Markides, Solar energy utilisation: Current status and roll-out potential, Appl Therm Eng 209 (2022) 118285. https://doi.org/https://doi.org/10.1016/j.applthermaleng.2022.118285.
- [124] H.M. Abbas, I.M. Ali, H.M.T. Al-Najjar, Experimental Study of Electrical and Thermal Efficiencies of a Photovoltaic Thermal (PVT) Hybrid Solar Water Collector

- with and Without Glass Cover, Journal of Engineering 27 (2021) 1–15. https://doi.org/10.31026/j.eng.2021.01.01.
- [125] S.S. Bhakre, P.D. Sawarkar, V.R. Kalamkar, Performance evaluation of PV panel surfaces exposed to hydraulic cooling A review, Solar Energy 224 (2021) 1193–1209. https://doi.org/https://doi.org/10.1016/j.solener.2021.06.083.
- [126] A. Anand, A. Shukla, H. Panchal, A. Sharma, Thermal regulation of photovoltaic system for enhanced power production: A review, J Energy Storage 35 (2021) 102236. https://doi.org/https://doi.org/10.1016/j.est.2021.102236.
- [127] J.J. Michael, I. S, R. Goic, Flat plate solar photovoltaic—thermal (PV/T) systems: A reference guide, Renewable and Sustainable Energy Reviews 51 (2015) 62–88. https://doi.org/https://doi.org/10.1016/j.rser.2015.06.022.
- [128] I. Guarracino, J. Freeman, A. Ramos, S.A. Kalogirou, N.J. Ekins-Daukes, C.N. Markides, Systematic testing of hybrid PV-thermal (PVT) solar collectors in steady-state and dynamic outdoor conditions, Appl Energy 240 (2019) 1014–1030. https://doi.org/10.1016/j.apenergy.2018.12.049.
- [129] I. Guarracino, A. Mellor, N.J. Ekins-Daukes, C.N. Markides, Dynamic coupled thermal-and-electrical modelling of sheet-and-tube hybrid photovoltaic/thermal (PVT) collectors, Appl Therm Eng 101 (2016) 778–795. https://doi.org/10.1016/j.applthermaleng.2016.02.056.
- [130] J.A. Duffie, W.A. Beckman, Solar Engineering of Thermal Processes, Wiley, 2013.
- [131] S.W. Churchill, A comprehensive correlating equation for laminar, assisting, forced and free convection, AIChE Journal 23 (1977) 10–16. https://doi.org/10.1002/aic.690230103.
- [132] J. ~H. Watmuff, W. ~W. ~S. Charters, D. Proctor, Solar and wind induced external coefficients Solar collectors, (1977) 56.
- [133] F.P. Incropera, D.P. DeWitt, T.L. Bergman, A.S. Lavine, Fundamentals of heat and mass transfer, Wiley New York, 1996.
- [134] F.P. Incropera, D.P. DeWitt, T.L. Bergman, A.S. Lavine, Fundamentals of heat and mass transfer, Wiley New York, 1996.
- [135] T.T. Chow, Performance analysis of photovoltaic-thermal collector by explicit dynamic model, Solar Energy 75 (2003) 143–152. https://doi.org/https://doi.org/10.1016/j.solener.2003.07.001.

- [136] D.L. Evans, Simplified method for predicting photovoltaic array output, Solar Energy 27 (1981) 555–560. https://doi.org/https://doi.org/10.1016/0038-092X(81)90051-7.
- [137] K. Nagano, T. Mochida, K. Shimakura, K. Murashita, S. Takeda, Development of thermal-photovoltaic hybrid exterior wallboards incorporating PV cells in and their winter performances, Solar Energy Materials and Solar Cells 77 (2003) 265–282. https://doi.org/https://doi.org/10.1016/S0927-0248(02)00348-3.
- [138] C. Yang, H. Chen, T. Miyazaki, Y.D. Kim, K. Thu, Unsteady-state entropy generation analysis of the counter-flow dew-point evaporative coolers, Appl Therm Eng 257 (2024). https://doi.org/10.1016/j.applthermaleng.2024.124443.
- [139] P. Hoang, V. Bourdin, Q. Liu, G. Caruso, V. Archambault, Coupling optical and thermal models to accurately predict PV panel electricity production, Solar Energy Materials and Solar Cells 125 (2014) 325–338. https://doi.org/https://doi.org/10.1016/j.solmat.2013.11.032.
- [140] P. Hoang, V. Bourdin, Q. Liu, G. Caruso, V. Archambault, Coupling optical and thermal models to accurately predict PV panel electricity production, Solar Energy Materials and Solar Cells 125 (2014) 325–338. https://doi.org/https://doi.org/10.1016/j.solmat.2013.11.032.
- [141] H.A. Zondag, D.W. de Vries, W.G.J. van Helden, R.J.C. van Zolingen, A.A. van Steenhoven, The yield of different combined PV-thermal collector designs, Solar Energy 74 (2003) 253–269. https://doi.org/https://doi.org/10.1016/S0038-092X(03)00121-X.
- [142] H.A. Zondag, D.W. de Vries, W.G.J. van Helden, R.J.C. van Zolingen, A.A. van Steenhoven, The yield of different combined PV-thermal collector designs, Solar Energy 74 (2003) 253–269. https://doi.org/https://doi.org/10.1016/S0038-092X(03)00121-X.
- [143] Y.D. Kim, K. Thu, H.K. Bhatia, C.S. Bhatia, K.C. Ng, Thermal analysis and performance optimization of a solar hot water plant with economic evaluation, Solar Energy 86 (2012) 1378–1395. https://doi.org/10.1016/j.solener.2012.01.030.
- [144] L. Yang, J.C. Lam, C.L. Tsang, Energy performance of building envelopes in different climate zones in China, Appl Energy 85 (2008) 800–817. https://doi.org/10.1016/j.apenergy.2007.11.002.

- [145] A. Costa, M.M. Keane, J.I. Torrens, E. Corry, Building operation and energy performance: Monitoring, analysis and optimisation toolkit, Appl Energy 101 (2013) 310–316. https://doi.org/10.1016/j.apenergy.2011.10.037.
- [146] L. Yang, H. Yan, J.C. Lam, Thermal comfort and building energy consumption implications - A review, Appl Energy 115 (2014) 164–173. https://doi.org/10.1016/j.apenergy.2013.10.062.
- [147] M. Lee, J. Ham, J.W. Lee, H. Cho, Analysis of thermal comfort, energy consumption, and CO2 reduction of indoor space according to the type of local heating under winter rest conditions, Energy 268 (2023) 126722. https://doi.org/10.1016/j.energy.2023.126722.
- [148] H. Sun, Z. Yang, B. Lin, W. Shi, Y. Zhu, H. Zhao, Comparison of thermal comfort between convective heating and radiant heating terminals in a winter thermal environment: A field and experimental study, Energy Build 224 (2020) 110239. https://doi.org/10.1016/j.enbuild.2020.110239.
- [149] R. Yang, H. Zhang, S. You, W. Zheng, X. Zheng, T. Ye, Study on the thermal comfort index of solar radiation conditions in winter, Build Environ 167 (2020) 106456. https://doi.org/10.1016/j.buildenv.2019.106456.
- [150] J. Dong, H. Lan, Y. Liu, X. Wang, C. Yu, Indoor environment of nearly zero energy residential buildings with conventional air conditioning in hot-summer and cold-winter zone, Energy and Built Environment 3 (2022) 129–138. https://doi.org/10.1016/j.enbenv.2020.12.001.
- [151] C. Wang, Y. Yang, F. Causone, M. Ferrando, Y. Ye, N. Gao, P. Li, X. Shi, Dynamic predictions for the composition and efficiency of heating, ventilation and air conditioning systems in urban building energy modeling, Journal of Building Engineering 96 (2024). https://doi.org/10.1016/j.jobe.2024.110562.
- [152] H. Wang, Q. Tang, D. Liu, A comprehensive evaluation index for indoor thermal comfort and energy utilization, Case Studies in Thermal Engineering 63 (2024). https://doi.org/10.1016/j.csite.2024.105335.
- [153] T. Al Mindeel, E. Spentzou, M. Eftekhari, Energy, thermal comfort, and indoor air quality: Multi-objective optimization review, Renewable and Sustainable Energy Reviews 202 (2024) 114682. https://doi.org/10.1016/j.rser.2024.114682.
- [154] S. Anisimov, D. Pandelidis, A. Jedlikowski, Performance study of the indirect

- evaporative air cooler and heat recovery exchanger in air conditioning system during the summer and winter operation, Energy 89 (2015) 205–225. https://doi.org/10.1016/j.energy.2015.07.070.
- [155] T. Miyazaki, I. Nikai, A. Akisawa, Simulation analysis of an open-cycle adsorption air conditioning system—numeral modeling of a fixed bed dehumidification unit and the maisotsenko cycle cooling unit, International Journal of Energy for a Clean Environment 12 (2011).
- [156] G. Priyadarshi, B. Kiran Naik, Experimental and numerical studies on moisture adsorption/desorption characteristics across the circular fin tube desiccant coated heat exchanger, Thermal Science and Engineering Progress 53 (2024) 102755. https://doi.org/10.1016/j.tsep.2024.102755.
- [157] S. Kumar, J. Mathur, S. Mathur, M.K. Singh, V. Loftness, An adaptive approach to define thermal comfort zones on psychrometric chart for naturally ventilated buildings in composite climate of India, Build Environ 109 (2016) 135–153. https://doi.org/10.1016/j.buildenv.2016.09.023.